Journal of Materials Research and Technology 32 (2024) 1868–1900

Contents lists available at ScienceDirect

Journal of Materials Research and Technology

journal homepage: www.elsevier.com/locate/jmrt

Research progress, application and development of high performance 6000 series aluminum alloys for new energy vehicles

Yi-Cheng Gao [a,b], Bai-Xin Dong [a,b,***], Hong-Yu Yang [a,b,**], Xiao-Yan Yao [a,b], Shi-Li Shu [a,c,****], Jie Kang [d], Jia Meng [e], Chang-Jie Luo [f], Cheng-Gang Wang [g], Kuang Cao [h], Jian Qiao [i], Ming Zhu [j], Feng Qiu [a,b,*], Qi-Chuan Jiang [a,b]

[a] State Key Laboratory of Automotive Simulation and Control, Jilin University, PR China
[b] Key Laboratory of Automobile Materials, Ministry of Education and Department of Materials Science and Engineering, Jilin University, Renmin Street NO. 5988, Changchun, Jilin Province, 130025, PR China
[c] School of Mechanical and Aerospace Engineering, Jilin University, Renmin Street NO. 5988, Changchun, 130025, PR China
[d] Jilin Liyuan Precision manufacturing Co., Ltd., No. 5729, Xi'ning Road, Economic Development Zone, LiaoYuan, Jilin Province, 136299, PR China
[e] Department and Test Center, FAW-Volkswagen Automotive Co., Ltd, Changchun, Jilin Province, 130011, PR China
[f] Shenzhen Cansinga Technology Co., Ltd. Building D, Central Avenue, Bao'an District, Shenzhen, Guangdong Province, 518101, PR China
[g] Technology Research and Development Casting & Forging Research Institute, FAW Foundry Co., Ltd, Crossing of Hexie Street & Bingwu Road Automotive Industry Development Zone Changchun, Jilin Province, 130013, PR China
[h] Jiangsu Dalishen Aluminum Industry Co., Ltd. No. 8 Shengchang West Road, Economic Development Zone, Danyang, Jiangsu Province, 212314, PR China
[i] School of Mechatronic Engineering and Automation, Foshan University, No. 33 Guangyun Road, Nanhai District, Foshan, Guangdong Province, 528231, PR China
[j] Zhenjiang Xianfeng Automotive Parts Co., Ltd, Dantu High tech Industrial Park, Zhenjiang, Jiangsu Province, 212000, PR China

ARTICLE INFO

Keywords:
Al-Mg-Si alloy
Alloying
Microstructure
Particle enhancement

ABSTRACT

For the development of new energy automobile industry and the trend of automobile lightweight have put forward a huge demand for high-strength lightweight materials, so developing high strength aluminum alloys is particularly momentous. As the most widely used aluminum alloy, 6000 series aluminum alloys (Al–Mg–Si alloys) have the advantages such as better mechanical properties, outstanding welding properties, excellent formability and fine processing capability, and therefore have obtained great attention as the structural materials. In addition, the Al–Mg–Si alloys with low density and corrosion resistance not only reduce the total weight of the car, but also extend the service life when subjected to chemical corrosion, which effectively achieve energy saving and emission reduction. This paper summarizes the research progress of 6000 series aluminum alloys, in particular, and reviews the methods of microalloying and particle strengthening, and their effects on the microstructure and properties of the alloy, thus providing a reference for the subsequent development of high-performance aluminum alloys in automobile and aerospace industries.

1. Introduction

With the global emphasis on environmental protection and sustainable development, new energy vehicles have become an important choice to solve the dual challenges of energy and environment. Passenger cars occupy an important position in new energy vehicles, and the development of high-performance aluminum alloys is one of the keys to promote the technological progress of new energy passenger cars. As a heat-treatable Al–Mg–Si alloy, with its excellent corrosion resistance and machinability, it is suitable for the manufacturing of complex structural components and is expected to replace steel as the profile of new energy vehicles, which will help achieve lightweight new energy vehicles to reduce energy loss and aluminum alloys are easier to recycle and more environmentally friendly than steel [1–5].

* Corresponding authors.
** Corresponding author.
*** Corresponding authors.
**** Corresponding author.
E-mail addresses: dongbx20@mails.jlu.edu.cn (B.-X. Dong), yanghongyu2021@jlu.edu.cn (H.-Y. Yang), shushili@jlu.edu.cn (S.-L. Shu), qiufeng@jlu.edu.cn (F. Qiu).

https://doi.org/10.1016/j.jmrt.2024.08.018
Received 8 May 2024; Received in revised form 21 July 2024; Accepted 6 August 2024
Available online 8 August 2024

The lightweight of new energy vehicles cannot be separated from the application of various lightweight materials (especially aluminum alloy) [6–12], but the lightweight aluminum alloy extrusion material used in the car is inevitably different from the ordinary industrial aluminum profile as heavy and single, it can not only be extruded but also can be fused and cast, and the thickness is relatively thin [13,14]. These involve structural innovation design method, multifunctional realization, performance evaluation and verification methods, which are extremely challenging for the entire automotive industry. In fact, in addition to lightweight, aluminum alloy parts in new energy vehicles have the following advantages [15–19]: (i) the processing process of aluminum alloy shell is simple compared with stainless steel and the welding process can be eliminated; (ii) good energy absorption effect, such as applied to the front protection structure of the vehicle, when the vehicle has a collision accident, the anti-collision beam of aluminum alloy can better absorb the impact energy, due to its soft special effects, can reduce the damage to the pedestrian hit; (iii) aluminum alloys are suitable for the integrated design of automotive bodies, which can reduce duplication and redundancy between components, making automotive systems more compact and improving overall efficiency. Fig. 1 gives some examples of aluminum alloys used in new energy vehicles. However, the simple 6xxx aluminum alloys are slightly insufficient in terms of strength and fatigue resistance [20], which is difficult to meet the demands of automobile bodies and parts required by industry. Therefore,

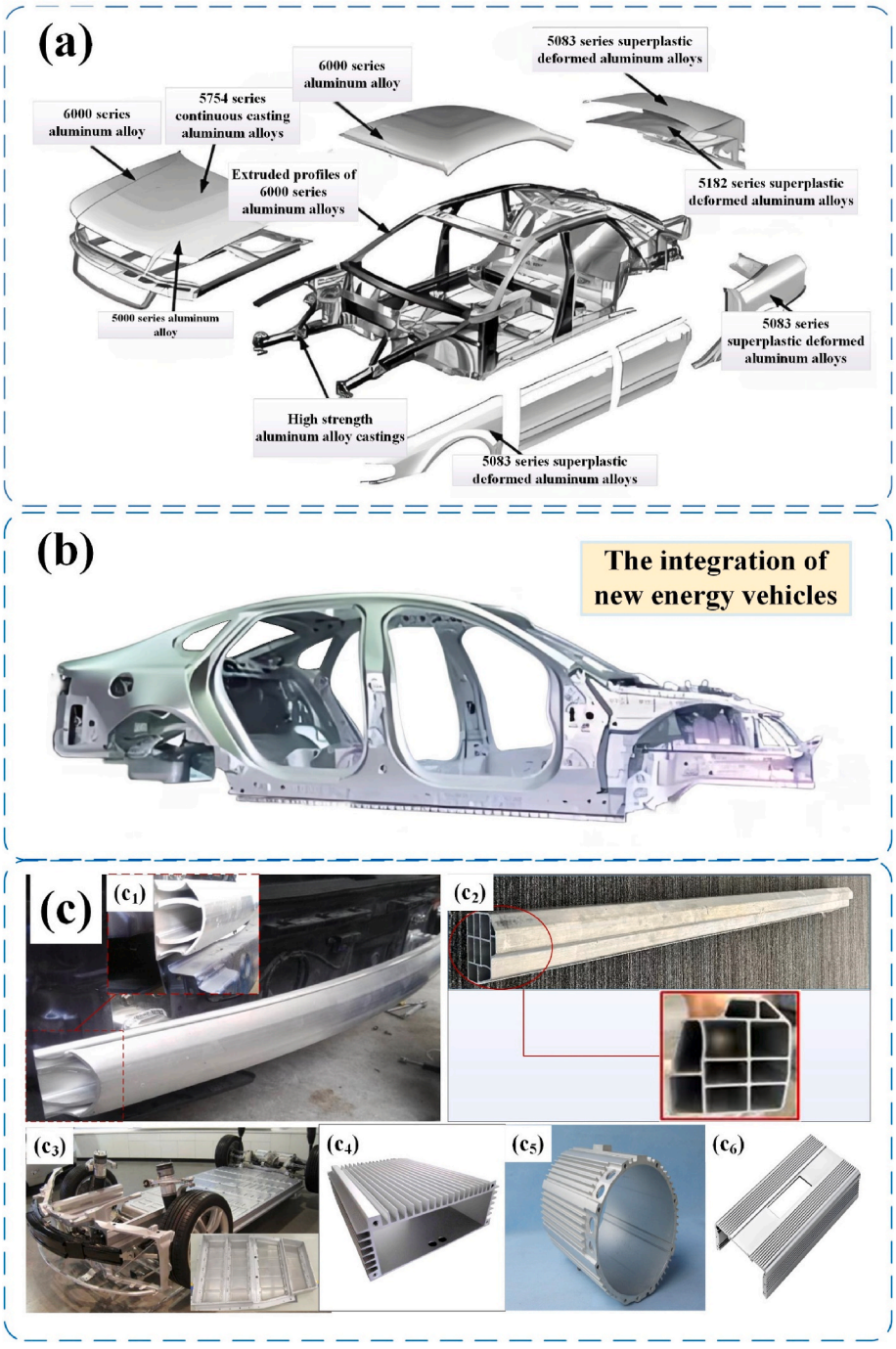

Fig. 1. (a) Aluminum alloys for new energy vehicle applications; (b) integration of new energy vehicles; (c) application of 6000 series aluminum alloy profiles or plates: (c_1) bumper beam, (c_2) door sill beams, (c_3) battery tray, (c_4) battery pack casing, (c_5) motor housing, (c_6) automobile cooling plate.

the potential of 6000 series aluminum alloys is continuously explored maintaining its welding, corrosion-resistant and high formability, especially, its mechanical properties for passenger cars should be further improved to achieve thin-wall lightweighting.

The strengthening of Al–Mg–Si alloy mainly comes from the strengthening effect brought by the nano-precipitated phase obtained by heat treatment [21,22], in order to improve their properties, controlling the distribution, orientation, size and composition of the precipitated phase are crucial. During the alloying process, the adjustment of the content of elements including those already present in the alloy (e.g. Mg, Si) or the introduction of other elements is almost always done in order to ensure an improvement in the precipitation phases and to obtain excellent properties. A host of studies have shown [22–24] that the purpose of precipitating more Mg_2Si strengthening phase has been achieved and the preparation of high-strength aluminum has been realized by increasing the Si content of aluminum alloy. Since excessive elemental content could cause elemental segregation to deteriorate performance, so the performance improvement only based on Si content is very limited, and relevant studies have also shown that Mg/Si ratio of 1.74 ensures the best performance [25]. This led to a focus on foreign elements, different elements will form different dispersoids in the aluminum matrix, which are summarized in Fig. 2. The appearance of some dispersoids could produce a strengthening effect that is similar to strengthening phase, meaning that the addition of elements brings conversion in the microstructure of the alloy and thus improves the performance. It has been reported that the pinning action of high-density Al_3Zr and Al_3Sc diffuse phases limits grain coarsening to bringing about the best mechanical properties [26,27]. Zheng et al. [28] found that Al–Mg–Si alloy with Sn and Sc addition obtained small dispersoids, which hindered dislocation movement and achieved high strength and good thermal stability, but the two elements has a completely different effect on the corrosion resistance.

Except for the improvement of properties by alloying, alloys obtained by relying on particle reinforcements have garnered significant interest due to their superior mechanical properties far beyond those of conventional metallic materials [29–32]. The particles not only influence the precipitated phase but also has a certain degree of influence on a series of microstructures such as solidification microstructure and the deformation microstructures [33,34], which also displays a more superior modification of the reinforcing particles. The study from Liu et al. showed that the addition of TiC to alloy was effective for slowing down the solidification rate of the alloy, inhibiting grain coarsening, reducing segregation and promoting uniform precipitation of the second phase, resulting in higher tensile properties [35]. In addition, the alloys prepared by incorporating reinforcement particles exhibit excellent properties, which is beneficial to their applications in various complex structural parts. Composite material, to a certain extent, combines the excellent molding ability and ductility of aluminum alloys [21,36] and the high elastic modulus and high strength of the enhanced particles [37–41], which indicates that the properties of the particles themselves have a certain impact on the performance of the composite material. It also lays a foundation for manipulating multi-phase particles, synthesizing their advantages and the synergistic effect of different particles to achieve better performance. However, too many particles or ineffective bonding of particles to the substrate interface not only leads to premature failure but also bring a series of defects, and thus resulting in the deterioration in performance [42,43].

Therefore, the investigation on how adjusting the alloy's composition and adding particles affect the microstructure and properties of the alloy is valued. This paper reviews the application and requirements of Al–Mg–Si alloy plate for new energy vehicles, the influence of the composition improvement on the performance, the complex function of particles in the manipulation of Al–Mg–Si alloy and the potential of enhanced particles to achieve high performance 6000 series aluminum alloys, aiming to provide a key support for the realization of clean and efficient new energy vehicles.

2. Automotive aluminum alloy sheet applications and requirements

Al–Mg alloys are prone to delayed yielding phenomenon during processing, which will lead to the emergence of Lydus bands, wrinkles and even the orange peel effect on the surface of the material after stamping [51–55]. By comparison, Al–Mg–Si alloys show good formability, edge compaction, corrosion resistance and collision performance in engineering, which lays a certain foundation for its application in the field of new energy vehicles. In particular, Al–Mg–Si alloys used as automotive plates have become the mainstream material used by automobile manufacturers for automobile exterior covering parts due to their many advantages, such as good formability, satisfactory surface finish after stamping, and significantly improved properties of alloy plates after baking and hardening after stamping [56–58]. It is applied in

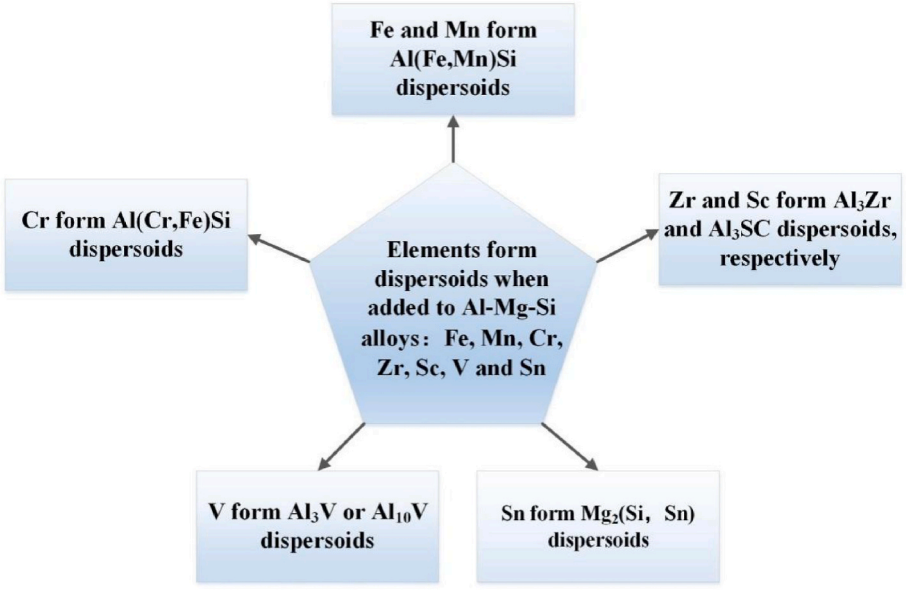

Fig. 2. Dispersoids formed by different elements in Al–Mg–Si alloys [28,44–50].

mainly the door, the back cover of the trunk and the hood of the car, which is often called "four doors and two covers" in the industry. Table 1 summarizes the service requirements of conventional Al–Mg–Si alloy body plates in order to use the relevant plates normally and give full play to the relevant advantages of aluminum alloy plates for different application scenarios. In addition, in order to meet the requirements of the strength of the body material and the vibration and noise reduction during the driving process of automobile, the panel coverings used in new energy vehicles are usually composed of two layers, the inner and outer panels. They are connected with the related parts through the flanging operation (Fig. 3(a)) [59–62], which not only improves the appearance of the sheet covering but also achieves better bonding strength. On the other hand, due to the complex geometry of automotive body panels, the application of aluminum alloy sheets in the car body requires different flanging methods according to different parts of the application in order to achieve a better combination effect (Fig. 3(b)) [63,64]. However, in the flanging process, the cracking of the outer surface layer is a major problem. That is to say, both the inner and outer double-layer plates will produce a large amount of plastic deformation after 180° flanging treatment, especially the outer layer is subjected to tensile deformation and the grains inside the alloy are constantly being elongated (Fig. 3(c)), which easily reaches the maximum strain value that can be withstood by the alloy and then Fracture occurs, forming macro cracks on the outer surface [65]. Therefore, the deformation of the alloy plate in the assembly process or in the service process will limit the use of the plate. In addition, Shi et al. [66] found that the uneven distribution or too large size of the second phase hard particles will significantly degrade the impact resistance of the alloy sheet. When the Al–Mg–Si alloy sheet subjected to the effect of external impact, the stress concentration around the particles will be obvious, which will ultimately evolve into the emergence of cracks and expand under the continuous effect of the external force until the failure of the alloy sheet (Fig. 3(d)). Although Al–Mg–Si alloy sheet has an influence the microstructure and mechanical properties of the alloy at each step of the production process (such as casting, homogenization treatment, after hot and cold rolling, pre-ageing treatment), the improvement of the process parameters on its in-service properties remains limited, so that the development of high-performance aluminum alloy sheet by new means is significant.

3. The influence of elements on properties and microstructure of 6000 aluminum alloys

For aluminum alloys, microalloying is one of the most common and effective means to improve the comprehensive properties of alloys. Adding different elements could affect the shape, distribution and volume fraction of precipitated phases (especially the β″ phase). In addition, some elements can also interact with the matrix to generate new reinforcing phases, affecting the strength and plastic toughness of the alloy. Different elements and their contents lead to different effects on the precipitated phases in the alloys, which in turn have different effects on the properties of the alloys.

3.1. The effect of Mg/Si on 6000 series aluminum alloys

Although that Al–Mg–Si alloys possess medium-strength, their strength and tensile properties can be further improved by solid solution and aging heat treatments. Al–Mg–Si alloys are aged from a supersaturated solid solution (SSS) state, and the order precipitation of various types is as follows [71–73]:

SSS → GP zones → β″ (Mg_5Si_6) → β′ → β (Mg_2Si), among them, the GP region (atomic clusters), β″ and β′ are spherical, fine needle-like and rod-like compounds, respectively. According to earlier research [74–77], β″ precipitates as well as GP zones are crucial for the strengthening of the alloy properties, the presence of the GP zones provides the main age-hardening and the spherical GP zones provides heterogeneous nucleation sites for the β″ precipitates. The strengthening effect of β″ precipitation and atomic clusters can be estimated by simulations [78–80]:

$$\sigma_y = \sigma_0 + \sigma_{sol} + \sqrt{\sigma_p^2 + \sigma_{cl}^2} \quad (1)$$

among them, σ_0, σ_{sol}, σ_p and σ_{cl} represent the strength of pure aluminum, the solid solution strengthening caused by the addition of Si and Mg elements, the strengthening effect of needle precipitates β″ and atomic clusters, respectively. However, the change in the Mg/Si ratio not only affects the formation of the GP zone and β″ precipitation during aging but also alters its stability. A relevant study has shown that the size distribution of precipitates in low Mg/Si ratio alloys was uniform as well as more diffusely distributed on the matrix both in the mid-ageing and the peak-ageing processes, while the precipitates of aluminum alloys with high Mg/Si ratios had a more disordered atomic structure and the TEM exhibited the coexistence of both long-needle and short-rock precipitates (Fig. 4(a–d)) [78]. This implies that the combined precipitated phase at higher Mg/Si ratios may be a coexisting body of the β″ phase and other phases.

The changes in the mass ratio and content of Mg and Si elements impact on the properties of the alloy. Gong et al. [77] found that keeping the content of Si at 1.2%, the Mg content is increased to exceed the maximum limit in 6000 series aluminum alloys (1.2%) [81–83], the strength and ductility are both enhanced by increasing Mg content. Sun et al. [84] investigated the microstructure and the properties of 6000 series aluminum alloys at Mg/Si ratios of 0.73, 1.19, and 1.30, respectively. They found that the extruded profiles were more homogeneous at the edges and centers, and the plasticity increased while the strength and hardness decreased slightly as the increasing Mg/Si ratio. This is due to the fact that the mutual entanglement of dislocations during deformation by applied external force hinders the movement of dislocations and increases the strength of the alloy, but the increasing Mg element eases the dislocation entanglement during deformation and reduces the rate of hardening, which in turn improves the plasticity of the alloy. Furthermore, raising the Mg/Si ratio brings a greater bias towards the formation of β″ in the alloy, which generates difficulty for Si to be polarized and enriched at grain boundaries, makes it less susceptible to along-granular fracture, and results in the reducing the generation of large-size precipitated phases to a certain extent. The decrease in Si content also reduces the precipitation of hard particles, which results in a decrease in strength and hardness. However, Mg/Si ratio less than 1.73 is considered to be an excess of elemental Si [85], when the content of the Mg_2Si phase is mainly controlled by the content of elemental Mg [71] as shown in Fig. 5. The content of the Mg_2Si phase in the alloy increases with the increase of Mg elements [86], and the increase in the

Table 1
Performance criteria for 6000 series aluminum alloy sheets for automotive bodies [56–58,67–70].

	Yield Strength (MPa)	Ultimate Tensile Streng (MPa)	Elongation (%)	Strain Hardening Exponent	Plastic Strain Ratio
Standard aluminum alloy	90–140	≥200	≥23	0.23	0.50
Bake-hardened reinforced aluminum alloys	100–150	≥200	≥22	0.23	0.50
High strength aluminum alloy	115–170	≥250	≥20	0.23	0.5
Aluminum alloy for reinforcement applications	110–160	≥200	≥21	0.23	0.5
Reinforced aluminum alloy with crimped edges	130	≥175	≥23	0.25	0.55

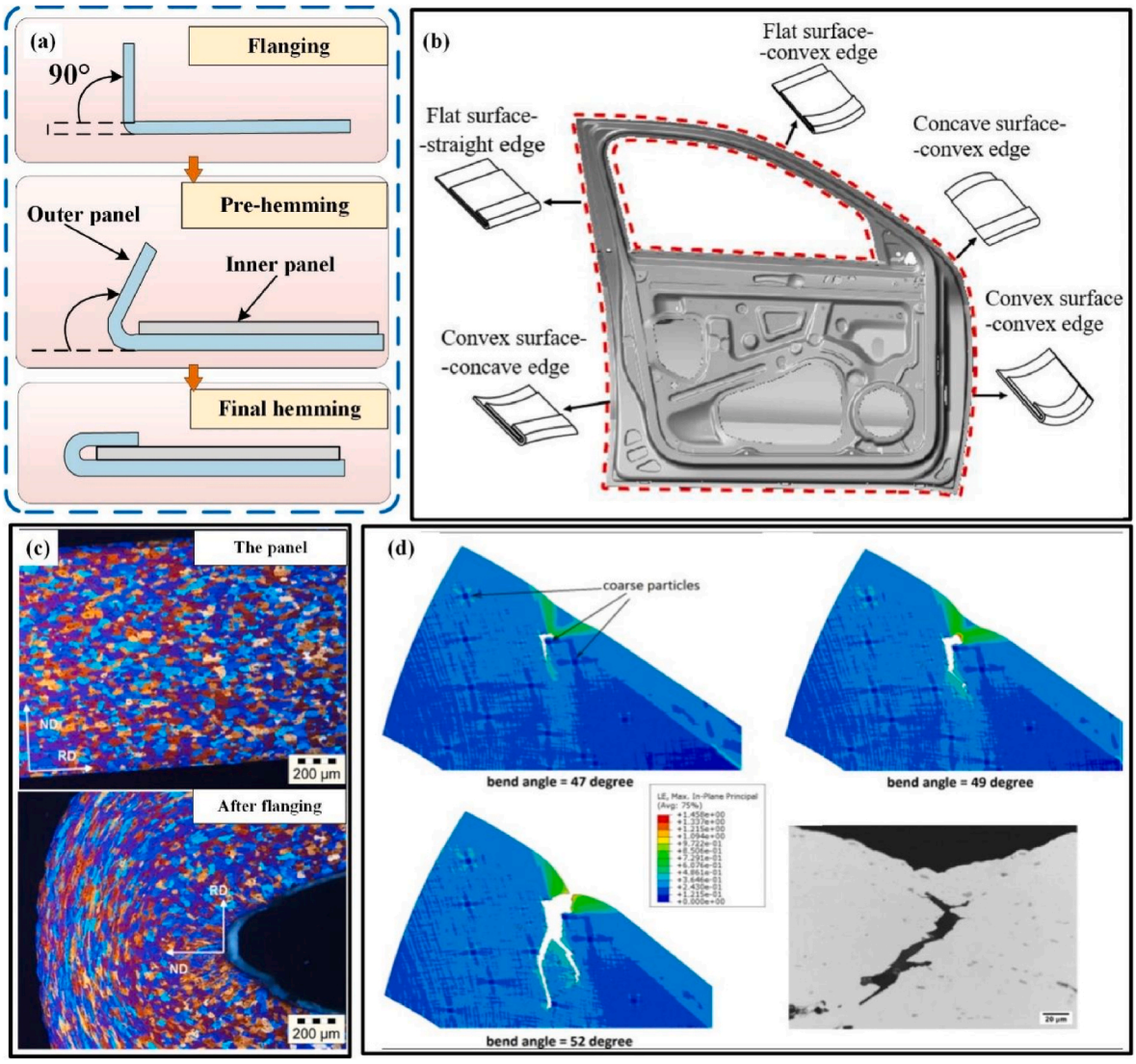

Fig. 3. (a) Schematic diagram of alloy sheet flanging; (b) types of flanging [64]; (c) comparison of microstructures of Al–Mg–Si alloy plates before and after flanging [65]; (d) plate failure from hard particles under impact [66].

Mg_2Si phase content from attenuating the unfavorable effect of reduced strength hardness due to the reduction of hard compounds.

Zupanič et al. [87] developed a high-strength aluminum alloy AA6086 based on AA6082, which possesses good fatigue resistance and mechanical properties, and the chemical elemental composition of AA6082 and AA6086 were given in Table 2. Apparently, AA6086 possessed a higher content of Si as well as the introduction of Zr elements compared to AA6082. They attributed the high performance of the alloy to the formation of intermetallic compounds such as α-AlMnSi and Mg_2Si during solidification and remained undissolved during homogenization. During the tensile process, many tough nests are formed at the intermetallic compounds. Meanwhile, the presence of sub-micron hard intermetallic compounds in the process of fatigue crack expansion from the surface to the inside, namely, α-AlMnSi, hinders the crack expansion and thus improves the fatigue resistance. Raising the Mg/Si ratio and Mg content brings more Mg_2Si phases in the alloy and the Si element is more inclined to the formation of β ″, but at much lower Si content may lead to a reduction in the total content of hard compounds, which can result in a slight decrease in the strength of the upgraded material. However, it is worth noting that the hard intermetallic compounds produced by the elevated Si content improve the fatigue resistance of the alloy. Therefore, in order to obtain the alloys with excellent properties, it is necessary to strictly control the ratio and content of Mg and Si to ensure that the precipitated phases in the alloy are favorable to the properties and uniformly distributed to avoid elemental segregation.

3.2. The effect of Cu on 6000 series aluminum alloys

As the main alloying element, the addition of Cu in 6xxx AA not only improves the precipitates' density and volume fraction, but also alters their structure, which produces an alloy with high strength [88–91]. Liu et al. and Weng et al. [91,92] observed the microstructure and phases of precipitation of the alloys after the addition of Cu. The results show that the density and volume fraction of precipitates in the alloy with Cu addition are effectively improved compared with those without Cu addition (Fig. 6(a and b)). The smaller point-like precipitates are GP zones, and the larger point-like precipitates or needle-like precipitates are β″. The Cu atoms enter into the interior of the β″ phase around the distribution of three Mg atoms and Si atoms (Fig. 6(c and d)) [93], which transform the original ordered β″ precipitate into disordered β″ phase. In addition, the homogenization process produces α-Al(Fe, Mn)Si diffuse phase [46,94]. Fig. 6(f_1-f_3) show the effect of Cu addition on the α-dispersive phase at 500 °C, holding for 4 h and 24 h, respectively. Cu element in alloys not only makes the dispersed phase denser, but also

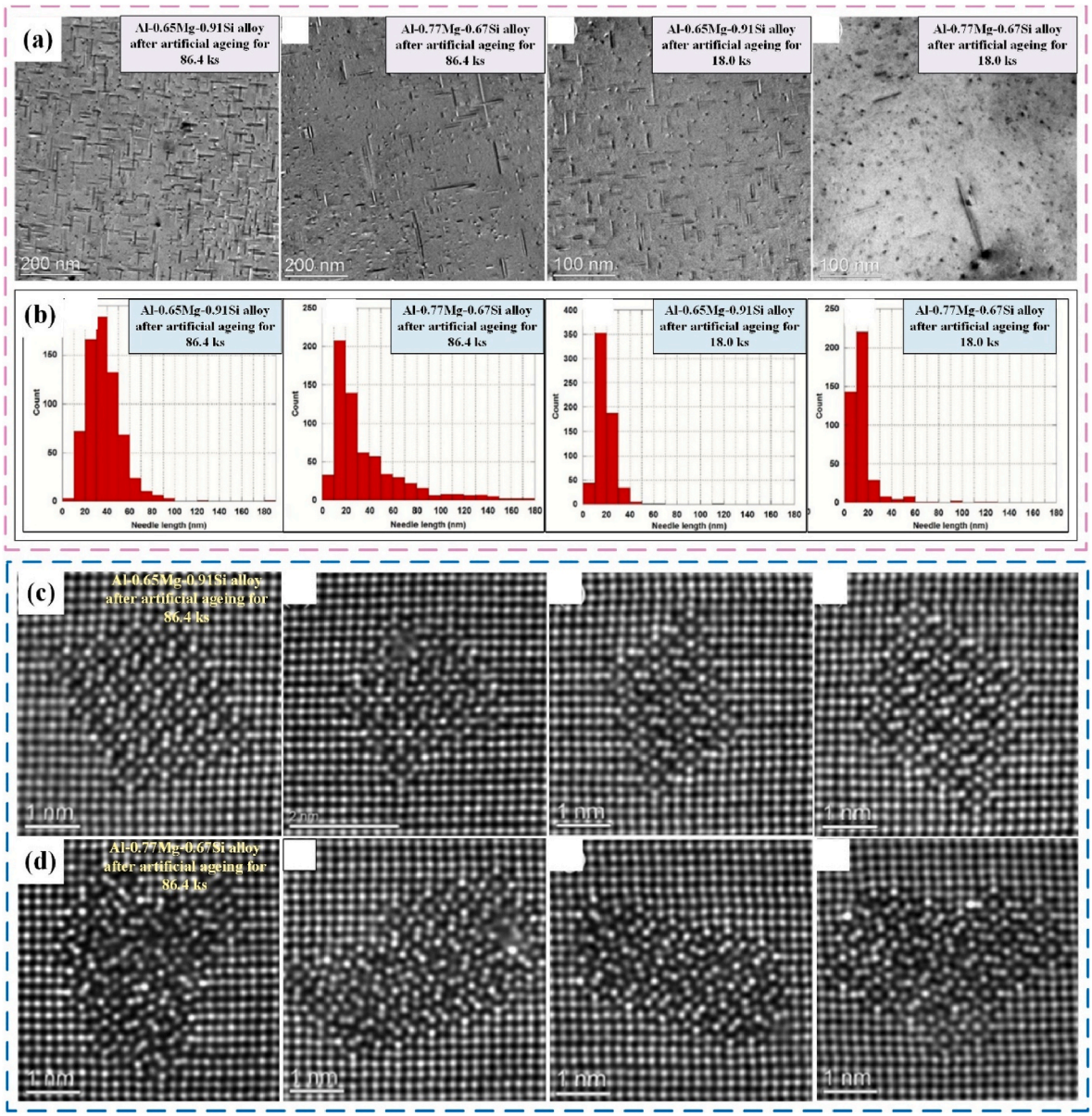

Fig. 4. (a) TEM maps of different alloys, (b) size distribution of precipitated phases, (c) and (d) showing the atomic structure of various alloys' precipitates [78].

encourages the phase transformation from flakes and rods to spheres, and thus leading to the reduction of its coarsening rate at high temperatures. It has been shown [95,96] that the alloy will possess better thermal stability because of smaller lattice mismatch between precipitates and precipitated phases. And the spherical α-Al(FeMn)Si dispersed phase presents a small lattice mismatch with the matrix, so the addition of Cu improves the high temperature mechanical properties. Wu et al. [97] reported center segregation and mechanical properties of twin-roll cast-rolled (TRC) aluminum sheets with different Cu contents. The results showed that the central segregation in the 0.8 wt% and 1.2 wt% alloys was dissolved, while the 1.6 wt% alloy still had serious segregation. In addition, the hardness and strength of the alloys with the addition of 0.8 wt% and 1.2 wt% Cu under quenching and peak aging were significantly enhanced, but no significant improvement in performance was observed when Cu reached 1.6 wt% (compared with 1.2 wt% Cu), as show in Fig. 6(g and h). The strengthening mechanisms of the alloy with the addition of Cu mainly include solid solution strengthening and precipitation strengthening. The improvement of segregation should be attributed to the formation of Q-AlCuMgSi and θ-Al_2Cu as well as the reduction of Mg_2Si precipitates after adding Cu [98]. The dissolution temperature of Q-AlCuMgSi and θ-Al_2Cu produced by Cu alloying is lower than that of Mg_2Si, so the segregation of the alloy can be improved [97]. The various Cu-rich phases are almost insoluble in the matrix when the Cu content is too high, resulting in more serious segregation.

Besides, some studies [99–101] have shown that 6000 series aluminum alloys in the presence of Cu element are more prone to intergranular corrosion (IGC) caused by the micro-current coupling between the copper film and the solute depletion active region. For example, Liang et al. [102] studied the corrosion kinetics of the alloys with 0.001 wt%, 0.30 wt% and 0.89 wt% Cu content under over-aging conditions. The results showed that the cathodic reaction kinetics accelerated with raising Cu content, which impaired the corrosion resistance of the alloy. Svenningsen et al. [99,103–105] shown that when the Cu content is very low, the alloy has excellent intergranular corrosion resistance due to the formation of continuous galvanic corrosion paths with nanometer size. However, when the mass fraction of Cu is higher than a certain value (0.12 wt%), the intergranular corrosion sensitivity of the alloy increases significantly, and the corrosion resistance becomes worse. In Cu-containing A1-Mg-Si alloys, it is

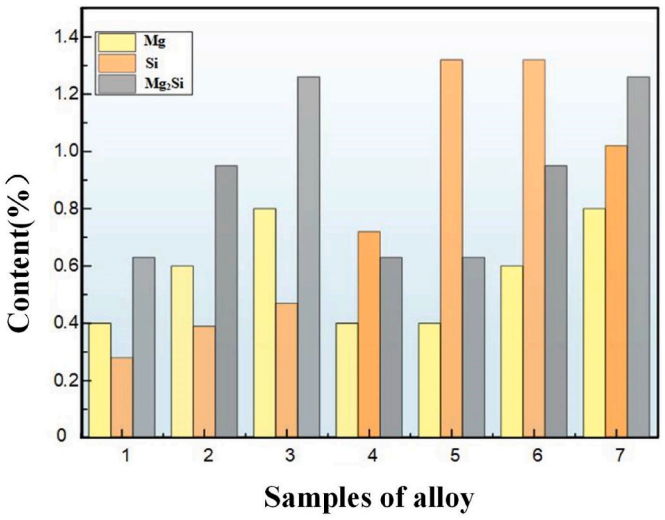

Fig. 5. The content of Mg_2Si in alloys with different Mg and Si content [86].

believed that the IGC occurs as a result of the precipitation free zone (PFZ) and the precipitation phase at the grain boundary, where the composition of the precipitation phase varies with the Cu content and Cu-rich films may be formed at the grain boundary with the increase of the Cu content. In Refs. [102,106–108], the exposed Cu-containing precipitated phase, the Cu-rich film and the corroded grain boundaries can act as cathodes. Under acidic conditions, Cu elements and Cu-containing precipitation phases in Cu-rich films dissolve and deposit at grain boundaries, ultimately accelerating IGC. In conclusion, the presence of the element Cu not only improves the strength of aluminum alloys by regulating the precipitation phase, but also ameliorates the central segregation produced during the TRC process. However, the appearance of Cu, especially when the Cu content is too high, will not only lead to a decrease in the corrosion resistance of the alloy, but also may result in more serious segregation. Therefore, it is necessary to strictly control the addition amount of Cu element to obtain alloys with better comprehensive properties in the process of Cu alloying.

3.3. The effect of Fe and Mn on 6000 series aluminum alloys

In most cases, the increase of Fe element and coarse Fe phase can worsen the bending properties of the alloy and is unfavorable to the recycling of Al in the alloy [109–111]. However, the appropriate addition of Mn element is beneficial to the formation of compounds with Fe element, and thus leading to the reduction of the adverse impact of Fe and the improvement in the heat resistance [112]. For example, Trink et al. [44,113] investigated the effects of adding Fe and Mn to Al–Mg–Si alloy and discovered that the alloy's strength increased without weakening its high plasticity persisted (Fig. 7(a–d)). Jovid et al. [114] studied the mechanical properties of extruded AA6082 with different Mn content (Fig. 7(e and f)). Because the solute diffusion accelerates the peak aging [115], the time required for the alloy after adding Mn is only 5 h, while it takes 8 h without adding Mn. Grain refinement, precipitation strengthening, solid solution strengthening, and other processes are responsible for the alloy's strengthening. This has a close connection to the alloy's altered microstructure. When the concentration of Fe and Mn increases, the precipitated phase of α-Al(FeMn)Si becomes coarser and its volume fraction of the precipitated phase is also improved (Fig. 8 (a–l)). The existence of the precipitated phase not only promotes the nucleation of recrystallized grains, but also inhibits the growth of grains [113,116]. In addition, there is a thermal expansion difference between the intermetallic compound and the matrix, which makes it difficult to deform, resulting in a geometrically necessary dislocation (GND) around matrix. The interaction between GND and the boundary can produce heterogeneous deformation-induced strengthening and improve the deformation resistance of the alloy [117]. In order to reduce the adverse effects of coarse phases, some special processing methods, such as T4 treatment (Fig. 8(g–l)) and rolling treatment (Fig. 8(m and n)), can significantly refine the intermetallic compounds, ensuring excellent properties of the alloy. However, Fe and Mn elements will be regarded as impurity elements, and when the content is too much, the sludge phase will be produced [118,119], the increase of Mn content indirectly lessens Si concentration in the matrix, leading to the decrease of the content of the main reinforcement phase β″ in the aluminum alloys [86, 120], which are the reason for the decrease of the properties of high Fe and high Mn content alloys (Fig. 7).

3.4. The effect of rare earth elements 6000 series aluminum alloys

The rare earth elements (REs) have attracted much attention in recent years, being viewed as a new type of alloy additives. The addition of small amounts of REs can significantly change the microstructure of an alloy, thus significantly affecting the alloys' mechanical and other properties. Wei et al. [121] investigated the microstructure of Al-0.5Mg-0.4Si with adding of 0.4 wt% Sc using resolved transmission electron microscopy and atomic probe chromatography, and found adding Sc accelerated forming GP zones, significantly refined the grain to improve the mechanical properties (Fig. 9(a–f)) as well as lowers PFZ to strengthen the corrosion resistance of alloys. Prach et al. [122] discovered that the yield strength (YS), ultimate tensile strength (UTS) and elongation (EL) of the alloy increased by 15.8%, 11.3% and 1.1%, respectively, compared with the base alloy when 0.1 wt% of Sc was added. The Al_3Sc ($L1_2$ structure) dispersions precipitated from the melt were produced after the addition of Sc during the solidification process, pinning the grain boundaries and dislocations hindering grains growth, obtaining a large degree of refinement [85,122–124]. At the same time, Al_3Sc dispersions are also effective in preventing grain growth at high temperatures (300 °C) [121,125]. Based on this, the grains can be stabilized by adding tiny Sc to 6000 series alloy to form the Al_3Sc dispersed phase, which prevents grain coarsening during artificial aging. Trudonoshyn et al. [126] investigated the properties of Al-5.5Mg-2.5Si-0.7Mn at different heat treatment temperatures and times after adding Sc, this study found that the strength of the alloy decreased visibly with the increase in aging temperature after aging temperature above 225 °C (Fig. 9(g and h)). Aging of Sc-containing alloys in the range of 250–500 °C, nanoscale Al_3Sc precipitates form in the Al matrix, engendering an aggrandizement in hardness. The decline in the strength of the alloy in the experiment may be due to the high aging temperature, the dissolution of β″ phase or even β′ precipitation and further formation of equilibrium β phase. Mahmoud et al. [127] studied the solidification behavior, microstructure evolution and property changes of AA6063 that had been deformed and had 1.0 wt% Ce added. It was found that the addition of Ce significantly refined the grain size, while resulted in

Table 2
Alloy composition of AA6082 and AA6086 [82,87].

Alloy	Major element (wt.%)								
	Mg	Si	Fe	Mn	Cu	Zn	Ti	Zr	Al
AA6082	0.6–1.2	0.7–1.3	<0.5	0.4–1	<1	<0.2	<0.1	–	Bal.
AA6086	1.01	1.58	0.18	0.71	0.55	0.17	0.04	0.17	Bal.

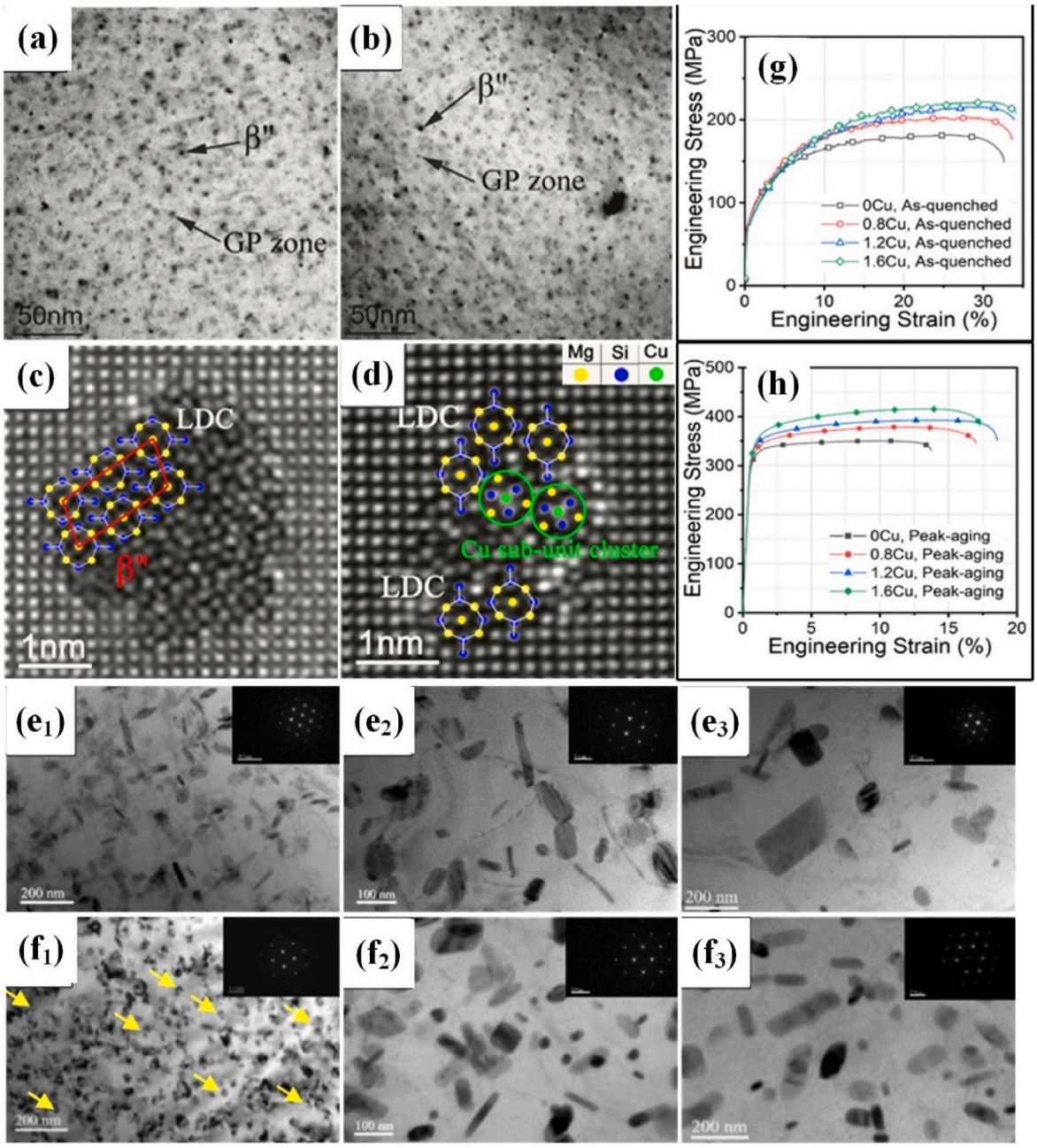

Fig. 6. TEM of bright-field images after PB treatment of Al-1.2Mg-0.68Si (a) and Al-1.2Mg-0.68Si with 0.21% Cu (b), HAADF-STEM images of the cross-sections of β″ precipitates of Al-1.2Mg-0.68Si (c) and Al-1.2Mg-0.68Si with 0.21% Cu (d), the red lines indicate β" cells, the green circles represent Cu substituent clusters, and the white lines refer to low-density cylinders (LDC) in the β" [92], TEM micrographs of α-dispersoids in Al-0.82Mg-1.07Si-0.71Mn-0.19Cr-0.05Fe alloy, (e_1, e_2, e_3) and Al-0.82Mg-1.07Si-0.58Cu-0.71Mn-0.19Cr-0.05Fe alloy (f_1, f_2, f_3) heated to 500 °C and soaked for 4 and 24 h, respectively [91]. Stress-strain curves of Al–Mg–Si alloys with different Cu contents in the quenched state (g) peak aging state (h) [97]. (For interpretation of the references to colour in this figure legend, the reader is referred to the Web version of this article.)

obvious decline of alloys' strength. Compared with the unalloyed AA6063, the alloy after Ce modification has Al–Ce precipitates and sharp plate-like Al–Si–Ce precipitates, and the Si element in the Al–Si–Ce precipitates comes from Mg_2Si, which leads to the decrease of the main enhanced precipitated phase Mg_2Si in the alloy, which leads to a sharp decline in the strength of the alloy. Zheng et al. [128] discovered that adding La can considerably boost the corrosion resistance of Al–Mg–Si alloys. Tiny concentrations of La not only preventing the development of Si particles, making them change from long lamellar shape to short rod-like morphology, but also can lower the volume percentage of Si particles at grain boundaries [129,130]. The addition of La is able to produce shells attached to the surface of Mg_2Si, which ensuring the stable presence of Mg_2Si and also prevents localized corrosion. Small amounts of Si particles at grain boundaries also prevent corrosion from extending along the grain boundaries [128]. Li et al. [131] incorporated two rare earth elements, La/Ce and La/Er, into Al–Mg–Si system alloys by resistance melting method, respectively, and they concluded that the La/Ce co-doped alloys had a higher tensile strength and the La/Er co-doped alloys exhibited a high electrical conductivity similar to that of La mono-doped alloys. Due to the addition of REs, more phases are precipitated from the matrix. These phases hinder the migration of grain boundaries or serve as heterogeneous nucleation sites to refine grains which improves the strength of the alloy [131–133]. In addition, although La, Ce and Er are all lanthanide elements, compared with Er,

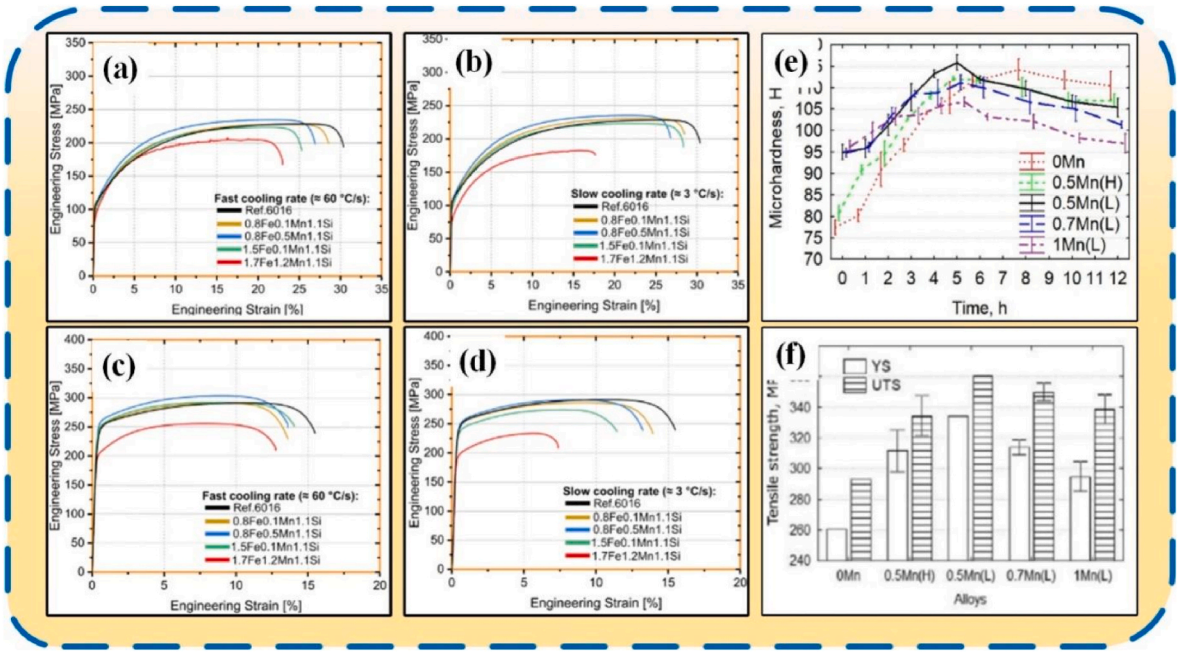

Fig. 7. Stress-strain curves for 14 days of natural aging (a, b) and 5 h of artificial aging at 185 °C (c, d) under fast-solidified (a, c) and slow-solidified conditions (b, d) [113]; Hardness versus time for 6082 extrusion alloy at different Mn contents (e) and tensile strength at conditions of T5 (f) [114].

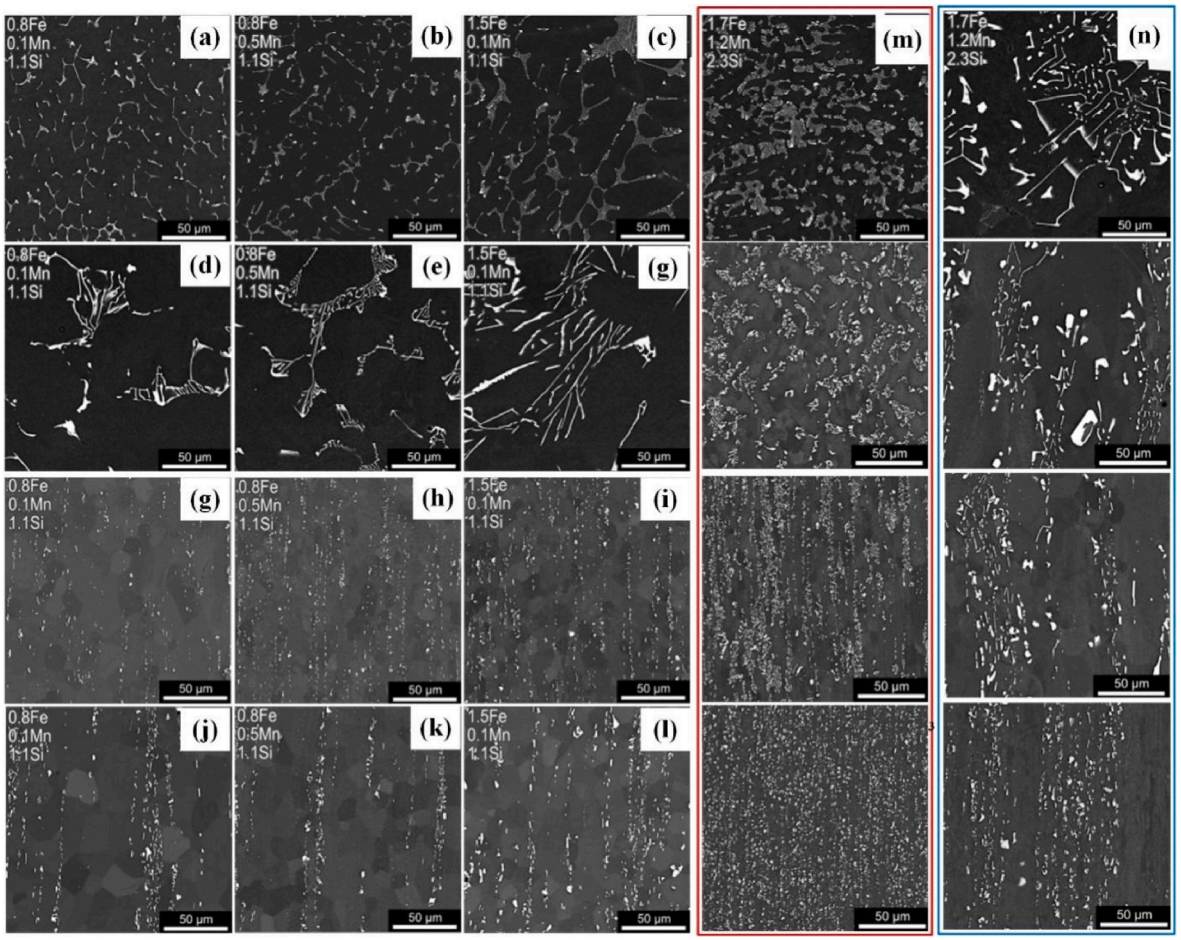

Fig. 8. BSE micrographs of alloys with different Fe and Mn elemental contents during fast (a–c) and slow (d–f) cooling; (g–l) represent BSE micrographs of the alloys after (a–f) T4 treatments, respectively; BSE micrographs of alloy 1.7Fe1.2Mn2.3Si during rolling at fast (m) and slow (n) cooling rates [113].

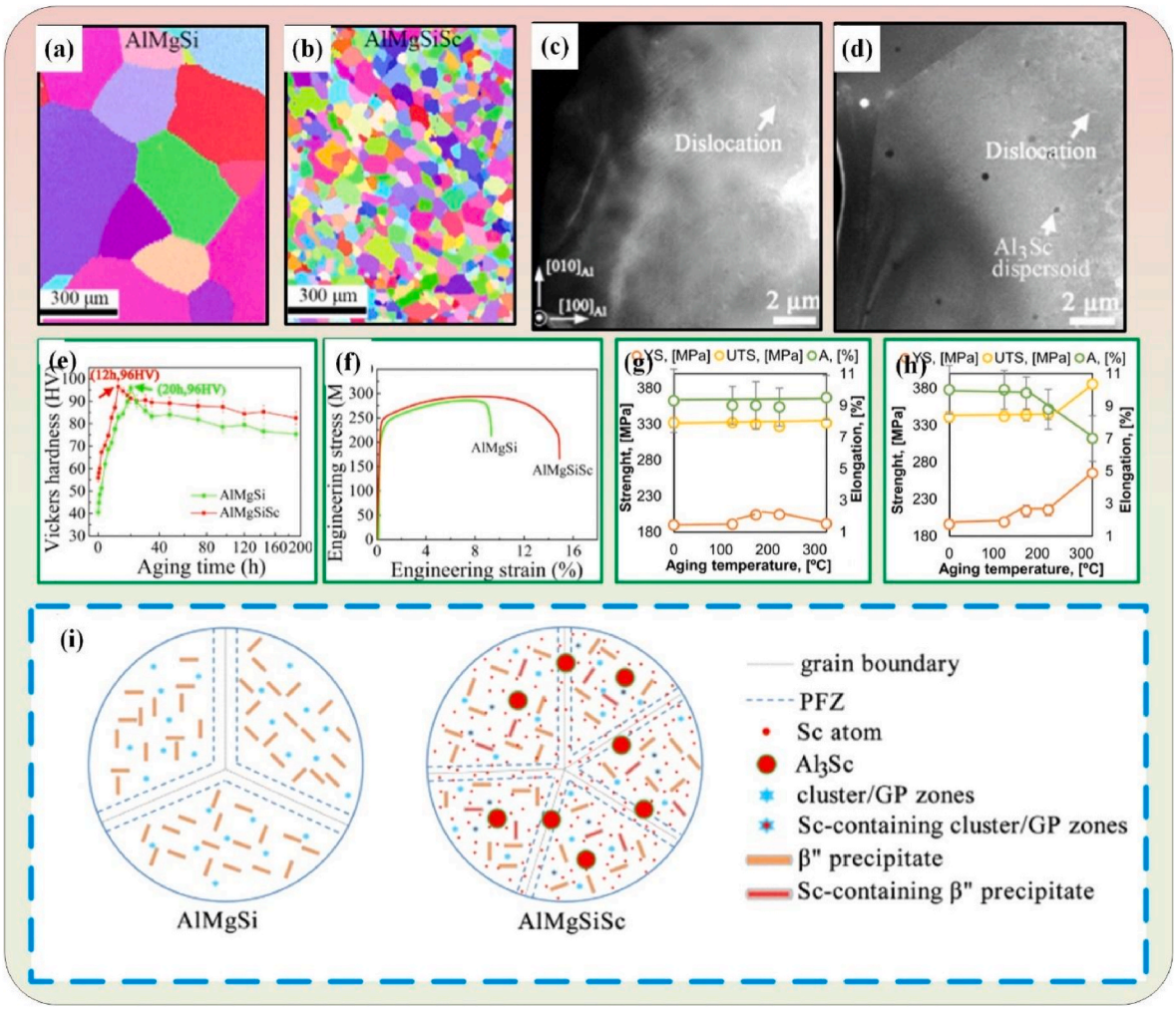

Fig. 9. Grain microstructures of AlMgSi (a) and AlMgSiSc (b) after solid solution treatment; microstructures of AlMgSi (c) and AlMgSiSc (d) samples in the quenched state; age-hardening curves (e) and stress-strain curves (f) at 170 °C [121]; properties of Al–Mg–Si–Mn alloys with 1.0 wt% Sc (g) and 2.0 wt% Sc (h) at different aging temperatures [126]; (i) the microstructures of AlMgSi and AlMgSiSc alloys [121].

the covalent radius of La and Ce are very small and have the same covalent bond structure. Therefore, it is easy to form atomic clusters in the lattice, which leads to the occurrence of co-precipitation, bringing about the raising of the density of surrounding dislocations. In brief, the addition of rare earth elements plays an obvious role in grain refinement, and the different precipitates or dispersion phases formed by different elements produce various degrees of effect on the properties. Especially, Sc not only reduces the PFZ and promotes the formation of the GP zone, but also forms precipitates Al_3Sc as a reinforcing phase and thus leads to the improvement in the properties of the alloys.

3.5. The influence of other elements

In addition to the above elements, trace elements Cr and Zr can also produce an obvious effect on the properties and microstructure of aluminum alloys [124,126,134,135]. Several studies have shown that Zr, similarly to Sc, also promotes the formation of $L1_2$-structured precipitates and generates high-temperature-resistant nanoscale precipitates in the matrix, effectively inhibiting grain growth through the Zener pinning mechanism [135–139]. When Zr and Sc are added at the same time, it not only leads to a significant increase in strength, but also improves creep resistance at high temperatures, so the cost can be reduced by partially substituting Zr to reduce the addition of Sc in the alloying process [124,140]. Zhang et al. [141] found that introducing 0.08 wt% of Zr element to AA6022 resulted in grain refinement and reduced macro-segregation, increasing the YS of alloy after T6 heat treatment by 5.3% and its EL as-cast by 2.7%. Wang et al. [142] found that the addition of 0.07 wt% Cr to AA6061 facilitated the formation of the $Al_{45}Cr_7$ phase as a heterogeneous nucleation sites for α-Al, which improved the microstructure and improved the YS, UTS, and EL at break of the T6 heat-treated alloy from 292 MPa, 327 MPa, and 15% to 301 MPa, 338 MPa and 18%, respectively. The Al_7Cr and Al_3Zr intermetallic phases, which serve as barriers to dislocation movement and boost the alloy's strength, are formed when Cr and Zr are added to the alloy. But Al_3Zr and Al_7Cr are coarse and brittle, which results in reducing tensile strength and EL at break [124]. In particular, Al_7Cr intermetallic compounds can also be observed in alloys with as little as 0.2 wt% Cr added, which significantly impairs the tensile and fracture strength. The coarse Al_3Zr slightly reduces the alloy EL, but when a little Sc is added, it changes the morphology of the Al_3Zr intermetallic compounds and eliminates the negative effect of coarse Al_3Zr, resulting in an increase in the toughening effect of the alloy [123]. It can be seen that the intermediate phase formed by the addition of trace elements Cr and Zr not only inhibits grain growth but also hinders the movement of dislocation lines, which leads to the enhancement of strength. However, both of them form a coarse and brittle intermediate phase, and even produce a sludge phase, which leads to the sacrifices of toughness.

The addition of Ag will be involved in the formation of clusters, which can be used as nucleation sites for subsequent precipitates to promote the precipitation of smaller and denser clusters and

precipitated phases during aging, thus enhancing the precipitation hardening response of the alloy [143]. Some studies have shown that alloys with Ag addition exhibit better mechanical properties due to the denser precipitation phases [143–145]. In addition, Marioara et al. [146] investigated the compositional changes of β′ in the alloy by HAADF-STEM characterization technique and found that the addition of Ag changed the crystal structure of β′ as well as its chemical composition from Mg_9Si_5 to $Mg_3Si_2Al_3Ag$. This is due to the fact that Ag can enter the β′ phase to take the place of Si atoms and polarize at the interface of many metastable phase (GP zone, β", β'/β′Ag), leading to the formation of β′Ag phases after over-ageing [147–149]. Therefore, the coexistence of several metastable precipitation phases appears in over-aged Ag-containing aluminum alloys. It is worth noting that Ag can enhance the pre-ageing effect of Al–Mg–Si alloys while inhibit the negative effects of natural ageing, which has great significance for automotive applications that require rapid hardening during the baking process [150,151]. Similar to the addition of Ag, the addition of Zn also significantly contributes to the intensification of age-hardening and the simultaneous presence of various precipitates [152–155]. Cai et al. [156] and Guo et al. [157] found that the generated Mg–Zn cluster after the introduction of Zn can be used as the nucleation particle of Mg–Si precipitation phase (such as GP region and β" phase), leading to the formation of a high-density Mg–Si precipitation phase and the enhancement of the aging hardening response ability of AI-Mg-Si alloy in the early artificial aging. Therefore, the hardness of the alloy increased significantly at the beginning of aging. Xu et al. [152] reported that the more finely dispersed β" precipitated phases produced at low levels of Zn resulted in higher strength and plasticity, but higher Zn contents (>2 wt%) resulted in a slight reduction in the strength of the alloys due to the reduction of the density of the precipitated phases. Apart from the effect of Zn addition on the precipitation and mechanical properties of Al–Mg–Si alloys, great attention has also been paid to its effect on improving the corrosion resistance of the alloys. Typically, the Zn addition alone can result in a wider PFZ, leading to an adverse effect on the corrosion resistance of the alloy [158–160]. IGC is very likely to occur at low Zn levels, and high Zn levels increase the tendency to stress corrosion. Nevertheless, Bartawi et al. [161] reported that the Zn element in alloys containing Cu elements reduced the IGC sensitivity of the alloy. Especially, the improvement of the corrosion resistance of the alloy was particularly obvious when the two elements had a similar content. The reason is that whether Zn is in the grain boundary or inside the crystal, and the potential difference of each part (matrix, grain boundary and PFZ) can be cleverly adjusted by adjusting the electrochemical potential. On the other hand, the Zn-rich film generated at the grain boundary reduces the catalytic effect of Cu element generated Cu-rich film on IGC due to the presence of Zn element [104,106,162]. Therefore, the introduction of Zn to Al–Mg–Si alloys containing Cu elements can improve the mechanical properties and bring about a more corrosion-resistant effect, which will extend the application of the alloys and facilitate longer service life under complex service conditions. In addition, the optimal strengthening effect can be achieved by controlling the element content and the coupling between different elements to achieve more excellent performance.

4. The effect of nanoparticles on microstructure of aluminum alloys

After alloying, although the properties of aluminum alloys can be improved, the strengthening effect is often very limited [163,164], the complex alloying system inevitably leads to the high cost of the material, and the addition of too many combined elements will make the precipitation phase as well as the precipitation order complex, At the same time, the high elemental content will lead to the generation of a coarse second phase and element-enriched segregation during solidification owing to the restricted solid solubility of various elements in aluminum [147,165,166], as well as certain adverse effects on the performance and use of the alloy [167]. These disadvantages make it difficult for pure alloying to meet the needs of aluminum alloys to replace steel as the main choice for new energy vehicles. However, nanoparticles as a new type of alloy reinforcing materials, not only have low raw material price, high elasticity modulus, oxidation and wear resistance, but also have a significant impact on improving grain boundaries to eliminate the negative effects of alloys in the process [168–170].

4.1. The effect of nanoparticles on solidification behaviors

By manipulating the microstructure of alloys, it is possible to improve mechanical performance and attain a balance between strength and ductility. The as-cast microstructure is influenced by solidification kinetics, whereas nanoparticles with an excellent crystal match to the matrix and high temperature stability (e.g. TiC, TiB_2) [171] present a major impact during the solidification process. There are few studies about the effect of nanoparticles on the solidification behavior of Al–Mg–Si alloys. The aluminum alloys have greater similarity in the solidification process, where α-Al is first precipitated and then other eutectic phases are precipitated, and the composition of the precipitated eutectic phases is closely related to the elements in their systems, but the precipitation process is almost the same. Researchers obtained the solidification curves of aluminum alloys by adding particles to different aluminum alloys [172–175], as shown in Fig. 10. The addition of nanoparticle significantly changed the solidification path of aluminum alloys and shifted the nucleation temperature of manipulated aluminum alloys upward to higher temperatures compared to the alloy without nanoparticles, suggesting that the introduction of the particles reduces the nucleation supercooling, promotes heterogeneous nucleation of α-Al, and increases the nucleation rate. According to the calculation of nucleation subcooling (ΔT_n) proposed by Turnbull [176]:

$$\Delta T_n = \frac{C_e}{\Delta S_v}\delta^2 \tag{2}$$

where C_e, ΔS_v and δ denote the elasticity coefficient, entropy per unit volume of phase transition and lattice mismatch, respectively. Nanoparticles have a good match with the matrix and can also be used as the sites of heterogeneous nucleation, thus promoting the nucleation of the primary phase and the eutectic phase and increasing the nucleation temperature of the primary phase as well as the transition temperature of the eutectic phase. The undercooling required for nucleation is reduced after adding the nanoparticles, which will be beneficial to the reduction of grain size. Liu et al. [177] and Geng et al. [178] manipulated 6061 aluminum alloys with dual-phase nano-TiC-TiB_2 and nano--TiC_p particles, respectively. The results showed that the as-cast microstructure was refined after the addition of nanoparticles (Fig. 11 (a_1-a_4)). By comparison, although 0.5 wt% of nanoparticles were added to the alloy in both works, the alloy reinforced with dual-phase nanoparticles possessed a superior refinement effect (52% refinement). This is due to the TiC–TiB_2 with dual scales (Fig. 11(b)), the larger particles will be preferentially excited as the substrate for heterogeneous nucleation of α-Al grains at a smaller undercooling [179], compared to a single nanoparticle, there will be more grain nucleation during solidification. Although larger particles provide a large number of potential heterogeneous nucleation sites, both heterogeneous nucleation and grain growth should be considered to achieve effective grain refinement. Previous studies have shown that only a very small number of nanoparticles can serve as the sites of heterogeneous nucleation [180,181], which implies that the remaining nanoparticles will either be captured by the solid-liquid interface or continue to exist in the liquid phase. However, due to the generally poor wettability of nanoparticles with Al, the bulk of nanoparticles are forced to the front of the dendrimer's solid-liquid interface to form a particles layer, while only a little portion are ingested by the interface and dispersed throughout the grain [182,183]. This physical limitation leads to the non-release of latent heat

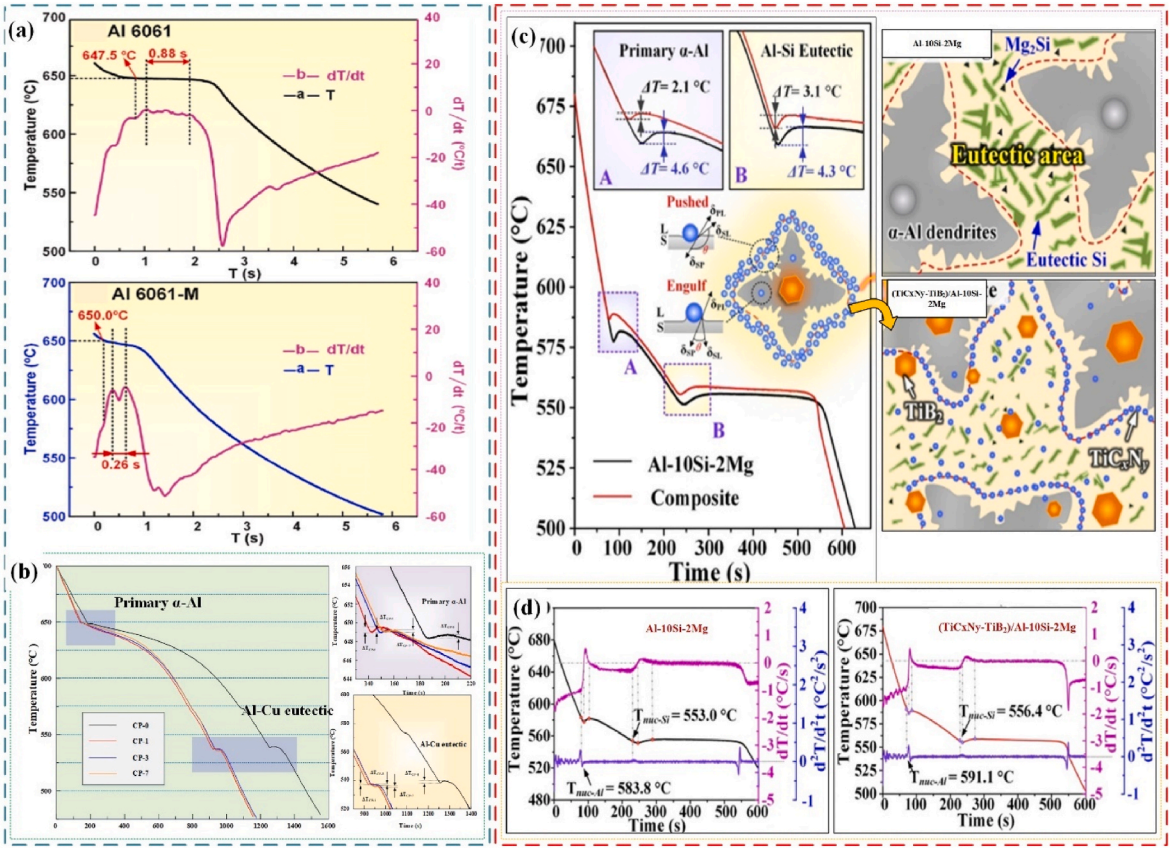

Fig. 10. The cooling curves of 6061 alloy (a), Al–Cu (b) and Al–10Si–2Mg (c); (d) first and second derivatives of the cooling curves in (d) [174,175,177].

when crystallizing as well as inhibiting atomic diffusion, which effectively prevents the rapid coarsening of α-Al dendrites (Fig. 11(c)). Nanoparticles as an efficient grain refiner [184–186], its effect is also reflected in the inhibition of grain growth during solidification and can inhibit the formation of dendrite arm, inducing the formation of equiaxed grains. Chen et al. [187] investigated the effect of TiC on the solidification microstructure of AA6063 alloys, they demonstrated that the manipulation of particles aided in the progressive release of latent heat, enhanced melt fluidity during casting and reduced thermal fractures, meanwhile, the presence of particles led to grain growth restriction, weakened the length of the dendritic grain arms and promoted the development of the grains toward spherical or equiaxed grains (Fig. 11 (d_1-d_4)). In addition, the content of nanoparticles also has a certain influence on the grain refinement effect. Ma et al. [175] reported the solidification microstructure Al–Cu alloys with varying amounts of in-situ TiC–TiB_2 particles. They found that the average grain sizes were refined by 37%, 58%, and 51% with the content of 0.1 wt%, 0.3 wt%, and 0 wt% of particles, respectively, as compared to the alloys without nanoparticles addition (Fig. 11(e_1-e_4)). Apparently, the best refining effect of particle addition occurs at 0.3 wt%, which is because high content particle addition leads to the difficulty in dispersion and local agglomeration of particles [188] and then hinders the grain refinement. As mentioned above, the regulation of solidification microstructure by nanoparticles is carried out through the particles as heterogeneous nucleation sites to promote the heterogeneous nucleation of α-Al as well as particles wrapped around the solid-liquid interface to impede dendrites growth. The grain size has also a certain effect on the transformation of dendrites to equiaxed grains during the process of solidification. However, the refinement effect will decrease when a large number of particles are difficult to disperse and agglomerate.

4.2. The influence of nanoparticles on segregation behaviors

In the process of alloy solidification, segregation behavior may occur due to the interaction between solute discharge and solute diffusion in solid-liquid phase. According to different scales, composition segregation can be divided into microsegregation and macrosegregation. Microsegregation refers to the uneven distribution of solute element between dendrites or the uneven chemical composition inside a grain during solidification. The macrosegregation is the composition difference at the overall scale of the solidified casting, and the alloy concentration in different parts of the casting changes significantly [189]. In the alloying process, the excessive introduction of elements leads to the coarsening of intermetallic compounds, which exacerbates the macroscopic segregation [190]. Due to the uneven distribution of alloying elements within the alloy, it can lead to a decrease in the strength, toughness, wear resistance and other performance indicators of alloys. This can not only affect the service life of the product, but also lead to safety problems. Especially for key components used in the automotive field, the presence of alloying element segregation may lead to premature fatigue or fracture of the components, and may even lead to major accidents in serious cases. In addition, TRC, as an effective means of producing aluminum alloy sheets from the melt, is susceptible to segregation due to its inherent characteristics, which leads to deterioration of properties [191–193]. However, heat treatment as we know it only significantly improves microscopic segregation, and there is still a high level of macroscopic segregation (central segregation) in plates prepared by the TRC process [194]. Previous studies have shown different external physical field effects have an obvious improvement on the macroscopic segregation in alloys with low alloying element content [195,196], whereas the improvement effect is limited for aluminum alloys with a high solute content [152]. Nanoparticles, as effective grain refiners [197] have outstanding effects on microstructure refinement

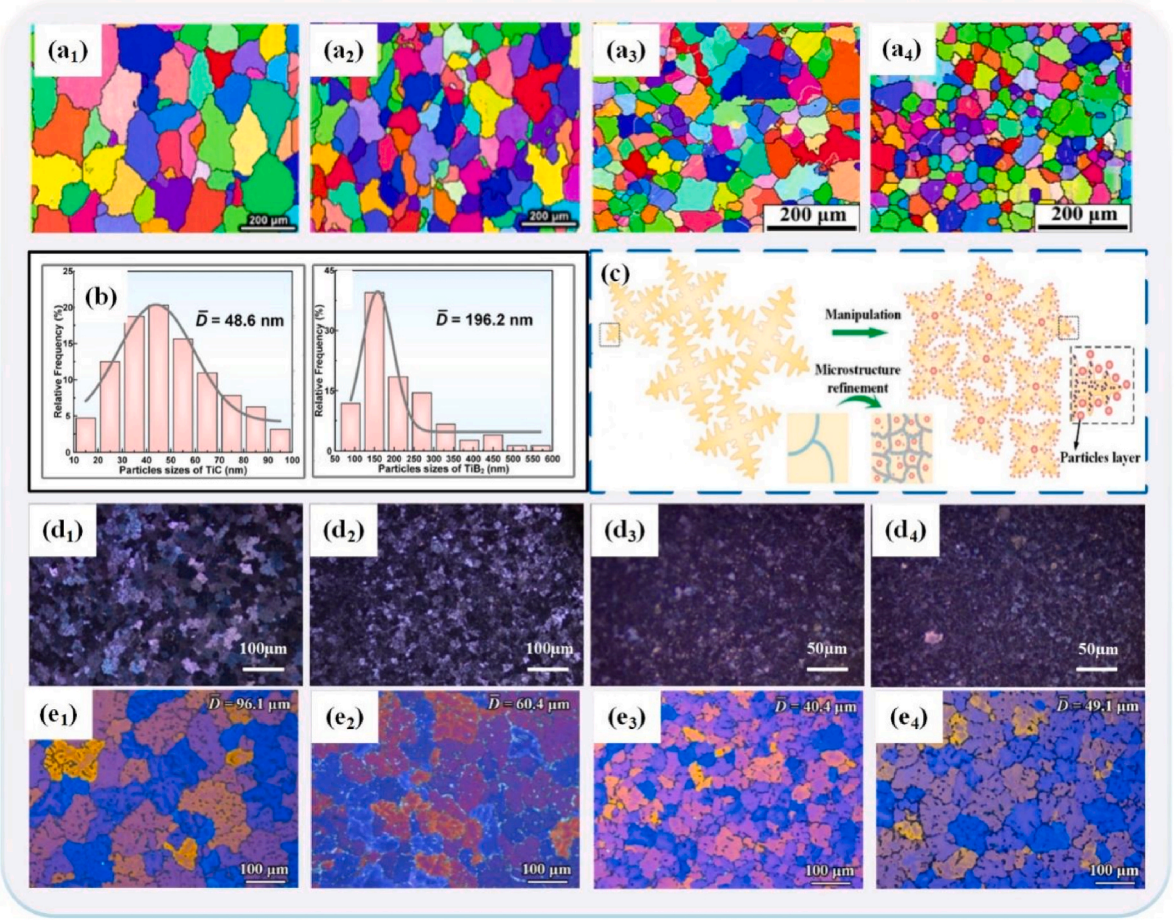

Fig. 11. (a_1-a_4) the EBSD images of AA6061 after adding 0,0.5 wt% TiC–TiB_2, 0.5 wt% TiC_p and 1.0 wt% TiC_p, respectively [177,178]; (b) particle size distribution of TiC and TiB_2 [177]; (c) the mechanism of grain refinement by nanoparticles [175]; (d_1-d_4) the polarized light microstructures of AA 6063 after addition of 0, 0.5, 1 and 2 vol% TiC, respectively [187]; (e_1-e_4) the as-cast organization of alloys after addition of 0.0, 0.1, 0.3 and 0.7 wt% TiC–TiB_2 particles, respectively [175].

and improvement of segregation. It was shown that the addition of TiC led to an increase in the coarsening of the secondary dendritic arms which in turn diluted the composition of the liquid phase and reduced microscopic segregation in the aluminum alloys [198]. For macroscopic segregation, Wang et al. [199] found that TiC particles not only refined the strip grain into equiaxial grains, but also successfully controlled the aggregation of solutes to the central region by impeding the growth of dendrites, thereby eliminating the central segregation zone (Fig. 12(a)). Another study showed [200] that the refinement of the α-Al(Mn, Fe)Si second phase in Al–Mn–Si strips after TiC–TiB_2 particle manipulation (Fig. 12(b_1, b_2)). At the same time, quite a little refined grains effectively divided the alloy melt based on the promotion of nanoparticles on the nucleation of α-Al, which significantly suppressed the elemental enrichment to the central region to achieve the elimination of segregation (Fig. 12(c and d)). As shown in Fig. 12(e and f), Liu et al. [191] added 0.5 wt% TiC particles to the Al–5Cu alloys and found that the segregation bands disappeared and the Cu-rich regions distributed between grains or dendrites became finer simultaneously (i.e., a more homogeneous distribution of Cu elements). According to the mechanism of central segregation proposed by Lv et al. [201], the solute will be enriched at the dendrite tip for the alloy with solute distribution coefficient $k < 1$. With the solidification and dendrite growth, the solute in the liquid phase is enriched, these bring about arising center segregation after solidification. Whereas, nanoparticles accelerate the nucleation of α-Al grains in melts and the grains produced during the solidification process are similar to equiaxed grains [202,203], these fine grains play a key role in impeding the further growth of dendrites and the segregation of solutes to the center (Fig. 12(g)). In addition, the particles promote grains nucleation and the increase in grain boundaries, impeding the flow of the solute-rich liquid phase to the center caused by external forces during the rolling process, thus eliminating the segregation zone. It can be seen that nanoparticles have a significant influence on the diffusion and distribution of solutes in aluminum alloys by regulating the microstructure, which in turn improves the segregation behaviors in the alloy and enhances the applicability of the alloy.

4.3. The impact of nanoparticles on the recrystallized microstructure

It is well known that the 6000 series aluminum alloys have excellent machinability, and the recrystallized microstructure greatly affects the grain size, morphology and other factors, which will significant effect on the performance of deformed aluminum alloys [204–206]. During material deformation, nanoparticles help to promote dynamic recrystallization [207], it is that particles promote the occurrence of recrystallization phenomena and particles inhibit the phenomenon of recrystallized grain growth. The currently suggested mechanism is mainly that the recrystallization drive is improved by enhancing the particles to be regulated by particle-stimulated nucleation (PSN) [208,209] for coarse enhancements larger than 1 μm and for fine nanoparticles hindering dislocation motion, the recrystallization drive can be obtained by promoting dislocation proliferation and pinning sub-grain boundary migration. The nature of recrystallization is the process of making Low-angle grain boundaries (LAGBs) form High angle grain boundaries (HAGBs) through the growth of sub-grains, at which time the sub-grain boundaries are pinned by nanoparticles and the growth of recrystallized grains will be hindered (Fig. 13(a)) [210]. Liu et al. [206]

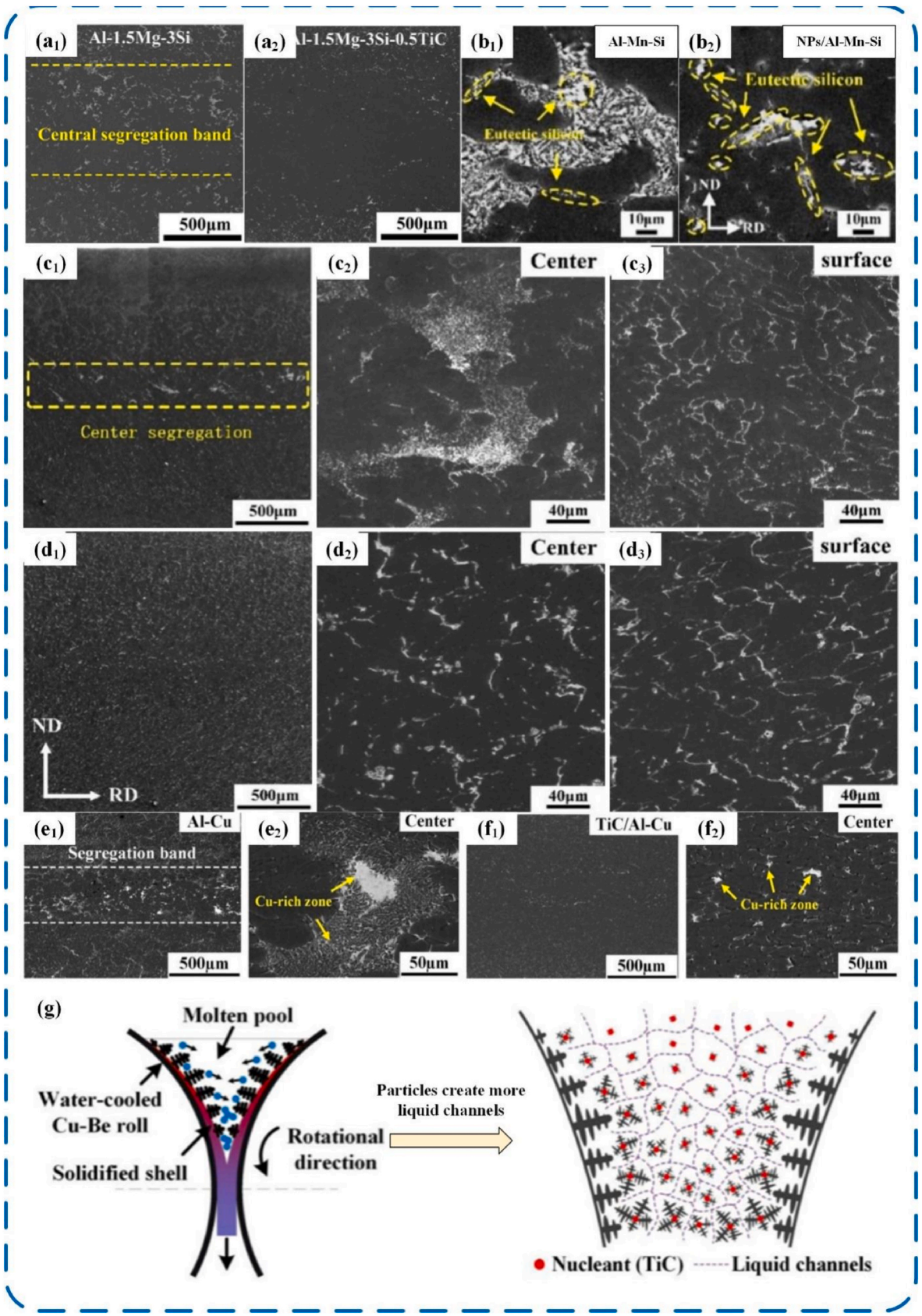

Fig. 12. SEM (a_1, a_2) and EBSD (b_1, b_2) images of TRC strips [199]; EDS maps of the second phase before (b_1) and after the manipulation of nanoparticles (b_2); SEMs of TRC Al–Mn–Si (c) and NP/Al–Mn–Si strips (d) [200]; BSE maps of Al–Cu (e_1, e_2) and TiC/Al–Cu stripes (f_1, f_2); (g) the mechanism of nanoparticles to inhibit the segregation during the TRC process [191].

investigated the grain size, recrystallization rate and substructure ratios of the molten core region after nanoparticle-enhanced friction stir welding (FSW). This study found a commonality: the phenomenon of increased recrystallization ratio and recrystallized grain refinement is appear after nanoparticle enhancement, which ultimately leaded to the transformation of the microstructures into fine isotropic crystals (Fig. 13 (b and c)). Meanwhile, Geng et al. [211] found the equal amounts of TiC and TiB_2 had almost the same refinement effect on the recrystallized tissues (Fig. 14(a)). Based on this phenomenon, Liu et al. [212] further investigated the effect dual-phase nanoparticles TiC–TiB_2 and single-phase nanoparticles TiC on recrystallization behavior. It was found that the recrystallization grain refinement rates after the addition of single-phase TiC particles as well as dual-phase TiC–TiB_2 particles were 6.7% and 32.0%, respectively, while the percentage of recrystallization fluctuates little, as shown in Fig. 14(b). After computer analysis, this is due to the fact that dual-phase nanoparticles have a greater retarding force for pinning at grain boundaries, suggesting that dual-phase nanoparticles have a better ability to refine recrystallized grains compared to single-phase particles. At the same time, the interfacial bonding between TiB_2 and Al matrix is stable, so even if the size of TiB_2 particles can not reach the range of coarse particles, there will still be the possibility of initiating PSN, which is beneficial to promote nucleation more efficiently during the recrystallization process. It is worth noting that not all nanoparticles have a positive effect on

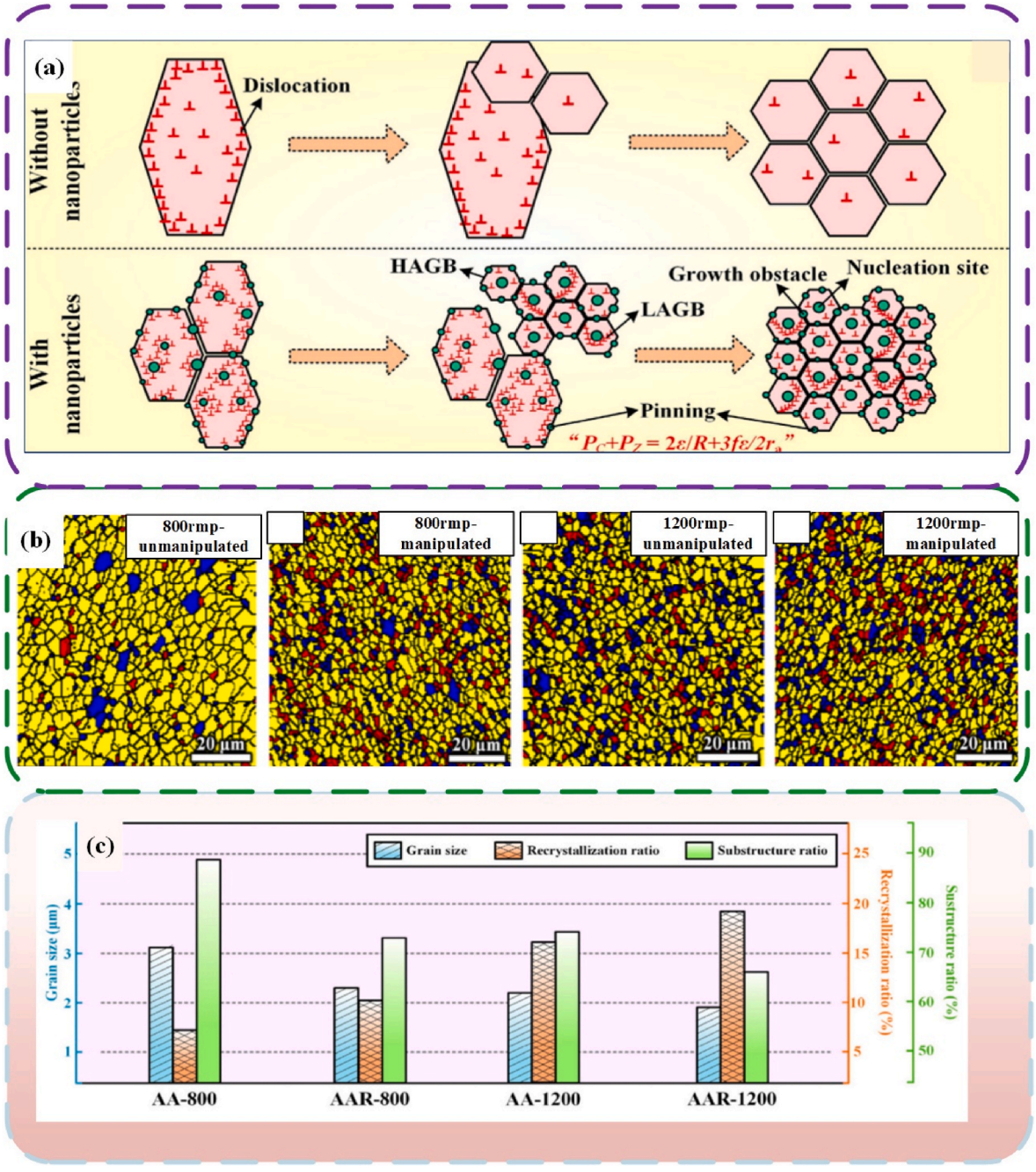

Fig. 13. (a) Mechanism of nanoparticles for recrystallization [212]; (b) recrystallization diagram of added particles at different rotational speeds, (c) trend diagram of recrystallized microstructures changes before and after particle enhancement [206]. **Note:** The red, yellow, and blue regions represent the deformation, sub-structure, and recrystallization of grains, respectively. (For interpretation of the references to colour in this figure legend, the reader is referred to the Web version of this article.)

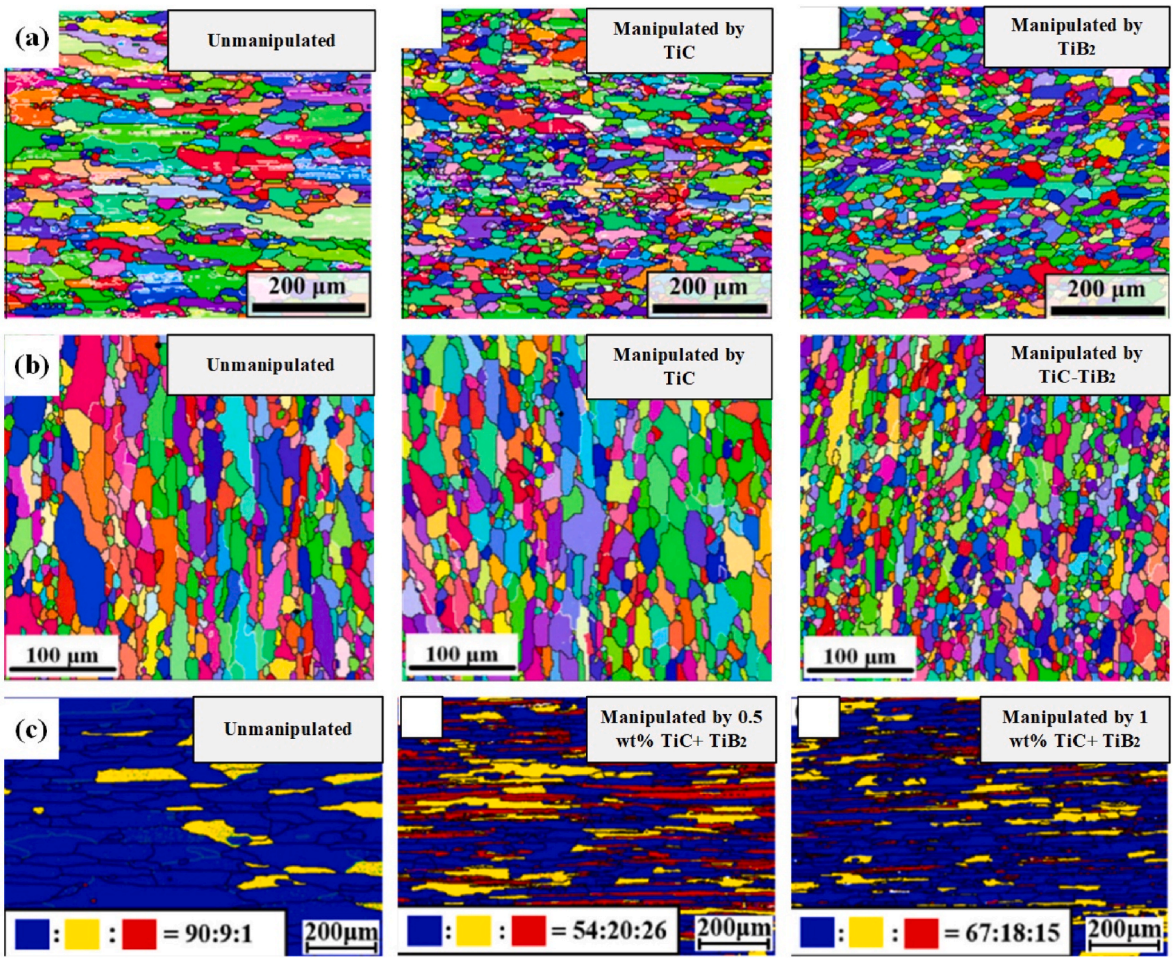

Fig. 14. (a) Recrystallized microstructures of 6061 obtained by treatment in TiC and TiB_2 [211]; (b) recrystallized microstructures obtained by single-phase and two-phase nanoparticle manipulated [212]; (c) recrystallization of nanoparticle manipulated 2055 alloy [213].

recrystallization. For example, Wang et al. [213] found that the recrystallization rates of aluminum alloys were reduced to varying degrees with the addition of 0.5 wt and 1.0 wt% TiC/TiB_2 particles (by 36% and 23%, respectively, as shown in Fig. 14(c). This phenomenon is linked to the agglomeration of particles in alloy, on the one hand, TiC/TiB_2 particles inhibit the migration of HAGBs by aggregating at grain boundaries, and on the other hand, the particles are pinned to dislocations and LAGBs, which prevents the subgrain boundaries from increasing the grain orientation by absorbing dislocations, and restricts the rotation and growth of the subgrains as well as the conversion of LAGBs into HAGBs to become recrystallized grains.

In addition, the content of nanoparticles affects the recrystallization process of aluminum alloys and the regulation of recrystallized grain size distribution to a certain extent. For example, Chen et al. [214] prepared reinforced alloys with different contents of TiB_2 particles and conducted a hot-extruded experiment at 450 °C. Then, the evolution of the dynamic recrystallized microstructures of the aluminum alloys by the addition of nanoparticles was analyzed using the EBSD technique. The experimental results show that the orientation difference between adjacent grains in the deformed alloy decreases continuously with the gradual increase of the nanoparticle content, and the LAGBs are continuously transformed into HAGBs increasing the quantity of HAGBs (Fig. 15(b)), which suggests that the increase of the particle content exacerbates the limitation on the dynamic recovery process and promotes the dynamic recrystallization. Geng et al. [178] reported that the number of coarse grains along the rolling direction was significantly reduced after nanoparticle manipulation, while the recrystallization rate was increased as well as the recrystallized grain size was refined with the increase of the nano-TiC_p content, and the grain size distributions of 0.5 wt% TiC_p/Al–Mg–Si composites and 1.0 wt% TiC_p/Al–Mg–Si composites have a narrower grain size distribution (Fig. 15(d)). The superior refinement of 1.0 wt% TiC_p nanoparticles compared to that of 0.5 wt% addition is due to the inherently finer as-cast microstructures in this treatment case. As mentioned in section 4.1, the increase of nanoparticle content in a certain range has a promoting effect on the refinement of the as-cast microstructures, leading to grain refinement after deformation, while the recrystallized nucleation can be formed at the grain boundaries, which promotes their recrystallized nucleation after deformation [215], at the same time, the increase of nanoparticle content may exacerbate the induction of the Zener pinning effect on grain boundaries to inhibit recrystallized grains growth (Fig. 15(e)). However, excessive particle content can easily lead to particle clustering [216,217]. Although the larger particle clusters can be used as nucleation sites for recrystallized grains through the PSN to promote recrystallization force [208,209,218,219], related studies [220] have suggested that the particle clusters can easily form a confined structure at the grain boundaries which is detrimental to recrystallization. Furthermore, when the ratio of the volume fraction of particles to their diameter is too large, recrystallization is usually impeded, excessive nanoparticles lead to delayed recrystallization nucleation and hysteresis effect on subsequent recrystallization by slowing down the motion of LAGBs and HAGBs. Therefore, based on the above study, appropriate reinforcing particles can be added to 6000 series aluminum alloys to manipulate the recrystallization microstructures. At the same time, although the increase in particle content

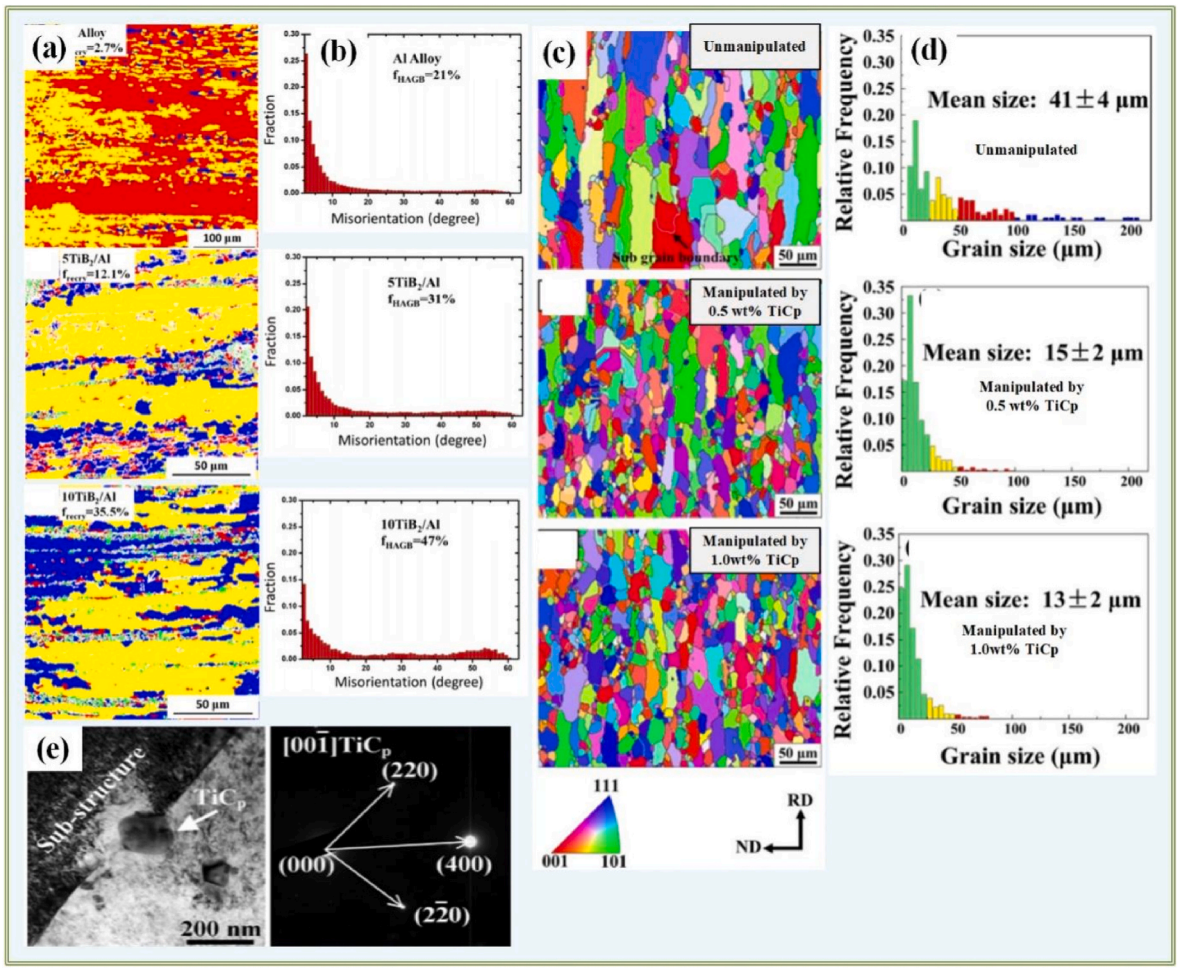

Fig. 15. (a) Distribution of deformed grains (red), substructured grains (yellow) and recrystallized grains (blue) in the alloy with different particle contents; (b) comparison of the volume fractions of HAGBs with different particle contents [214]; EBSD microstructures of 6061 (c) and corresponding statistics of grain-size distributions (d); (e) TiC_p particles pinned to the subgrain boundaries [178]. (For interpretation of the references to colour in this figure legend, the reader is referred to the Web version of this article.)

is conducive to the conversion of LAGB into HAGB to become recrystallized grains and more effective pinning of grain boundaries to further refine the recrystallization microstructures, in view of the adverse effects of agglomeration phenomenon on the recrystallization caused by the excessive particle content, the amount of additive needs to be strictly controlled in the actual control process.

4.4. The effect of nanoparticles on the heat treatment processes

As mentioned in section 3, Al–Mg–Si alloys, as heat-treatable Al alloys, the alloying elements not only promote the changes in grain size and morphology, but also produce precipitation phases after certain heat treatments [165,221]. A large number of researchers have studied nanoparticle-reinforced aluminum alloys and found that nanoparticles not only refine the α-Al and eutectic phases, but also have a significant impact on the size and distribution of the second phase during the heat treatment process [175,222]. Liu et al. [177] found that after TiC–TiB_2 enhancement, the precipitation of GP zone and β″ phase was expedited, and the precipitated Mg_2Si in the alloy was more fine and diffuse (Fig. 16 (a and b)). This is because the production of α-Al grain refinement after particle manipulation is beneficial to the solid solution and uniform diffusion of alloying elements during the heat treatment solid solution process. In addition, due to the existence of thermal stresses at the TiC/Al and TiB_2/Al interfaces, the density of dislocations around the particles is increased (Fig. 16(e and f)), and the high-density dislocations can serve as a base for heterogeneous nucleation and accelerate the nucleation of the precipitation phase as well as a diffusion channel for solute atoms [223], which promotes the formation of clusters and the homogeneous diffusion of elements. In addition, the intensification of nucleation of the second phase lead to a certain limitation of the number of atoms in the clusters (Fig. 16(g)), resulting in an increase in the number of precipitated phases but the growth is inhibited. Geng et al. [178] compared the effect of different contents of nano-TiC_p on the precipitated phases and counted the size of the precipitated phases (Fig. 16(i)), and found that the addition of the particles not only increased the number of the precipitated phases but also promoted the refinement of the precipitated phases. Besides, the number of β″ precipitated phases increased significantly and the refinement effect was more obvious with increasing nanoparticle content. The dislocation density caused by thermal mismatch of particle expansion can be expressed according to the formula [224]:

$$\rho_{CET} = \frac{4V_p \Delta T \Delta C}{b(1-V_p)}\left(\frac{1}{t_1}+\frac{1}{t_2}+\frac{1}{t_3}\right) \tag{3}$$

where, ρ_{CTE} represents the dislocation density, V_p represents the volume fraction of reinforcing particles, ΔT and ΔC represent the temperature difference from room temperature to processing temperature and the coefficient of thermal expansion (CTE) difference between the reinforcement and the substrate, respectively. b is the magnitude of the Burgers vector in Al, t_1, t_2 and t_3 are the three dimensions of the particle,

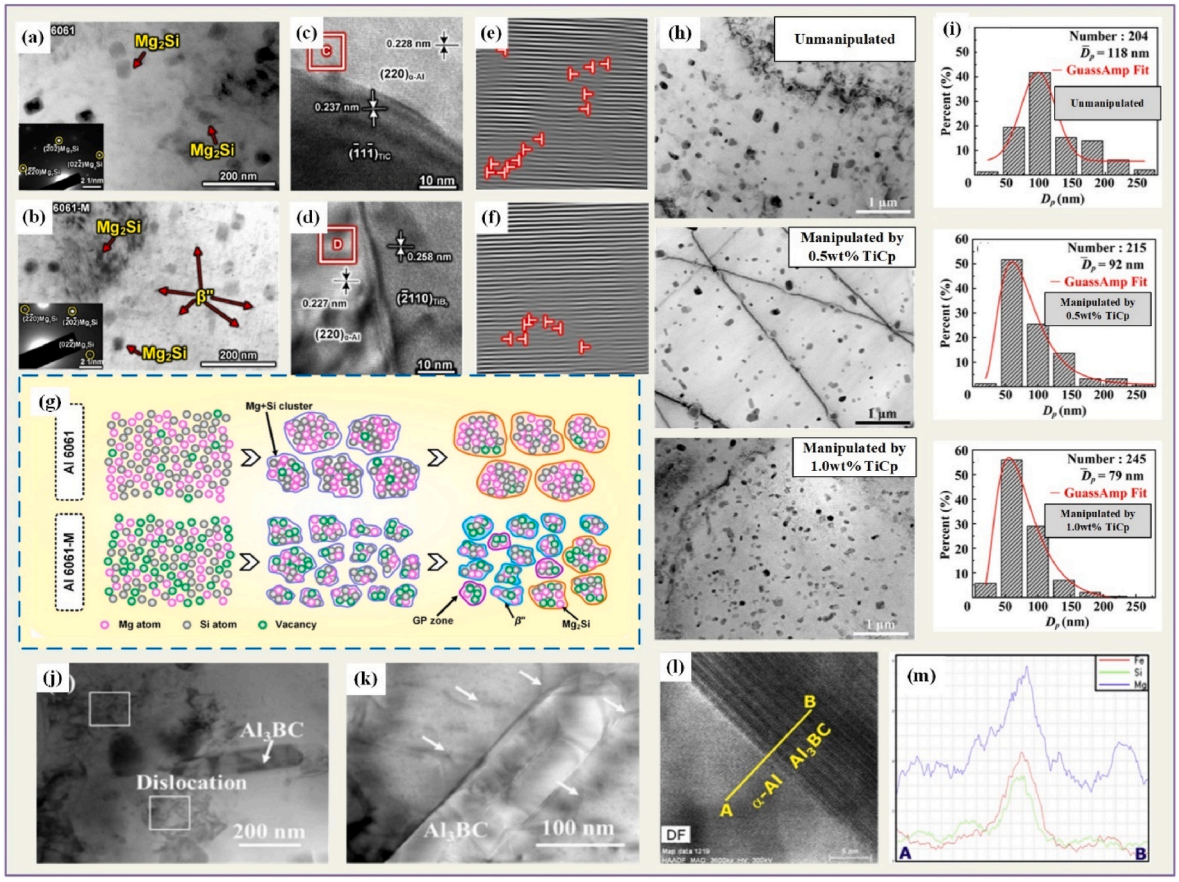

Fig. 16. (a, b) shows the unadded and added particle precipitation phases, respectively; (c, d) HRTEM images of TiC/Al interface and TiB_2/Al interface, respectively; (e, f)) inverse fast-Fourier transform images of areas (c, d), respectively; (g) mechanism of nanoparticles affecting the precipitated phases of Al 6061 [177]; (h) TiC_p particles with different contents in the TEM micrographs of the composites after T6 treatment, (i) statistical plot of the size of the precipitated phase [178]; (j, k) dislocations induced by the introduction of Al_3BC particles in the composites, (l) an ABF image of the Al_3BC/Al interface, (m) the result of the EDS line scanning of the elements along the line shown in image (l) [223].

respectively. From this formula, it can be seen that raising particle content contributes to the improvement of the dislocation density and the production of the β'' phase, which explains that more particle addition in the above experiments enhances the optimization for the precipitation process. At the same time, the second phase precipitated particles produced during the aging period have varying number of defects due to the different CET of various particles [225], which not only explains the different dislocation densities produced by the two particles in Fig. 16(e and f), but also shows all the differences in aging kinetics and time to reach peak aging [226–229]. Zheng et al. [230] reinforced Al–Mg–Si alloys to expedite the dissolution and precipitation of the alloying elements through the addition of TiC nanoparticles and found that the TiC nano-reinforced alloys reached peak aging in a shorter time than that of the matrix alloys, whereas Alfred et al. [226] investigated the aging kinetics of SiC/Al-based composites and found that the composites had a lower concentration of vacancies and an insufficient density of dislocations that required a longer time to reach peak aging compared to the matrix materials. Furthermore, nanoparticles may interact with elements in the alloy to influence the distribution and even reduce the number of precipitated phases during heat treatment [231,232]. Zhao et al. [223] fabricated 15 wt% Al_3BC/6061 Al composites by solid-liquid reaction method and investigated the effect of aging precipitation of the composites. It was shown that Al_3BC particles can effectively shorten the peak aging time to accelerate the aging kinetics of 6061 Al alloys, but in their study, the addition of particles had a dual effect on the generation of precipitated phases in the composites, which includes a positive effect on increasing dislocation density due to the mismatch between particles and matrix, at the same time, the interface combination of particles and matrix also has adverse effects on reducing vacancy concentration and inhibiting the formation of GP region [233]. In addition, the presence of Mg, Si elemental bias at the Al_3BC/Al interface results in the formation of β'' phases (Fig. 16(l and m)), which are precipitated mainly uniformly distributed in the Al_3BC-free region while almost no precipitated phases are observed in the vicinity of the Al_3BC particles. To sum up, nanoparticles can contribute to precipitated phase kinetics during heat treatment through the enhancement of geometrically necessary dislocations induced by thermal mismatches between them and the matrix. Moreover, the thermal mismatch is related to the content and type of the particles and the particles may also react with the alloying elements, leading to a decrease in the content of the precipitated phase.

5. The effect of particles on the properties of 6000 series aluminum alloy

It is worth noting that nanoparticles as excellent reinforcement to aluminum matrix composites (AMC) excellent reinforcement, not only is an excellent modifier to regulate the microstructure of the metal material, more importantly, the microstructure of the change and the particles as the AMC reinforcement will be a certain enhancement of the performance of the alloy, which will be conducive to the development of high-performance aluminum alloys to replace the steel as an important material for the new energy vehicles.

5.1. The effect of nanoparticles on room temperature tensile properties of 6000 series aluminum alloys

To date, TiC and TiB_2 particles are commonly used as reinforcements to improve the properties of alloys through microstructure improvement. For example, Zhen et al. [230] found that the manipulation of nanoparticles facilitates the dissolution of the alloying elements, which brings the high strength as well as the toughness of the composites (Fig. 17(a)). Liu et al. [234] found that the addition of only 0.5 wt% of TiC–TiB_2 nanoparticles increased the YS and UTS of AA6061 sheets by 31.3% and 16.3%, respectively, and furthermore, the YS and UTS of the welded joints were increased by 30.2% and 7.8%, respectively, with the ductility remaining at a high level. The strength of the welded joints was still improved at different levels precisely because the ultra-fine grains resulting from particle enhancement were retained even after post-weld heat treatment. Besides, Liu et al. [235] further systematically investigated and compared the effect of nano-TiC and nano-TiC-TiB_2 on the properties of the alloys, the results show that the materials reinforced by dual-phase nanoparticles exhibited higher strength and toughness, as shown in Fig. 17(b). This is due to the more excellent microstructure of aluminum alloys reinforced with dual-phase nanoparticles. On the other hand, TiC nanoparticles, which are approximately spherical in shape and the hexagonal TiB_2 particles (shown in Fig. 17(c)), TiB_2 particles produces more channels for elemental diffusion during deformation due to its morphological features, which facilitates elemental diffusion to form a finer second phase. At present, it is widely believed that the strengthening mechanism of nanoparticles for room temperature tensile properties is mainly orowan strengthening, fine grain strengthening and

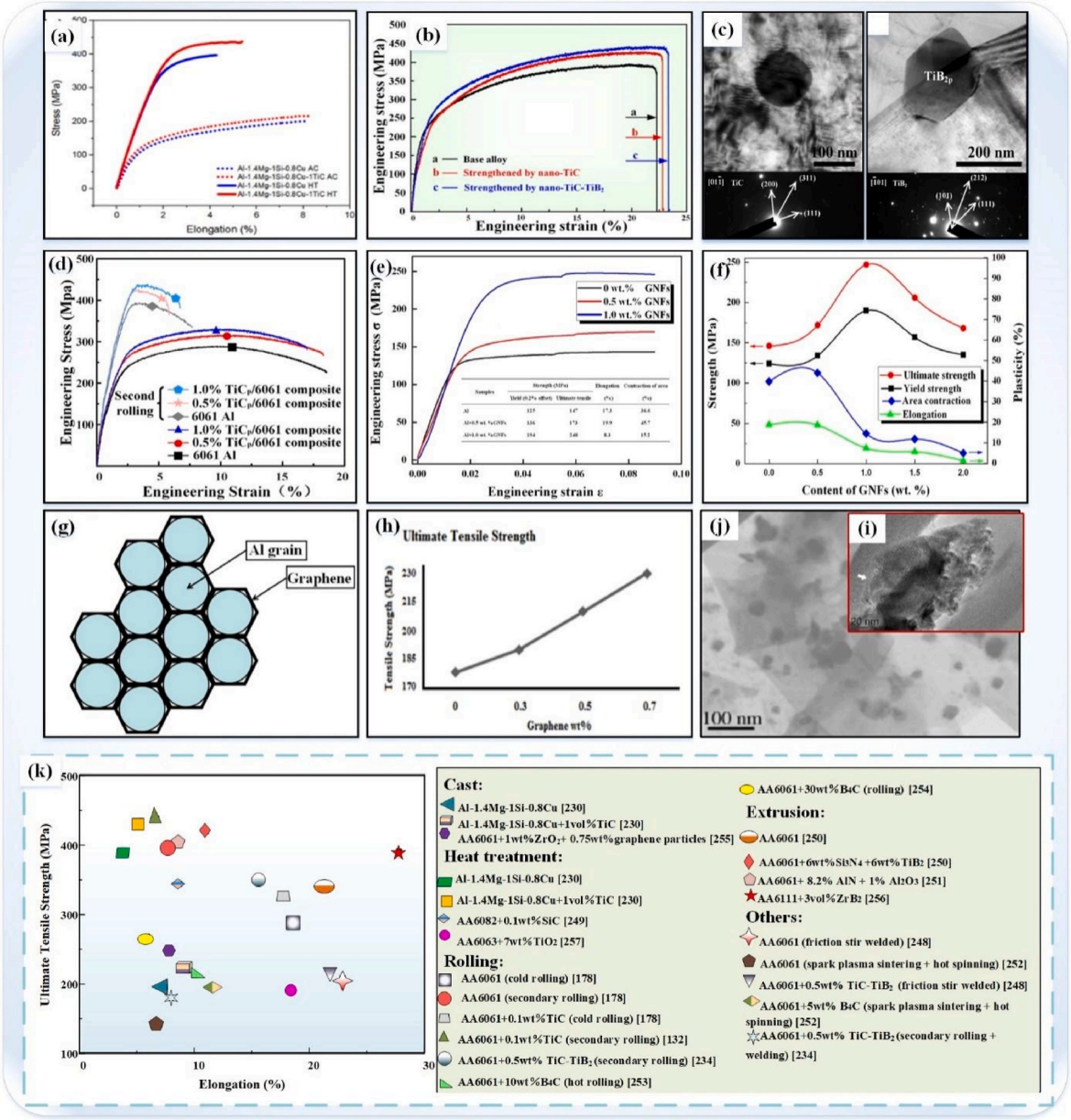

Fig. 17. (a) Stress-strain curves of Al–Mg–Si–Cu and Al–Mg–Si–Cu/TiC [230]; (b) stress-strain curves of alloys with different particle reinforcement [235]; (c) morphology of TiC and TiB_2 particles [247]; (d) engineering stress-strain curves of 6061 aluminum alloy and nano TiC/6061 composites [178]; (e) engineering stress-strain curves and tensile properties of composites reinforced with 0, 0.5, and 1.0 wt% graphene at room temperature, (f) tensile properties of composites as a function of the weight fraction of graphene (0–2.0%) at room temperature, and (g) Interfacial structure in the Al matrix constituted with nanographene [238]; (h) tensile strength of composites with different weight percentages of graphene for samples with constant SiC particle content [244]; (i) HRTEM image of GNS-coated SiC particles, (j) TEM image of SiC particles in composite powder [245]; (k) room temperature tensile properties of various aluminum alloy.

thermal mismatch strengthening caused by dislocations and other defects in the vicinity of reinforcing particles because of the difference in CTE between metal matrix and reinforcing particles. The size of the precipitated phase as well as incremental YS induced by fine grain strengthening can be expressed through the previous relationship between particle and dislocation density [236]:

$$\Delta\sigma_{H-P} = k_y\left(d^{-\frac{1}{2}} - d_0^{-\frac{1}{2}}\right) \tag{4}$$

where, d_0 and d are the average grain size of unreinforced material and reinforced composite, respectively. d can be expressed by Zener equation [237]:

$$d = \frac{4\alpha d_p}{3v_p} \tag{5}$$

where, α is a constant, d_p and v_p are the enhanced phase particle size and volume fraction, respectively. Obviously, when the particle content is increased, not only the thermal mismatch strengthening due to the increase of defect density will be enhanced, but also the effect of fine grain strengthening will be more obvious. Subsequently, Geng et al. [178] prepared TiC/6061 composites with different contents of nanoparticles and found that the addition of nano-TiC improved the strength of alloys under both cold rolling (CR) and secondary rolling (SR) treatment processes, as shown in Fig. 17(d), the improvement in the additions of nano-TiC provided a better strengthening effect, which was precisely due to the enhancement of the effects of the matrix microstructure refinement caused by raising content of the particles and the dislocation defects.

In addition to the above nanoparticles, graphene nanoflake (GNF) also show great potential to reinforce aluminum matrix composites. For example, Li et al. [238] investigated the room-temperature tensile properties of the materials with various contents of GNF, Fig. 17(e, f) display the outcome, which showed that both 0.5 wt% and 1 wt% GNF-aluminum matrix composites exhibited higher YS and UTS compared with that of the composites without GNF, in which YS increased by 8.8% and 55.2%, and UTS increased by 17.7% and 68.7%, respectively. The increase in strength in composites can be explained in three ways. Firstly, GNF in composites not only possesses ultra-high strength, but also disperses homogeneously as a reinforcement of this aluminum matrix material (Figure 17(g)). Furthermore, similar to other nanoparticles [178,234,235,239], GNF can also achieve the reinforcing effect of nanostructures by refining matrix grains. Lastly, nanographene in the Al matrix constituting a clean interface can effectively transfer the loading to graphene. However, the strength and ductility decreased significantly at high GNF content (more than 1 wt%) (Fig. 17(f)), which may be attributed to the loosening of the interfacial bonding in the composites due to the agglomeration of GNFs at the grain boundaries of the matrix, which ultimately leads to the decrease in strength and toughness. Moreover, when the addition of reinforcing particles was further raised, they would be more difficult to uniformly dispersed into the matrix and exacerbate particle agglomeration [240], resulting in performance degradation.

Researchers have suggested that the diffuse distribution of nanoparticles in the matrix is closely associated with the reinforcement of composite properties, but even very low levels of nanoparticles are difficult to disperse uniformly [241,242]. Yar et al. [243] promoted the dispersion of particles by stir casting, but its effect was not significant. Another approach is to promote the dispersion of nanoparticles through the coupling between different particles. The researchers prepared 10% SiC/6061 composites and added different levels of graphene nanoparticles to them [244]. They found that the strength of the composites increased continuously with the increase of graphene content and the tensile strength reached a maximum value of 230 MPa at 0.7 wt% addition. This is attributed to the fact that the SiC particles wrapped by graphene shells reduce the possibility of particle agglomeration in the matrix [245], and the graphene shells that wrap the particles can also hinder the dislocation motion, which suggests that the GNF dispersed in the composites and SiC particles show a synergistic effect in hindering the dislocation motion to increase the toughness of the composites (Figure 17(j)). Similarly, Ding et al. [246] found that the addition of Al_2O_3 particles to Sn–9Zn–1Al_2O_3/6061 composites improved the flowability of the composite brazing material as well as the diffusion of the nanoparticles contributed to the formation of the precursor film, which led to the improvement in the strength of the composite brazed joints. Fig. 17(k) and Table 3 list some properties of the alloy after particle reinforcement, the results show that nanoparticles as a potential reinforcement material, making the properties of particle-reinforced aluminum alloys advantageous in many ways, especially at low-levels of additions where the composites show even better strong and tough properties.

5.2. The improvement of high temperature tensile properties of aluminum alloys by reinforcing particles

New energy vehicle chassis structure and battery shell in the driving process will be subject to complex mechanical and thermal effects, so Al–Mg–Si alloy used as the components of new energy battery shell and chassis are usually required to be still have good mechanical properties

Table 3
Room temperature tensile properties of system 6000 series aluminum alloys after nanoparticle reinforcement.

Alloy	Nanoparticle	Processing method	YS (MPa)	UTS (MPa)	EL (%)
Al-1.4 Mg–1Si-0.8Cu [230]	1 vol% TiC	as-cast	128.7	219.3	9.39
		T6 heat treated	349.5	434.5	5.38
AA6061 [178]	0.1 wt% TiC	cold rolling	275	330	17.9
		secondary rolling	426	438	6.7
AA6061 [234]	0.5 wt% TiC–TiB_2	secondary rolling	302	350	15.3
		secondary rolling + welding	125	180	8.0
AA6061 [248]	0.5 wt% TiC–TiB_2	friction-stir-welded	167	216	21.8
AA6082 [249]	0.1 wt% SiC	T6	161.8	344.21	8.69
AA6061 [250]	6 wt% Si_3N_4 + 6 wt% TiB_2	hot extrusion + T6	353	420	11
AA6061 [251]	8.2% AlN + 1% Al_2O_3	hot extrusion + T6	320	400	806
AA6061 [252]	5 wt% B_4C	spark plasma sintering + hot spinning	143.2	195.2	11.6
AA6061 [253]	10 wt% B_4C	hot rolling	155	213	10
AA6061 [254]	30 wt% B_4C	rolling	180	268	5.9
AA6061 [255]	1 wt% ZrO_2+ 0.75 wt% graphene particles	as-cast	182	250	7.8
Al−1.08% Mg−0.63% Si [244]	10 wt% SiC + 0.7 wt% graphene particles	as-cast	–	270	–
AA6111 [256]	3 vol% ZrB_2	hot extrusion + T6	–	390.7	27.8
AA6063 [257]	7 wt% TiO_2	T4	121	194	18.4
AA6090 [258]	25 vol% SiC	T6	200	541	–

at the temperature of 150 °C. At the same time, the automotive braking system in the braking and operation process near the exhaust system will generate high temperatures, so the study on Al–Mg–Si alloys at high-temperature environment can help to optimize the choice of materials for braking components and exhaust systems, ensuring the efficiency of the parts and the life of the case of replacing the other materials to further realize the new energy vehicle lightweight. Therefore, it is of great significance to study the high temperature performance of Al–Mg–Si alloys.

As we known, the strengthening effect of unstable precipitated phase on the tensile property is weakened under high temperature conditions compared with that at room temperature [259,260]. On the one hand, the softening and loosening of grain boundaries are easy to slide relatively, resulting in the strengthening effect of fine grains almost disappearing, when temperatures rise, additional dislocation slip systems will initiate as a result of thermal activation, which leads to insufficient strength of the alloy during stretching [261]. On the other hand, the movement of the dislocation at high temperature is no longer around the particles but through climbing [262], which reduces the orowan strengthening effect and leads to the weakening of the particle strengthening effect at high temperature. This situation also suggests that the selection of particles to manipulate the alloys must have high-temperature stability to obtain stronger reinforcement efficiency [263,264]. He et al. [265] reported an increase in the strength of composites at different temperatures after reinforcement with thermally stable TiCN ceramic particles (Fig. 18(a)) and they attributed this phenomenon to the pinning of grain boundaries by submicron particles. Li et al. [266] in situ synthesized high mass fraction $MgAlB_{4w}$ whisker reinforced aluminum matrix composites and investigated the tensile properties from 25 °C–300 °C. The results (Fig. 18(b)) showed that the UTS of the alloy reinforced by particles increased by 70% (10 wt% $MgAlB_{4w}$) and 166% (20 wt% $MgAlB_{4w}$) at 200 °C compared with that of the unreinforced alloys, respectivley, with specific values of 170 MPa and 266 MPa. When temperature achieved to 300 °C, there was an increase in the UTS over the unreinforced alloys by 49% (10 wt% $MgAlB_{4w}$) and 98% (20 wt% $MgAlB_{4w}$), respectively, but the EL for the composites with 20 wt% $MgAlB_{4w}$ was significantly decreased. They also found that an increase in the content of reinforcing particles also improved the high temperature tensile strength (HTTS) of the alloys, which was consistent with the results in the particle-reinforced Al–Cu alloys reported by Tian [260] (Fig. 18(c)), which is due to the fact that the reinforcing particles not only present within the grains to trap and pin dislocations as well as to increase the density of the dislocations, but also present in the inter-grain to stabilize grain boundaries and increase the strength of the boundaries, an increase in particle content enhances both of these enhancement effects, resulting in higher HTTS (Fig. 18(d)). Nevertheless, a high-content of particles weakens the coordinated deformations ability of alloys because raising particles strengthens the dislocation density and the pinning of dislocations, so it is difficult to reduce the stress concentration through the dynamic softening of the matrix, and thus leads to the rapid expansion of cracks, causing excessive loss of toughness in composites.

Besides, particles that have been well enhanced at room temperature may fail at high temperatures. Some studies have shown that ordinary TiC particles are difficult to stabilize at high temperatures because the abundance of C-atom vacancies within them affects their structural stability [267–270], which in turn makes it difficult to enhance the properties. To avoid the TiC particles from destabilizing at high temperatures and losing their reinforcement, Ren et al. [271] modified TiC with B element and applied it to aluminum matrix composites. It was found that the YS and UTS of the modified TiC particle composites reached 184 MPa and 187 MPa at 350 °C, respectively, which were 31.4% and 30.8% higher than that of the unreinforced alloys. Xie et al. [251] found that the slip system was activated more easily at high temperatures, which made the dislocations tend to accumulate at grain boundaries and eventually annihilate, and thus led to the poor HTTS of the specimens before and after the particles reinforcement. However, the high-temperature tensile properties of 6061 were effectively improved by the addition of both AlN nanoparticles and submicron Al_2O_3 particles (YS, UTS and EF increased by 75.4%, 77.8% and 0.6%, respectively). This can be attributed to the fact that the particles stabilized the grain boundaries and prevented them from sliding to avoid the loosening of the boundaries damage to strength at high temperatures.

On the basis of the above studies, in order to further investigated the HTTS of aluminum matrix composites manipulated with multi-sized particles. For example, Bian et al. [272] designed and prepared multi-phase reinforced aluminum matrix composites by extrusion using in-situ synthesis, they found that the high temperature properties of (4.2 wt% Al_2O_3 + 4.8 wt% ZrB_2 + 6.5 wt% AlN)/Al were significantly improved (UTS increased up to 200 MPa) and exhibited excellent thermal stability, this is because adding AlN (size less than 100 nm) favors the heat resistance of the matrix, while ZrB_2 (size less than 300 nm) and Al_2O_3 (size less than 1 μm) favor the hardness and thermal stability. By observing the particle distribution, it is found that the in situ synthesized Al_2O_3 and ZrB_2 are uniformly dispersed in the matrix, while the more abundant AlN nanoparticles are presented as interconnected in the form of particle chains (as shown in Fig. 18(g)), and the complementary distribution of the three kinds of particles complements not only show the multiscale skeleton of the composites, but also exhibit the uniform dispersion of the particles as a whole in the matrix. Based on this, it is known that the improvement in the properties of multiphase particle-reinforced aluminum matrix composites is a result of the contribution of the particles themselves to the high-temperature properties and their synergistic effect. They demonstrated the feasibility of the idea of obtaining superior overall performance by utilizing different reinforcing particles in the alloy. Similarly, Li et al. [250] designed groups of particle reinforcements with different size combinations (coarse Si_3N_{4p} + coarse TiB_{2p} (CSCT), fine Si_3N_{4p} + fine TiB_{2p} (FSFT) and fine Si_3N_{4p} + coarse TiB_{2p} (FSCT)) for the manipulation of 6061 aluminum alloys, comparing the tensile conditions of different particle groups at 300 °C (tensile results are shown in Fig. 18(h and i)). They found that different particle groups improved the HTTS of the alloys to some extent and FSFT possessed the best strengthening properties. As can be seen from Fig. 18(j), each group of particles is able to be dispersed, but due to the decrease in particle size brings an elevated distributed number of particles, FSFT is more effective in pinning grain boundaries and dislocations and thus obtaining stronger HTTS.

The HTTS of different aluminum alloys are shown in Fig. 18(k) and Table 4. Evidently, the high temperature tensile characteristics of aluminum alloys can be markedly enhanced by adding thermally stable particles, but too high particles content may result in excessive plasticity loss and weaken the strengthening effect due to stress concentration. Moreover, relying on the synergistic effect of multiphase particles in the matrix and the selection of smaller particles to increase the number of uniformly dispersed particles can get a better strengthening effect.

5.3. Fatigue resistance of particle reinforced aluminum matrix composites

Fatigue refers to the sudden rupture and failure phenomenon of materials subjected to long-term cyclic stress or strain [276]. In engineering, ε-N and S–N curves are usually used to describe the fatigue properties of materials, where the S–N curves describe the number of times the corresponding cyclic stresses are loaded (fatigue life N) at different stress amplitudes (fatigue strength S), and stipulates that the maximum stress that does not rupture when cycling for 10^7 cycles is used as the conditional fatigue limit for aluminum alloys [277,278]. Additionally, fatigue failure of metal-based materials consists mainly of crack initiation and fatigue crack extension [279,280].

Walaa et al. [281] summarized the factors influencing the fatigue behavior of metal matrix composites, including loading conditions and the machining and forming process of composites, and investigated the effect of particles on the fatigue properties of composites. However, the

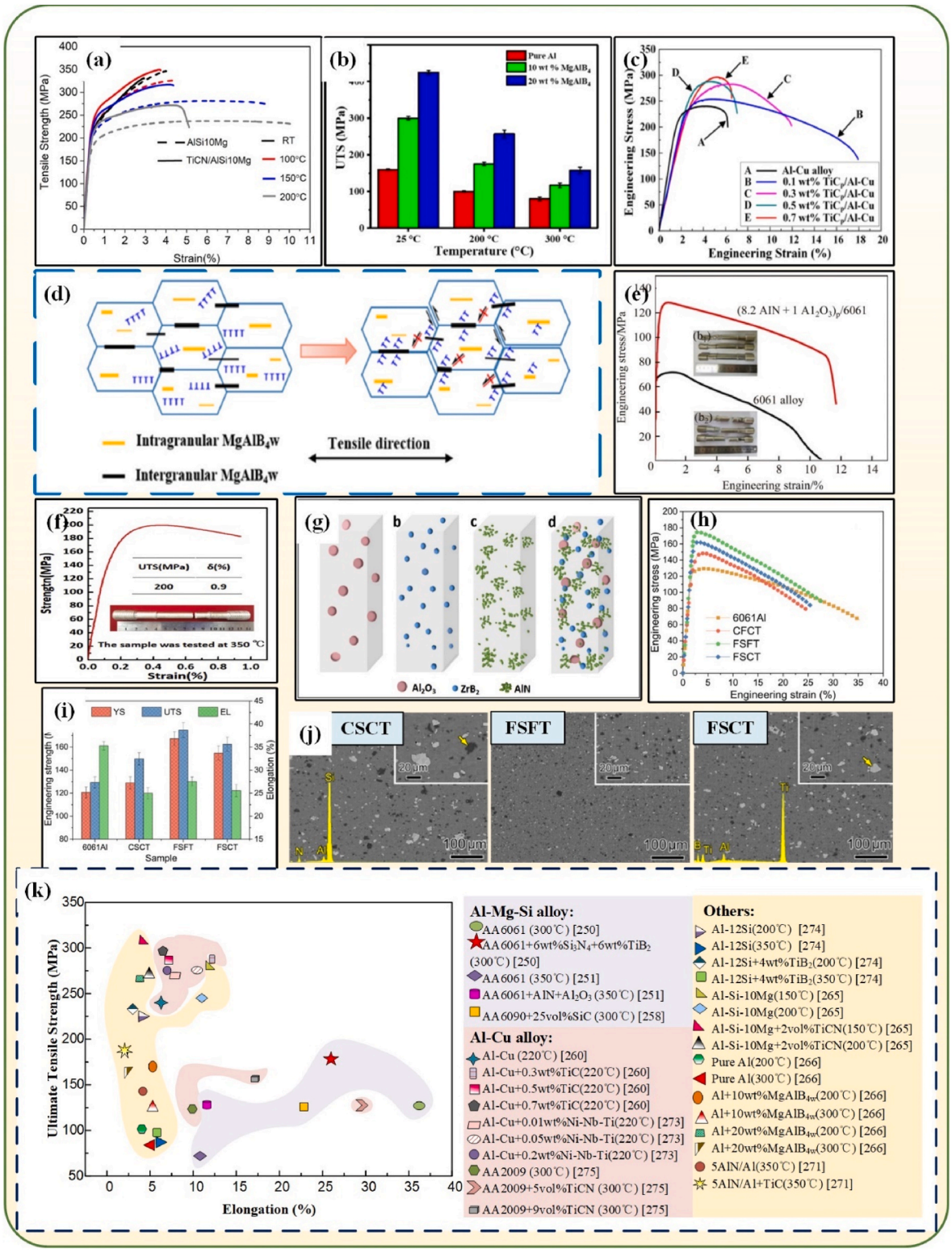

Fig. 18. (a) Stress-strain curves of TiCN/AlSi10Mg composites with AlSi10Mg at different temperatures [265]; (b) UTS of the alloys at different temperatures [266]; (c) high-temperature tensile curves of the composites with different contents of TiC [260]; (d) mechanisms of particles in intra- and inter-granularity [266]; (e) comparison of the tensile curves of (8.2 AlN + $1Al_2O_3)_p$/6061 and 6061 tensile curves [251]; (f) high-temperature tensile curves of composites, (g) schematic diagram of the distribution of multiphase particles in the matrix [272]; (h) stress-strain curves after manipulation of 6061 with different particle combinations at 300 °C, (i) statistics of high-temperature tensile strength of different particle combinations, (j) distribution of different particle combinations in the matrix [250]; (k) the high temperature tensile properties of various aluminum alloys.

Table 4
A summary of the high temperature tensile properties for various Al alloy.

Alloy	Nanoparticle	Tensile temperature (°C)	YS (MPa)	UTS (MPa)	EL (%)
AlSi10Mg [265]	unenhanced	150	213	282	11.5
		200	194	245	11
	2 vol% TiCN	150	235	308	4.2
		200	209	270	4.9
Al [266]	unenhanced	200	81	100	4.05
		300	77	84	5.21
	10 wt% $MgAlB_{4w}$	200	156	170	5.16
		300	118	125	5.30
	20 wt% $MgAlB_{4w}$	200	243	266	3.8
		300	158	166	2.38
AA6090 [258]	25 vol% SiC	300	–	126	23
5AlN/Al [271]	unenhanced	350	140	143	4.2
	TiC	350	184	187	2.1
AA6061 [251]	unenhanced	350	69	72	10.8
	8.2% AlN + 1% Al_2O_3	350	121	128	11.6
Al-Cu [260]	unenhanced	220	210	241	6.2
	0.3 wt% TiC	220	234	283	11.9
	0.5 wt% TiC	220	242	288	7
	0.7 wt% TiC	220	254	297	6.6
Al-Cu [273]	0.01 wt% Ni–Nb–Ti	220	–	270	7.89
	0.05 wt% Ni–Nb–Ti	220	–	275.7	10.45
	0.2 wt% Ni–Nb–Ti	220	–	275.9	6.98
Al–12Si [274]	unenhanced	200	184	225	4.0
		350	80	88	6.0
	4 wt% TiB_2	200	189	233	3.0
		350	84	96	5.8
AA2009 [275]	unenhanced	300	107	124	9.9
	5 vol% TiCN	300	105	127	29.3
	9 vol% TiCN	300	139	157	17.2
AA6061 [250]	unenhanced	300	120	128	36.2
	6 wt% Si_3N_4 + 6 wt% TiB_2	300	169	178	26

presence of particles in particle-reinforced composites has two sides to the fatigue resistance. On the one hand, under the cyclic action of stress, cracks are not only easy to initiate in coarse intermetallic compounds, but also the existence of particles in composite materials may lead to cracks, which are mainly manifested in three aspects [282–284]: (i) The particles may interact with the Al matrix interface to produce precipitates with obvious tips and then the stress concentration is produced under load, triggering crack initiation. (ii) The inhomogeneous dispersion of particles also contributes to cracking, which is represented by the interface desticking caused by the failure of the interface bonding between particle clusters formed by particle agglomeration and Al matrix, and the local strength deficiency caused by the particle barren zone of the composite material, which is more likely to promote the initiation of cracks. (iii) During the cyclic loading process, due to the stress concentration in particles, dislocations will be generated, the larger size particles result in insufficient reinforcement effect and fractured particles will form a crack sprouting source to promote crack generation. Hall et al. [285] found that micro-cracks were induced at the fracture site of SiC particles. On the other hand, the reinforcing particles will have an impact on fatigue crack propagation mainly through changing the microstructure of the composite material, which are reflected in the following aspects [286–288]: (i) The orowan reinforcement by small-sized hard particles (nano-size) leads to a bypassing mechanism of the dislocations passing through the particles, which increases the resistance of the dislocation motion and creates unfavorable conditions for crack propagation. (ii) When the crack expansion encounters grain boundaries, only when the cyclic stress continues to act to cause new tiny cracks on the grain boundaries and make the original cracks continue to expand, but particles acted on the grain refinement brings more grain boundaries, which leads to frequent stagnation in the crack expansion process in the composite material to improve the fatigue resistance. (iii) The difference in roughness between the matrix and the reinforcement leads to crack closure, which also attenuates the rate of crack expansion and prevents premature material failure.

Numerous studies have also illustrated that the presence of particles mainly slows down the rate of crack propagation to achieve an improvement in fatigue resistance, for example, Alalkawi Hussain et al. [289] added 10 wt% Al_2O_3 particles to 6061 and it was found that the presence of particles acted as a buffer barrier to crack propagation to some extent and hence improved the fatigue strength as well as fatigue life. As shown in Fig. 19(a) [290], the fatigue strength (σ_{FS}) showed a certain positive correlation trend with the tensile strength (σ_{TS}) according to the defined correlation trend between σ_{FS} and σ_{TS} [291]:

$$m = \frac{\sigma_{FS}}{\sigma_{TS}} \tag{6}$$

They found that the increase in the content of multi-walled carbon nanotubes (MWCNTs) led to an increase in m, suggesting that the addition of MWCNTs brings about a positive correlation trend of greater strength and an increase in the content of MWCNTs leads to higher fatigue strength (Fig. 19(b)). This is because the existence of pull-out MWCNTs at the crack, like a bridge, shares the cyclic load that causes crack extension to a certain extent, causing a certain resistance to the further development of the crack (Fig. 19(c)), and the increase of MWCNTs exacerbates this resistance to obtain a higher fatigue life. Zhang et al. [256] prepared ZrB_2/AA6111 composites by in-situ synthesis, they found that the fatigue resistance of the composites is better than the basic alloys, so the composites withstand more stresses under the same cyclic stress. The fracture analysis results indicated that the fatigue fracture of the composite is rougher with dense tearing edges, and the rounded shape of the particles can effectively prevent the crack initiation caused by the tip stress concentration, as shown in Fig. 19(d). However, it is observed from the statistical S–N diagrams for different contents of ZrB_2 shown in Fig. 19(e) that the increase in the content of particles did not positively correlate with the strengthening of fatigue resistance, the same result was found from the report of Mamoon et al. [292], this may be due to the weakening of the grain refinement effect caused by excessive particle content as mentioned in Chapter 4, so that the number of grain boundaries encountered in the process of crack growth is reduced. Another explanation can be explained by the particle-enriched band, the particle-enriched band will have a tendency to widen as particle content increases, and it has been shown in that when the width of the particle-enriched band is too high (>10 μm), there will be a lot of the second phase inside and the fracture of the second phase accelerates the crack extension, which will ultimately show that the reinforcing body promotes the crack extension more than mitigates the effect, as shown in Fig. 19(f, g) [280].

Generally speaking, fine particles are more effective in improving the microstructure, which results in the improvement in the fatigue strength and tensile properties of the composite material after particle reinforcement. The reduction in the size of the reinforcement reduces the damage of the material at a given stress, increases the stress of fracture of the alloys during cycling, and improves the high circumferential fatigue properties dominated by crack initiation, as shown in Fig. 20(a and b). Chen et al. [284] found that smaller particles exhibited fatigue strength similar to that of the substrate, while oversized particles exhibited a significant reduction in fatigue strength. This is closely related to the crack extension mode and budding. At lower applied stress (130 MPa), the increase in particle size effectively attenuates the small crack extension rate, but at higher stress (145 MPa), particles with larger diameter will accumulate more cracks at the particle and expand them simultaneously, leading to a sharp increase in the crack expansion rate (da/dN) (Fig. 20(c)), and Fig. 20(d) also demonstrates that the crack extension process also results in the fragmentation of large particles,

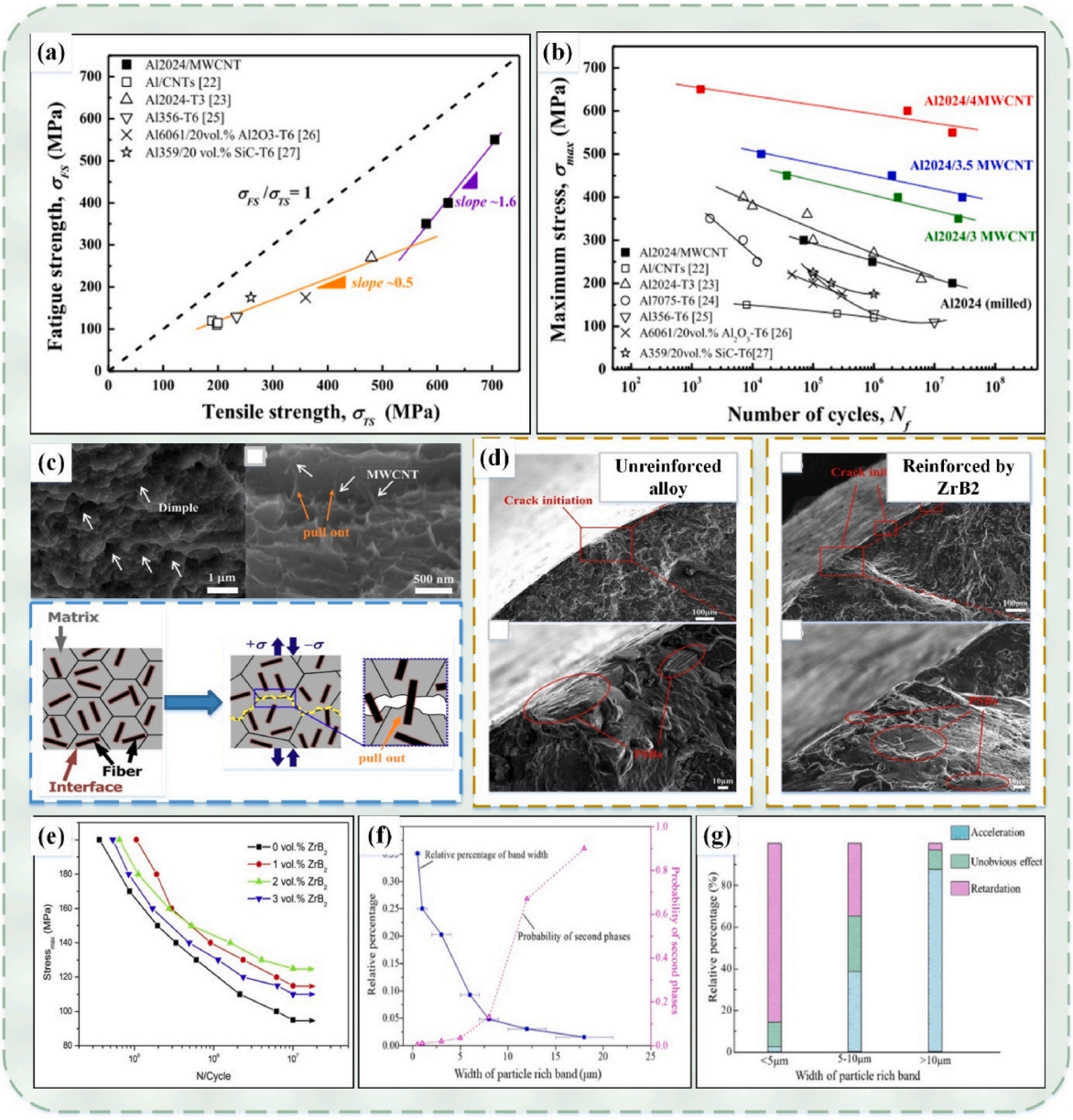

Fig. 19. (a) Relationship between fatigue strength and tensile strength of different composites, (b) statistical plots of the number of cycles of different composites at different stresses, (c) fatigue fracture surfaces of MWCNT-reinforced aluminum alloys and their mechanism of action [290]; (d) SEM photographs of the crack sprouting zone, (e) S–N curves of composites with different ZrB_2 contents after T6 treatment [256]; (f) the possibility of a second phase in particle-enriched zones of different widths, (g) the role of particle-enriched zones of different widths on crack propagation [280].

generating a new source of crack sprouting. Based on that study, Uematsu et al. [293] investigated the fatigue behavior of SiC aluminum matrix composites with different dimensions at different temperatures and the result showed that the fatigue resistance of the particle-reinforced material at high temperatures decreased (Fig. 20(e)). Fig. 20(f) reveals the causes of fatigue ageing crack production under different particle sizes and temperatures conditions. The composites with a particle size of 5 μm are almost always cracked at the test temperature due to cracking of the matrix caused by cyclic stress, while the composites with particle size of 20 μm and 60 μm will be cracked at 150 °C and 250 °C, respectively, which are due to particle fracture caused by cracking and the particles and matrix interface bonding failure that becomes a crack sprouting point. The loss of matrix softening strength at high temperatures can easily cause large plastic deformation at the tip of the emerging cracks, specifically the rapid growth of cracks and the poor fatigue strength at high temperatures, and the improvement of reinforced particles on the fatigue performance of the material appears to be unsatisfactory, and even can lead to a reduction in the fatigue life. The crack extension can not be effectively inhibited by the addition of particles due to the matrix softening and the extension of the enhanced particle-matrix interface at high temperatures. Similar studies have shown [294] that the composites reinforced with a mixture of nano-sized and micron-sized Al_2O_3 exhibit a higher fatigue life and fatigue strength than that of the composites reinforced with only micron particles. This is due to the fact that the presence of nano-sized particles leads to stronger reinforced interfaces that are less prone to cracking of the matrix interface or particles, while the denser entanglement of dislocations caused by the nanoparticles induces a superior strengthening effect. This suggests that finer sized particles provide a better reinforcement effect, while single nanoparticles that are prone to agglomeration, especially at high levels, which not only reduces the density of particles dispersed in the matrix, but also results in larger aggregates

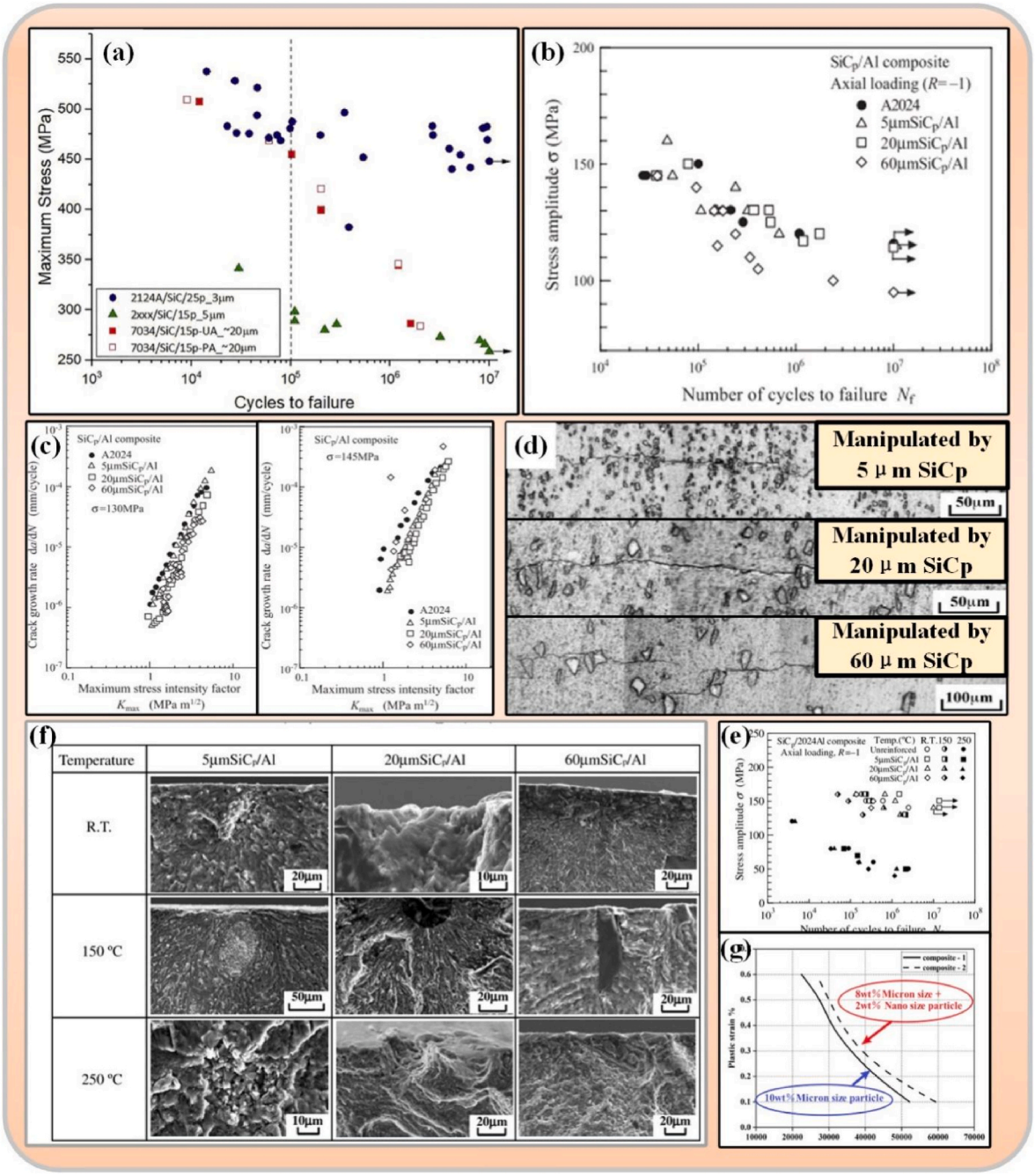

Fig. 20. (a) Comparison of fatigue properties of different metal matrix composites [297]; (b) S–N curves of SiC/Al composites of different sizes, (c) crack extension rate under different stress conditions and (d) crack extension in particle reinforced materials [284]; (e) S–N curves of different composites at different temperatures and (f) SEM images of crack initiation points [293] (g) comparison of fatigue resistance of composites reinforced by nano-sized and micrometre-sized hybrid particles and micrometre-sized particles [294].

that can cause stress concentrations and crack propagation [295,296]. Table 5 gives the fatigue properties of different aluminum alloys, and we can speculate that the selection of the size of reinforcement particles and the control of the appropriate content range are beneficial to the improvement in the fatigue properties.

6. Summary and outlook

This paper reviews the use of microalloying and the addition of reinforcing particles for the development of high-strength and fatigue-resistant aluminum alloys used in new energy vehicles to replace the conventional steel to achieve lightweight design of new energy vehicles, and focus on the effects of the content of some elements, types of reinforcing particles, sizes, contents, morphology and coupling effects of some of the particles on the properties of aluminum alloys as well as the corresponding mechanisms. It is revealed that alloying elements play an important role in the formation of the precipitated phases. Compositional changes not only change the content, distribution and even morphology of the original precipitated phases in the Al–Mg–Si alloy (β″ phase, Al(FeMn)Si phase, etc.), but also generate new precipitated phases, which will have an outstanding effect on the improvement of the properties of alloys in various aspects (mechanical properties, corrosion resistance, and processing and forming properties, etc.). However, the excessive addition of alloy elements will not only cause the coarsening of

Table 5
A summary of fatigue properties of various aluminum alloys.

Matrix	Particle type	Particle size	Frequency (Hz)	Tensile temperature (°C)	Fatigue strength/limit (MPa)	Cycles endured
AA6061 [289]	Unmanipulated	–	–	–	80	1.3×10^5
	10 wt% Al_2O_3	50 nm	–	–	80	2.2×10^5
AA6111 [256]	Unmanipulated	–	20	20–25	97	10^7
	2 vol% ZrB_2	5–60 nm	20	20–25	125	10^7
	3 vol% ZrB_2	5–60 nm	20	20–25	110	10^7
AA6063 [257]	Unmanipulated	–	23.34	–	103	4.2×10^4
	7 wt% TiO_2	40 nm	23.34	–	103	5×10^4
AA6061 [292]	Unmanipulated	–	–	–	60	4×10^5
	2 wt% SiC	10 nm	–	–	60	6.3×10^5
	2.5 wt% SiC	10 nm	–	–	60	4.2×10^5
AA2024 [284]	Unmanipulated	–	10	Room temperature	115	10^7
	10 wt% SiC	5 μm	10	Room temperature	115	10^7
	10 wt% SiC	60 μm	10	Room temperature	95	10^7
AA2024 [293]	10 wt% SiC	5 μm	10	150	130	10^6
	10 wt% SiC	5 μm	10	250	75	10^5
	10 wt% SiC	60 μm	10	250	40	10^6
AA2124 [297]	25 vol% SiC	3 μm	20	–	448	10^7
AA2024 [290]	Unmanipulated	–	5	20–25	200	10^7
	3 vol% MWCNT	20 nm	5	20–25	350	10^7
	4 vol% MWCNT	20 nm	5	20–25	550	10^7
AA7034 [298]	15 vol% SiC	20 μm	5	120	350	10^6
A359 [299]	20 vol% SiC	17 μm	5	–	130	10^6
Al–Si–10Mg [300]	0.1 wt% boron nitride nanosheet	30–50 nm	15	Room temperature	60	10^6

the precipitated phases, but also aggravate the generation of some harmful phases (such as sharp slate-like Al–Si–Ce precipitates), and even reduce the β″ phases due to the competition between the various types of precipitated phases in the process of precipitation, which will deteriorate the performance of the alloy and is harmful to alloy processing and forming. These issues can make it difficult for the alloys to meet the requirements of plates and profiles used in new energy vehicles. Moreover, it is shown that the addition of nanoparticles to aluminum alloys exhibits a remarkable enhancement of the mechanical properties by improving the microstructure. Particles not only refine the microstructure and homogenize the composition to prevent the detrimental effects of segregation, but also act as fine precipitation phases to induce orowan strengthening. Furthermore, the introduction of different particles of mixed size will integrate the benefits of coarse particles and fine particles in refining grains to show more amazing results and play a more meritorious strengthening effect.

In order to meet the more demanding engineering requirements, the content of elements in the alloying process should be controlled in the appropriate range and the precipitation phases of certain elements should be uniformly dispersed to avoid the possible hazards (especially Fe). On the other hand, in response to the call of environmental protection and green initiatives, seeking and using alloying schemes of renewable resources to achieve high recycling efficiency of aluminum alloys will be one of the key research directions in the future. At present, there is insufficient in-depth research on the processing and forming of aluminum alloys with particles, so further investigations are needed to fully explore the particles' influence on the welding performance, corrosion performance and impact resistance of aluminum alloys reinforced. How to achieve uniform dispersion of particles, develop more efficient reinforcing particles, and take advantage of the coupling between different particles (type and size) to achieve the best reinforcing effect are the key to the development of materials for new energy vehicles. In the future, combining the advantages of both particles and alloying to achieve full-cycle control of aluminum alloys and the thin-walled lightweight with large extrusion ratio, fulfill microstructure refinement and homogenization and obtain high-strength, high-performance, corrosion-resistant thin-walled materials or profiles under the condition of ensuring the rigidity. In addition, developing the aluminum alloys that are more tolerant of impurity elements to enable recycling of aluminum alloys. These initiatives will continue to promote the progress of lightweight material technology for new energy vehicles, play an important role in various fields and focus on the development direction of environmental protection, sustainability and functionality.

Funding

This work was supported by the National Natural Science Foundation of China (NNSFC, No. 52371109) and the Science and Technology Development Program of Jilin Province, China (No. 20230201145GX).

Institutional review board statement

Not applicable.

Informed consent statement

Not applicable.

Data availability statement

Not applicable.

Declaration of competing interest

The authors declare that they have no known competing financial interests or personal relationships that could have appeared to influence the work reported in this paper.

References

[1] Yan ZJ, Liu XS, Fang HY. Effect of sheet configuration on microstructure and mechanical behaviors of Dissimilar Al–Mg–Si/Al–Zn–Mg aluminum alloys friction stir welding joints. J Mater Sci Technol 2016;32:1378–85. https://doi.org/10.1016/j.jmst.2016.10.011.

[2] Pan D, Pan Q, Yu Q, Li G, Liu B, Deng Y, et al. Microstructure and fatigue behavior of MIG-welded joints of 6005A aluminum alloy with trace amounts of scandium. Mater. Charact 2022;194:112482. https://doi.org/10.1016/j.matchar.2022.112482.

[3] Sozhamannan GG, Mohamed Yusuf M, Aravind G, Kumaresan G, Velmurugan K, Venkatachalapathy VSK. Effect of applied load on the wear performance of 6061 Al/nano Ticp/Gr hybrid composites. Mater. Today. SAVE Proc 2018;5:6489–96. https://doi.org/10.1016/j.matpr.2017.12.262.

[4] Tang K, Wei L, Huang H, Wang J, Li D, Jiang H, et al. Effect of grain size and second phase on the corrosion behavior of MIG-welded Al–Mg–Si–Mn–Cr alloy. J Mater Sci 2023;58:10782–801. https://doi.org/10.1007/s10853-023-08689-9.

[5] Li SS, Yue X, Li QY, Peng HL, Dong BX, Liu TS, et al. Development and applications of aluminum alloys for aerospace industry. J Mater Res Technol 2023;27:944–83. https://doi.org/10.1016/j.jmrt.2023.09.274.

[6] Liu B, Yang J, Zhang XY, Li XQ. Development and low cost control of glass fiber reinforced thermoplastic composites-based electric vehicle tailgate. J Mater Eng Perform 2023. https://doi.org/10.1007/s11665-023-08609-7.
[7] Kulkarni SS, Hale F, Taufique MFN, Soulami A, Devanathan R. Investigation of crashworthiness of carbon fiber-based electric vehicle battery enclosure using finite element analysis. Appl Compos Mater 2023;30:1689–715. https://doi.org/10.1007/s10443-023-10146-4.
[8] Han W, Liang QH, Huang LS, Wang WX. Design and analysis of hot core box mold for new energy vehicle motor shell. Int J Metalcast 2018;12:779–84. https://doi.org/10.1007/s40962-017-0208-x.
[9] He X, Lin Y, Ding Y, Abdullah AM, Lei Z, Han Y, et al. Reshapeable, rehealable and recyclable sensor fabricated by direct ink writing of conductive composites based on covalent adaptable network polymers. Int. J. Extreme Manuf 2021;4:015301. https://doi.org/10.1088/2631-7990/ac37f2.
[10] Sui S, Guo S, Ma D, Guo C, Wu X, Zhang Z, et al. Additive manufacturing of magnesium and its alloys: process-formability-microstructure-performance relationship and underlying mechanism. Int. J. Extreme Manuf 2023;5:251–95. https://doi.org/10.1088/2631-7990/acf254.
[11] Zhang H, Zhu X, Tai Y, Zhou J, Li H, Li Z, et al. Recent advances in nanofiber-based flexible transparent electrodes. Extreme Manuf 2023;5:150–204. https://doi.org/10.1088/2631-7990/acdc66.
[12] Shao C, Li H, Zhu Y, Li P, Yu H, Zhang Z, et al. Nano-additive manufacturing of multilevel strengthened aluminum matrix composites. Int. J. Extreme Manuf 2022;5:260–70. https://doi.org/10.1088/2631-7990/ac9ba2.
[13] Abd El-Baky MA, Hegazy DA, Hassan MA. Advanced thin-walled composite structures for energy absorption applications. Appl Compos Mater 2022;29:1195–233. https://doi.org/10.1007/s10443-022-10016-5.
[14] Cheng T, Li P, Lu F, Wang C, Zhang H, Yang Y. The improvement in mechanical properties and strengthening mechanism of the new type of cast aluminum alloy with low silicon content for automotive purposes. Trans Indian Inst Met 2022;75:1245–54. https://doi.org/10.1007/s12666-021-02479-0.
[15] Dai HB, Liang GC, Liu LJ, Pan SG. Research on friction stir welding of electric control system accessories of new energy vehicle charger. Trans Indian Inst Met 2023;77:405–16. https://doi.org/10.1007/s12666-023-03079-w.
[16] Liu B, Yang J, Zhang XY, Li XQ. Topology optimization and lightweight platform development of pure electric vehicle frame-type aluminum body considering crash performance. J Mater Eng Perform 2024. https://doi.org/10.1007/s11665-024-09239-3.
[17] Li ZH, Deng YF, Zeng JC, Hu L, Zhou YT, Qiu ZR. Achievement of defect-free and high-properties multilayer copper foils flexible connection by friction stir welding. Weld World 2023. https://doi.org/10.1007/s40194-023-01665-6.
[18] Venugopal A, Venugopal P, Thomas BG, Koshy CP, Varghese JT. Numerical study on aluminium 5056 alloy hexagonal honeycomb cells as a possible material for energy absorption during vehicle crash. Indian Inst. Met 2023;76:2515–24. https://doi.org/10.1007/s12666-023-02993-3.
[19] Moodispaw MP, Chen B, Luo AA, Wang Q. Achieving Metallurgical bonding in aluminum/steel Bimetallic castings. Int J Metalcast 2024;130:235–41. https://doi.org/10.1007/s40962-023-01241-0.
[20] Lin YC, Luo SC, Yin LX, Huang J. Microstructural evolution and high temperature flow behaviors of a homogenized Sr-modified Al-Si-Mg alloy. J Alloys Compd 2018;739:590–9. https://doi.org/10.1016/j.jallcom.2017.12.278.
[21] Jin D, Li HY, Zhu ZX, Yang CL, Chen BA, Miao YJ. Effects of cooling rate in homogenization on microstructure, hot deformation resistance and subsequent age-hardening behavior of an Al–Mg–Si alloy. J Mater Res Technol 2023;27:3283–300. https://doi.org/10.1016/j.jmrt.2023.10.156.
[22] Dong QP, Zhang Y, Wang JH, Huang LJ, Nagaumi H. Enhanced strength-conductivity trade-off in Al-Mg-Si alloys with optimized Mg/Si ratio. J Alloys Compd 2024;970:172682. https://doi.org/10.1016/j.jallcom.2023.172682.
[23] Sun Y, Wu GH. Preparation and characterization of Al-Mg-Si matrix composites reinforced with Ti2(Al,Si)C solid solution. Mater Lett 2023;353:135266. https://doi.org/10.1016/j.matlet.2023.135266.
[24] Zang RJ, Ding LP, Ehlers FJH, Jia ZH, Xu SQ, Li YJ, et al. The influence of Cu content and Mg/Si ratio on the strength and formability in Al-Mg-Si-Cu alloys. Mater. Charact 2023;205:113355. https://doi.org/10.1016/j.matchar.2023.113355.
[25] Baruah M, Borah A. Processing and precipitation strengthening of 6xxx series aluminium alloys: a review. International J. Mater. Sci 2020;1:40–8. https://doi.org/10.22271/27078221.2020.v1.i1a.10.
[26] Wang WY, Pan QL, Wang XD, Liu B. Improved heat and corrosion resistance of high electrical conductivity Al-Mg-Si alloys by multi-alloying of Ce, Sc and Y. Corros. Sci 2024;226:111695. https://doi.org/10.1016/j.corsci.2023.111695.
[27] Elasheri A, Parson N, Chen XG. Microstructure, tensile and bending properties of extruded Al–Mg–Si 6xxx alloys with individual and combined additions of Zr and Mn. Mater Sci. Eng A 2024;894:146156. https://doi.org/10.1016/j.msea.2024.146156.
[28] Zheng DH, Li JH, Wei B, Liang TB, Yang ZC, Wang Z, et al. Sn–Sc microalloying-induced property improvement and micromechanisms of an Al–Mg–Si alloy. J Mater Res Technol 2023;27:472–89. https://doi.org/10.1016/j.jmrt.2023.09.307.
[29] Huang ZY, Zhang XX, Xiao B, Ma ZY. Hot deformation mechanisms and microstructure evolution of SiCp/2014Al composite. J Alloys Compd 2017;722:145–57. https://doi.org/10.1016/j.jallcom.2017.06.065.
[30] Xiao YK, Chen H, Bian ZY, Sun TT, Ding H, Yang Q, et al. Enhancing strength and ductility of AlSi10Mg fabricated by selective laser melting by TiB_2 nanoparticles. J Mater Sci Technol 2022;109:254–66. https://doi.org/10.1016/j.jmst.2021.08.030.
[31] Maivizhi Selvi, Saravana Kumar A, Isaac D R G, Keerthana N, Madhanagopal GD, Nikhilesh G. Influence of MoS2 on microstructure and mechanical Behaviours of Al6061-Al2O3 hybrid composite. Appl Mech Mater 2015;813–814:62–6. https://dx.doi.org/10.4028/www.scientific.net/AMM.813-814.62.
[32] Housaer FB, Touzin F, Tingaud M, Legris D, Addad A. A. Interfacial characterization in carbon nanotube reinforced aluminum matrix composites. Mater. Charact 2015;110:94–101. https://doi.org/10.1016/j.matchar.2015.10.014.
[33] Li DX, Zhao K, Han MX, Liu GL, Sun QQ, Liu SD, et al. Optimizing microstructure and enhancing mechanical properties of Al–Si–Mg–Mn–based alloy by novel C-doped TiB2 particles. J Mater Res Technol 2023;26:9450–66. https://doi.org/10.1016/j.jmrt.2023.09.206.
[34] Liu TS, Dong BX, Yang HY, Qiu F, Shu S-L, Jiang Q-C. Review on role of intermetallic and ceramic particles in recrystallization driving force and microstructure of wrought Al alloys. J Mater Res Technol 2023;27:3374–95. https://doi.org/10.1016/j.jmrt.2023.10.098.
[35] Liu X, Zhao QL, Jiang QC. Effects of cooling rate and TiC nanoparticles on the microstructure and tensile properties of an Al–Cu cast alloy. Mater Sci. Eng A 2020;790:139737. https://doi.org/10.1016/j.msea.2020.139737.
[36] Fang X, Li K, Ma MH, Shang JH, Feng XL, Hou YH, et al. Microstructure and properties of a novel high-performance Al-Si-Mg alloy fabricated by wire-arc directed energy deposition. Mater Lett 2024;360:136010. https://doi.org/10.1016/j.matlet.2024.136010.
[37] Shu SL, Lu JB, Qiu F, Xuan QQ, Jiang QC. High volume fraction TiCx/Al composites with good comprehensive performance fabricated by combustion synthesis and hot press consolidation. Mater Sci. Eng A 2011;528:1931–6. https://doi.org/10.1016/j.msea.2010.11.052.
[38] Zhou DS, Qiu F, Jiang QC. Simultaneously increasing the strength and ductility of nano-sized TiN particle reinforced Al–Cu matrix composites. Mater Sci. Eng A 2014;596:98–102. https://doi.org/10.1016/j.msea.2013.12.049.
[39] Gangolu S, Rao AG, Prabhu N, Deshmukh VP, Kashyap BP. Microstructure evolution and flow behavior of hot-rolled aluminum – 5% B4C composite. Mater Des 2014;53:581–7. https://doi.org/10.1016/j.matdes.2013.07.025.
[40] Hua ZT, Shan TT, Geng R, Zhao QL. Effect of hot-plate rolling on the microstructure evolution and mechanical properties of in-situ nano-TiCP/Al-Mg-Si composites. J Wuhan Univ Technol 2022;37:513–7. https://doi.org/10.1007/s11595-022-2559-2.
[41] Yan Y-F, Kou S-Q, Yang H-Y, Shu S-L, Qiu F, Jiang Q-C, et al. Ceramic particles reinforced copper matrix composites manufactured by advanced powder metallurgy: preparation, performance, and mechanisms. Int. J. Extreme Manuf 2023;5:206–40. https://doi.org/10.1088/2631-7990/acdb0b.
[42] Shaga A, Shen P, Sun C, Jiang Q. Lamellar-interpenetrated Al–Si–Mg/SiC composites fabricated by freeze casting and pressureless infiltration. Mater Sci. Eng A 2015;630:78–84. https://doi.org/10.1016/j.msea.2015.02.012.
[43] Zhang LJ, Xuan QQ, Wang JG, Qiu F, Jiang QC. Effects of TiB2 content and alloy elements (Mg, Mo, V) on the compression properties of high-volume-fraction TiB2/Al composites. Mater Sci. Eng A 2014;607:28–32. https://doi.org/10.1016/j.msea.2014.03.131.
[44] Trink B, Weißensteiner I, Uggowitzer PJ, Strobel K, Pogatscher S. High Fe content in Al-Mg-Si wrought alloys facilitates excellent mechanical properties. Scr. Mater 2022;215:114701. https://doi.org/10.1016/j.scriptamat.2022.114701.
[45] Zhang XZ, Wang DT, Nagaumi H, Zhou YX, Yu W, Chong XY, et al. Morphology, thermal stability, electronic structure and mechanical properties of α-AlFeMnSi phases with varying Mn/Fe atomic ratios: experimental studies and DFT calculations. J Alloys Compd 2022;901:163523. https://doi.org/10.1016/j.jallcom.2021.163523.
[46] Lodgaard L, Ryum N. Precipitation of dispersoids containing Mn and/or Cr in Al–Mg–Si alloys. Mater Sci. Eng A 2000;283:144–52. https://doi.org/10.1016/S0921-5093(00)00734-6.
[47] Cassell AM, Robson JD, Race CP, Eggeman A, Hashimoto T, Besel M. Dispersoid composition in zirconium containing Al-Zn-Mg-Cu (AA7010) aluminium alloy. Acta Mater 2019;169:135–46. https://doi.org/10.1016/j.actamat.2019.02.047.
[48] De Luca A, Shu S, Seidman DN. Effect of microadditions of Mn and Mo on dual L12- and α-precipitation in a dilute Al-Zr-Sc-Er-Si alloy. Mater. Charact 2020;169:110585. https://doi.org/10.1016/j.matchar.2020.110585.
[49] Karnesky RA, Van Dalen ME, Dunand DC, Seidman DN. Effects of substituting rare-earth elements for scandium in a precipitation-strengthened Al–0.08at. %Sc alloy. Scr. Mater 2006;55:437–40. https://doi.org/10.1016/j.scriptamat.2006.05.021.
[50] Meng Y, Cui J, Zhao Z, Zuo Y. Effect of vanadium on the microstructures and mechanical properties of an Al–Mg–Si–Cu–Cr–Ti alloy of 6XXX series. J Alloys Compd 2013;573:102–11. https://doi.org/10.1016/j.jallcom.2013.03.239.
[51] Dunwoody BJ. The production of automotive body panels in 5083 SPF aluminium alloy. Mater Sci Forum 2001;357–359:59–64. https://dx.doi.org/10.4028/www.scientific.net/MSF.357-359.59.
[52] Yuan Z, Li F, He M. Fast fourier transform on analysis of portevin-le chatelier effect in Al 5052. Mater Sci. Eng A 2011;530:389–95. https://doi.org/10.1016/j.msea.2011.09.101.
[53] Li J, Liu WC, Yuan H, Gao YK. Comparison of earing behavior between continuous cast and direct chill cast AA 5182 aluminum alloys during cold rolling and annealing. J Mater Process Technol 2010;210:2007–15. https://doi.org/10.1016/j.jmatprotec.2010.07.017.
[54] Hu Q, Zhang Q, Fu S, Cao P, Gong M. Influence of precipitation on the Portevin-Le Chatelier effect in Al-Mg alloys. Theor. Appl. Mech. Lett. 2011;1:011007. https://doi.org/10.1063/2.1101107.

[55] Schneider R, Grant RJ, Heine B, Börret R, Burger S, Zouaoui Z. An analysis of the surface quality of AA5182 at different testing temperatures. Mater Des 2014;64:750–4. https://doi.org/10.1016/j.matdes.2014.08.028.
[56] Li Z, Zang R, Zhao P, Jia Z. Effects of pre-aging and natural aging on the clusters, strength and hemming performance of AA6014 alloys. Mater Sci. Eng A 2020;782:139206. https://doi.org/10.1016/j.msea.2020.139206.
[57] Engler O, Hirsch J. Texture control by thermomechanical processing of AA6xxx Al–Mg–Si sheet alloys for automotive applications—a review. Mater Sci. Eng A 2002;336:249–62. https://doi.org/10.1016/S0921-5093(01)01968-2.
[58] Zhong H, Rometsch PA, Estrin Y. The influence of Si and Mg content on the microstructure, tensile ductility, and Stretch formability of 6xxx alloys. Metall. Mater. Trans. A. 2013;44:3970–83. https://doi.org/10.1007/s11661-013-1740-9.
[59] Jimbert P, Eguia I, Perez I, Gutierrez MA, Hurtado I. Analysis and comparative study of factors affecting quality in the hemming of 6016T4AA performed by means of electromagnetic forming and process characterization. J Mater Process Technol 2011;211:916–24. https://doi.org/10.1016/j.jmatprotec.2010.08.022.
[60] Zhang K, He Q, Rao JH, Wang Y, Zhang R, Yuan X, et al. Correlation of textures and hemming performance of an AA6XXX aluminium alloy. J Alloys Compd 2021;853:157081. https://doi.org/10.1016/j.jallcom.2020.157081.
[61] Hu X, Lin ZQ, Li SH, Zhao YX. Fracture limit prediction for roller hemming of aluminum alloy sheet. Mater Des 2010;31:1410–6. https://doi.org/10.1016/j.matdes.2009.08.039.
[62] Le Maoût N, Thuillier S, Drawing Manach PY. Flanging and hemming of metallic thin sheets: a multi-step process. Mater Des 2010;31:2725–36. https://doi.org/10.1016/j.matdes.2010.01.030.
[63] Zhang G, Hao H, Wu X, Hu SJ, Harper K, Faitel W. An experimental investigation of curved surface-Straight edge hemming. J Manuf Process 2000;2:241–6. https://doi.org/10.1016/S1526-6125(00)70025-9.
[64] Wang S, Zhu W, Li M. Differential geometry modeling and application of roller pose and trajectory of robot roller hemming for complex curved surface-curved edge panels. RoboT Cim-Int Manuf 2023;83:102565. https://doi.org/10.1016/j.rcim.2023.102565.
[65] Mattei L, Daniel D, Guiglionda G, Klöcker H, Driver J. Strain localization and damage mechanisms during bending of AA6016 sheet. Mater Sci. Eng A 2013;559:812–21. https://doi.org/10.1016/j.msea.2012.09.028.
[66] Shi Y, Jin H, Wu PD, Lloyd DJ, Embury D. Failure analysis of fusion clad alloy system AA3003/AA6xxx sheet under bending. Mater Sci. Eng A 2014;610:263–72. https://doi.org/10.1016/j.msea.2014.05.047.
[67] Mori K, Maki S, Ishiguro M. Improvement of product strength and formability in stamping of Al–Mg–Si alloy sheets having bake hardenability by resistance heat and artificial aging treatments. Int. J. Mach. Tool. Manu 2006;46:1966–71. https://doi.org/10.1016/j.ijmachtools.2006.01.011.
[68] Li M. Micromechanisms of deformation and fracture in shearing aluminum alloy sheet. Int J Mech Sci 2000;42:907–23. https://doi.org/10.1016/S0020-7403(99)00034-X.
[69] Paraianu L, Banabic D. Characterization of the plastic behaviour of AA6016-T4 aluminium alloy. Adv Eng Forum 2013;8–9:293–300. https://dx.doi.org/10.4028/www.scientific.net/AEF.8-9.293.
[70] Kamat RG, Butler Jr JF, Murtha SJ, Bovard FS. Alloy 6022-T4E29 for automotive sheet applications. Mater Sci Forum 2002;396–402:1591–6. https://doi.org/10.4028/WWW.SCIENTIFIC.NET/MSF.396-402.1591.
[71] Ji YL, Zhong H, Hu P, Guo F. Use of thermodynamic calculation to predict the effect of Si on the ageing behavior of Al–Mg–Si–Cu alloys. Mater Des 2011;32:2974–7. https://doi.org/10.1016/j.matdes.2011.01.014.
[72] Baruah M, Borah A. Structure–property correlation of Al–Mg–Si alloys micro-alloyed with Sn. Int J Metalcast 2021;16:924–44. https://doi.org/10.1007/s40962-021-00652-1.
[73] Lin S, Dang J, Wang Z, Sun Y, Xiang Y. Enhanced strength and toughness in Al-Mg-Si alloys with addition of Cr, Mn, and Cu elements. J Mater Eng Perform 2022;32:1039–50. https://doi.org/10.1007/s11665-022-07191-8.
[74] Wang C, Wang ZJ, Xu H, Zhang GW. Decreased dislocation density as an origin for the quench sensitivity of the Al-Si-Mg alloys with high Si content. J Alloys Compd 2022;910:165011. https://doi.org/10.1016/j.jallcom.2022.165011.
[75] Mao H, Kong Y, Cai D, Yang M, Peng Y, Zeng Y, et al. β'' needle-shape precipitate formation in Al-Mg-Si alloy: phase field simulation and experimental verification. Comput Mater Sci 2020;184:109878. https://doi.org/10.1016/j.commatsci.2020.109878.
[76] Yang MJ, Chen HN, Orekhov A, Lu Q, Lan XY, Li K, et al. Quantified contribution of β″ and β′ precipitates to the strengthening of an aged Al–Mg–Si alloy. Mater Sci. Eng A 2020;774:138776. https://doi.org/10.1016/j.msea.2019.138776.
[77] Gong WY, Li RX, Xie MJ, Wu Y, Zhang JS. Precipitation behaviors of multi-scale precipitation strengthened Al–Mg–Si–Cu–Zn alloys controlled by Mg content. J Mater Res Technol 2021;13:651–68. https://doi.org/10.1016/j.jmrt.2021.04.057.
[78] Shishido H, Aruga Y, Murata Y, Marioara CD, Engler O. Evaluation of precipitates and clusters during artificial aging of two model Al–Mg–Si alloys with different Mg/Si ratios. J Alloys Compd 2022;927:166978. https://doi.org/10.1016/j.jallcom.2022.166978.
[79] Myhr OR, Grong Ø, Fjær HG, Marioara CD. Modelling of the microstructure and strength evolution in Al–Mg–Si alloys during multistage thermal processing. Acta Mater 2004;52:4997–5008. https://doi.org/10.1016/j.actamat.2004.07.002.
[80] Engler O, Marioara CD, Aruga Y, Kozuka M, Myhr OR. Effect of natural ageing or pre-ageing on the evolution of precipitate structure and strength during age hardening of Al–Mg–Si alloy AA 6016. Mater Sci. Eng A 2019;759:520–9. https://doi.org/10.1016/j.msea.2019.05.073.
[81] Esmaeili S, Lloyd DJ, Poole WJ. A yield strength model for the Al-Mg-Si-Cu alloy AA6111. Acta Mater 2003;51:2243–57. https://doi.org/10.1016/S1359-6454(03)00028-4.
[82] Özkan Z, Gökmen U, Ocak SB. Analyses of Gamma and Neutron Attenuation Properties of the AA6082 composite material doped with boron carbide (B_4C). Radiat Phys Chem 2023;206:110810. https://doi.org/10.1016/j.radphyschem.2023.110810.
[83] Hirth SM, Marshall GJ, Court SA, Lloyd DJ. Effects of Si on the aging behaviour and formability of aluminium alloys based on AA6016. Mater Sci. Eng A 2001;319–321:452–6. https://doi.org/10.1016/S0921-5093(01)00969-8.
[84] Liang S, Wei LZ, Yu Z, Li Y, Jun LY, Zhuo WH, et al. Effect of mass ratio of Mg to Si on the properties of 6 series aluminum alloys. Nonferrous Met. Mater. Eng 2020;41:35–40. https://doi.org/10.13258/j.cnki.nmme.2020.02.006.
[85] Jiang SY, Wang RH. Grain size-dependent Mg/Si ratio effect on the microstructure and mechanical/electrical properties of Al-Mg-Si-Sc alloys. J Mater Sci Technol 2019;35:1354–63. https://doi.org/10.1016/j.jmst.2019.03.011.
[86] Gupta AK, Lloyd DJ, Court SA. Precipitation hardening in Al–Mg–Si alloys with and without excess Si. Mater Sci. Eng A 2001;316:11–7. https://doi.org/10.1016/S0921-5093(01)01247-3.
[87] Zupanič F, Klemenc J, Steinacher M, Glodež S. Microstructure, mechanical properties and fatigue behaviour of a new high-strength aluminium alloy AA 6086. J Alloys Compd 2023;941:168976. https://doi.org/10.1016/j.jallcom.2023.168976.
[88] Marioara CD, Andersen SJ, Stene TN, Hasting H, Walmsley J, Van Helvoort ATJ, et al. The effect of Cu on precipitation in Al–Mg–Si alloys. Philos Mag 2007;87:3385–413. https://doi.org/10.1080/14786430701287377.
[89] Marioara CD, Andersen SJ, Røyset J, Reiso O, Gulbrandsen-Dahl S, Nicolaisen T-E, et al. Improving thermal stability in Cu-containing Al-Mg-Si alloys by precipitate optimization. Metall Mater Trans A 2014;45:2938–49. https://doi.org/10.1007/s11661-014-2250-0.
[90] Sunde JK, Marioara CD, Van Helvoort ATJ, Holmestad R. The evolution of precipitate crystal structures in an Al-Mg-Si(-Cu) alloy studied by a combined HAADF-STEM and SPED approach. Mater. Charact 2018;142:458–69. https://doi.org/10.1016/j.matchar.2018.05.031.
[91] Liu F-Z, Qin J, Li Z, Yu C-B, Zhu X, Nagaumi H, et al. Precipitation of dispersoids in Al–Mg–Si alloys with Cu addition. J Mater Res Technol 2021;14:3134–9. https://doi.org/10.1016/j.jmrt.2021.08.123.
[92] Weng YY, Jia ZH, Ding LP, Liu MP, Wu XZ, Liu Q. Combined effect of pre-aging and Ag/Cu addition on the natural aging and bake hardening in Al-Mg-Si alloys. Prog Nat Sci: Mater Int 2018;28:363–70. https://doi.org/10.1016/j.pnsc.2018.04.007.
[93] Ding LP, Jia ZH, Nie JF, Weng YY, Cao LF, Chen HW, et al. The structural and compositional evolution of precipitates in Al-Mg-Si-Cu alloy. Acta Mater 2018;145:437–50. https://doi.org/10.1016/j.actamat.2017.12.036.
[94] Hu R, Ogura T, Tezuka H, Sato T, Liu Q. Dispersoid Formation and recrystallization behavior in an Al-Mg-Si-Mn alloy. J Mater Sci Technol 2010;26:237–43. https://doi.org/10.1016/S1005-0302(10)60040-0.
[95] Knipling K. Precipitation evolution in Al–Zr and Al–Zr–Ti alloys during aging at 450–600°C. Acta Mater 2008;56:1182–95. https://doi.org/10.1016/j.actamat.2007.11.011.
[96] Liu CW, Li YS, Zhu LH, Shi SJ. Effect of Coherent lattice mismatch on the morphology and kinetics of ordered precipitates. J Mater Eng Perform 2018;27:4968–77. https://doi.org/10.1007/s11665-018-3572-7.
[97] Wu X, Guan ZP, Yang ZZ, Wang X, Qiu F, Wang HY. Effect of Cu content on central-segregation composition and mechanical properties of Al–Mg–Si alloys produced by twin-roll casting. Mater Sci. Eng A 2023;869:144782. https://doi.org/10.1016/j.msea.2023.144782.
[98] Chakrabarti DJ, Laughlin DE. Phase relations and precipitation in Al–Mg–Si alloys with Cu additions. Prog Mater Sci 2004;49:389–410. https://doi.org/10.1016/S0079-6425(03)00031-8.
[99] Svenningsen G, Lein JE, Bjørgum A, Nordlien JH, Yu Y, Nisancioglu K. Effect of low copper content and heat treatment on intergranular corrosion of model AlMgSi alloys. Corros. Sci 2006;48:226–42. https://doi.org/10.1016/j.corsci.2004.11.025.
[100] Larsen MH, Walmsley JC, Lunder O, Mathiesen RH, Nisancioglu K. Intergranular corrosion of copper-containing AA6xxx AlMgSi aluminum alloys. J Electrochem Soc 2008;155. https://doi.org/10.1149/1.2976774.
[101] Hou XK, Qi P, Li BL, Wen SP, Wei W, Qi YT, et al. Precipitation behavior and mechanical properties of Al–1.0Mg–0.6Si–Cu (wt.%) alloy controlled by Cu content. Appl. Phys. A 2023;129:281. https://doi.org/10.1007/s00339-023-06580-7.
[102] Liang WJ, Rometsch PA, Cao LF, Birbilis N. General aspects related to the corrosion of 6xxx series aluminium alloys: exploring the influence of Mg/Si ratio and Cu. Corros. Sci 2013;76:119–28. https://doi.org/10.1016/j.corsci.2013.06.035.
[103] Svenningsen G, Larsen MH, Nordlien JH, Nisancioglu K. Effect of thermomechanical history on intergranular corrosion of extruded AlMgSi(Cu) model alloy. Corros. Sci 2006;48:3969–87. https://doi.org/10.1016/j.corsci.2006.03.018.
[104] Svenningsen G, Larsen MH, Walmsley JC, Nordlien JH, Nisancioglu K. Effect of artificial aging on intergranular corrosion of extruded AlMgSi alloy with small Cu content. Corros. Sci 2006;48:1528–43. https://doi.org/10.1016/j.corsci.2005.05.045.
[105] Svenningsen G, Larsen MH, Nordlien JH, Nisancioglu K. Effect of high temperature heat treatment on intergranular corrosion of AlMgSi(Cu) model

alloy. Corros. Sci 2006;48:258–72. https://doi.org/10.1016/j.corsci.2004.12.003.
[106] Zou Y, Liu Q, Jia Z, Xing Y, Ding L, Wang X. The intergranular corrosion behavior of 6000-series alloys with different Mg/Si and Cu content. Appl Surf Sci 2017;405:489–96. https://doi.org/10.1016/j.apsusc.2017.02.045.
[107] Kairy SK, Rometsch PA, Diao K, Nie JF, Davies CHJ, Birbilis N. Exploring the electrochemistry of 6xxx series aluminium alloys as a function of Si to Mg ratio, Cu content, ageing conditions and microstructure. Electrochim Acta 2016;190:92–103. https://doi.org/10.1016/j.electacta.2015.12.098.
[108] Li H, Zhao P, Wang Z, Mao Q, Fang B, Song R, Zheng Z. The intergranular corrosion susceptibility of a heavily overaged Al-Mg-Si-Cu alloy. Corros. Sci 2016;107:113–22. https://doi.org/10.1016/j.corsci.2016.02.025.
[109] Sarkar J, Kutty TRG, Wilkinson DS, Embury JD, Lloyd DJ. Tensile properties and bendability of T4 treated AA6111 aluminum alloys. Mater Sci. Eng A 2004;369:258–66. https://doi.org/10.1016/j.msea.2003.11.022.
[110] Lievers WB, Pilkey AK, Lloyd DJ. The influence of iron content on the bendability of AA6111 sheet. Materials Mater Sci. Eng A 2003;361:312–20. https://doi.org/10.1016/S0921-5093(03)00535-5.
[111] Österreicher JA, Arnoldt AR, Gneiger S, Kunschert G. Tolerance of Al–Mg–Si wrought alloys for high Fe contents: the role of effective Si. Metall Mater Trans A 2023;54:4472–80. https://doi.org/10.1007/s11661-023-07180-z.
[112] Qian Z, Liu XF, Zhao DG, Zhang GH. Effects of trace Mn addition on the elevated temperature tensile strength and microstructure of a low-iron Al–Si piston alloy. Mater Lett 2008;62:2146–9. https://doi.org/10.1016/j.matlet.2007.11.035.
[113] Trink B, Weißensteiner I, Uggowitzer PJ, Strobel K, Hofer-Roblyek A, Pogatscher S. Processing and microstructure–property relations of Al-Mg-Si-Fe crossover alloys. Acta Mater 2023;257. https://doi.org/10.1016/j.actamat.2023.119160.
[114] Rakhmonov J, Liu K, Rometsch P, Parson N, Chen XG. Effects of Al(MnFe)Si dispersoids with different sizes and number densities on microstructure and ambient/elevated-temperature mechanical properties of extruded Al–Mg–Si AA6082 alloys with varying Mn content. J Alloys Compd 2021;861. https://doi.org/10.1016/j.jallcom.2020.157937.
[115] Sigli C, De Geuser F, Deschamps A, Lépinoux J, Perez M. Recent advances in the metallurgy of aluminum alloys. Part II: age hardening. Comptes C. R. Phys 2018;19:688–709. https://doi.org/10.1016/j.crhy.2018.10.012.
[116] Qian XM, Parson N, Chen XG. Effects of Mn addition and related Mn-containing dispersoids on the hot deformation behavior of 6082 aluminum alloys. Mater Sci. Eng A 2019;764. https://doi.org/10.1016/j.msea.2019.138253.
[117] Zhu YT. Introduction to Heterostructured materials: a fast emerging field. Metall Mater Trans A 2021;52:4715–26. https://doi.org/10.1007/s11661-021-06438-8.
[118] Bösch D, Pogatscher S, Hummel M, Fragner W, Uggowitzer PJ, Göken M, Höppel HW. Secondary Al-Si-Mg high-pressure die casting alloys with enhanced ductility. Metall Mater Trans A 2014;46:1035–45. https://doi.org/10.1007/s11661-014-2700-8.
[119] Taghaddos E, Hejazi MM, Taghiabadi R, Shabestari SG. Effect of iron-intermetallics on the fluidity of 413 aluminum alloy. J Alloys Compd 2009;468:539–45. https://doi.org/10.1016/j.jallcom.2008.01.079.
[120] Roy S, Allard LF, Rodriguez A, Porter WD, Shyam A. Comparative evaluation of cast aluminum alloys for automotive cylinder heads: Part II—mechanical and thermal properties. Metall Mater Trans A 2017;48:2543–62. https://doi.org/10.1007/s11661-017-3986-0.
[121] Wei B, Pan S, Liao GZ, Ali A, Wang SB. Sc-containing hierarchical phase structures to improve the mechanical and corrosion resistant properties of Al-Mg-Si alloy. Mater Des 2022;218. https://doi.org/10.1016/j.matdes.2022.110699.
[122] Prach O, Trudonoshyn O, Randelzhofer P, Körner C, Durst K. Effect of Zr, Cr and Sc on the Al–Mg–Si–Mn high-pressure die casting alloys. Mater Sci. Eng A 2019;759:603–12. https://doi.org/10.1016/j.msea.2019.05.038.
[123] Trudonoshyn O, Prach O. Multistep nucleation and multi-modification effect of Sc in hypoeutectic Al-Mg-Si alloys. Heliyon 2019;5:e01202. https://doi.org/10.1016/j.heliyon.2019.e01202.
[124] Prach O, Trudonoshyn O, Randelzhofer P, Körner C, Durst K. Multi-alloying effect of Sc, Zr, Cr on the Al-Mg-Si-Mn high-pressure die casting alloys. Mater. Charact 2020;168. https://doi.org/10.1016/j.matchar.2020.110537.
[125] Xu P, Jiang F, Tang ZQ, Yan N, Jiang JY, Xu XD, Peng YY. Coarsening of Al_3Sc precipitates in Al-Mg-Sc alloys. J Alloys Compd 2019;781:209–15. https://doi.org/10.1016/j.jallcom.2018.12.133.
[126] Trudonoshyn O, Prach O, Randelzhofer P, Durst K, Körner C. Heat treatment of the new high-strength high-ductility Al–Mg–Si–Mn alloys with Sc, Zr and Cr additions. Materialia 2021;15:100981. https://doi.org/10.1016/j.mtla.2020.100981.
[127] Mahmoud MG, Mosleh AO, Mohamed MS, El-Moayed MH, Khalifa W, Pozdniakov AV, Salem S. The impact of Ce-containing precipitates on the solidification behavior, microstructure, and mechanical properties of Al-6063. J Alloys Compd 2023;94:169805. https://doi.org/10.1016/j.jallcom.2023.169805.
[128] Zheng QJ, Wu J, Jiang HX, Zhang LL, Zhao JZ, He J. Effect of micro-alloying element La on corrosion behavior of Al-Mg-Si alloys. Corros. Sci 2021;179:109113. https://doi.org/10.1016/j.corsci.2020.109113.
[129] Zheng QJ, Zhang LL, Jiang HX, Zhao JZ, He J. Effect mechanisms of micro-alloying element La on microstructure and mechanical properties of hypoeutectic Al-Si alloys. J Mater Sci Technol 2020;47:142–51. https://doi.org/10.1016/j.jmst.2019.12.021.
[130] Wang SH, Zhou HP, Kang YP. The influence of rare earth elements on microstructures and properties of 6061 aluminum alloy vacuum-brazed joints. J Alloys Compd 2003;352:79–83. https://doi.org/10.1016/S0925-8388(02)01117-9.
[131] Li DQ, Cai SL, Gu J, Liu SC, Si JJ. Co-doping of La/Ce and La/Er induced precipitation strengthening for designing high strength Al-Mg-Si electrical conductive alloys. Mater Today Commun 2023;36:106666. https://doi.org/10.1016/j.mtcomm.2023.106666.
[132] Jiang HX, Li SX, Zheng QJ, Zhang LL, He J, Song Y, Deng CK, Zhao JZ. Effect of minor lanthanum on the microstructures, tensile and electrical properties of Al-Fe alloys. Mater Des 2020;195:108991. https://doi.org/10.1016/j.matdes.2020.108991.
[133] Pandee P, Gourlay CM, Belyakov SA, Patakham U, Zeng G, Limmaneevichitr C. AlSi2Sc2 intermetallic formation in Al-7Si-0.3Mg-xSc alloys and their effects on as-cast properties. J Alloys Compd 2018;731:1159–70. https://doi.org/10.1016/j.jallcom.2017.10.125.
[134] Mikhaylovskaya AV, Esmaeili Ghayoumabadi M, Mochugovskiy AG. Superplasticity and mechanical properties of Al–Mg–Si alloy doped with eutectic-forming Ni and Fe, and dispersoid-forming Sc and Zr elements. Mater Sci. Eng A 2021;817:141319. https://doi.org/10.1016/j.msea.2021.141319.
[135] Mochugovskiy AG, Mikhaylovskaya AV. Comparison of precipitation kinetics and mechanical properties in Zr and Sc-bearing aluminum-based alloys. Mater Lett 2020;275:128096. https://doi.org/10.1016/j.matlet.2020.128096.
[136] Dorin T, Ramajayam M, Lamb J, Langan T. Effect of Sc and Zr additions on the microstructure/strength of Al-Cu binary alloys. Mater Sci. Eng A 2017;707:58–64. https://doi.org/10.1016/j.msea.2017.09.032.
[137] Li M, Pan Q, Shi Y, Sun X, Xiang H. High strain rate superplasticity in an Al–Mg–Sc–Zr alloy processed via simple rolling. Mater Sci. Eng A 2017;687:298–305. https://doi.org/10.1016/j.msea.2017.01.091.
[138] Sitdikov O, Avtokratova E, Markushev M. Influence of strain rate on grain refinement in the Al-Mg-Sc-Zr alloy during high-temperature multidirectional isothermal forging. Mater. Charact 2019;157:109885. https://doi.org/10.1016/j.matchar.2019.109885.
[139] Mochugovskiy AG, Mikhaylovskaya AV, Zadorognyy MY, Golovin IS. Effect of heat treatment on the grain size control, superplasticity, internal friction, and mechanical properties of zirconium-bearing aluminum-based alloy. J Alloys Compd 2021;856. https://doi.org/10.1016/j.jallcom.2020.157455.
[140] Meng Y, Zhao ZH, Cui JZ. Effect of minor Zr and Sc on microstructures and mechanical properties of Al–Mg–Si–Cu–Cr–V alloys. Trans. Nonferrous Met. Soc. China 2013;23:1882–9. https://doi.org/10.1016/S1003-6326(13)62673-4.
[141] Zhang MX, Ning H, Wang C, Guan K, Wang X, Li Z-G, et al. Effectively mitigated macro-segregation and improved tensile properties of twin-roll cast Al–Mg–Si (6022) alloy strips via Zr addition. Mater Sci. Eng A 2023;880:145318. https://doi.org/10.1016/j.msea.2023.145318.
[142] Wang X, Ma PK, Meng ZY, Zhang SY, Liu X, Wang C, et al. Effect of trace Cr alloying on centerline segregations in sub-rapid solidified Al–Mg–Si (AA6061) alloys fabricated by twin-roll casting. Mater Sci. Eng A 2021;825:141896. https://doi.org/10.1016/j.msea.2021.141896.
[143] Weng Y, Jia Z, Ding L, Pan Y, Liu Y, Liu Q. Effect of Ag and Cu additions on natural aging and precipitation hardening behavior in Al-Mg-Si alloys. J Alloys Compd 2017;695:2444–52. https://doi.org/10.1016/j.jallcom.2016.11.140.
[144] Weng Y, Jia Z, Ding L, Liu M, Wu X, Liu Q. Combined effect of pre-aging and Ag/Cu addition on the natural aging and bake hardening in Al-Mg-Si alloys. Prog Nat Sci: Mater Int 2018;28:363–70. https://doi.org/10.1016/j.pnsc.2018.04.007.
[145] Khangholi SN, Javidani M, Maltais A, Chen XG. Effect of Ag and Cu addition on the strength and electrical conductivity of Al-Mg-Si alloys using conventional and modified thermomechanical treatments. J Alloys Compd 2022;914:165242. https://doi.org/10.1016/j.jallcom.2022.165242.
[146] Marioara CD, Nakamura J, Matsuda K, Andersen SJ, Holmestad R, Sato T, et al. HAADF-STEM study of β′-type precipitates in an over-aged Al–Mg–Si–Ag alloy. Philos Mag 2012;92:1149–58. https://doi.org/10.1080/14786435.2011.642319.
[147] Weng Y, Ding L, Zhang Z, Jia Z, Wen B, Liu Y, et al. Effect of Ag addition on the precipitation evolution and interfacial segregation for Al–Mg–Si alloy. Acta Mater 2019;180:301–16. https://10.1016/j.actamat.2019.09.015.
[148] Mørtsell EA, Andersen SJ, Friis J, Marioara CD, Holmestad R. Atomistic details of precipitates in lean Al–Mg–Si alloys with trace additions of Ag and Ge studied by HAADF-STEM and DFT. Philos Mag 2017;97:851–66. https://10.1080/14786435.2017.1281461.
[149] Singh P, Ramacharyulu DA, Kumar N, Saxena KK, Eldin SM. Change in the structure and mechanical properties of Al–Mg–Si alloys caused by the addition of other elements: a comprehensive review. J Mater Res Technol 2023;27:1764–96. https://doi.org/10.1016/j.jmrt.2023.09.220.
[150] Oe Y, Matsuda K, Nakamura J, Ikeno S. Effect of Cu/Ag addition on age-precipitation in two step aged Al-Mg-Si alloys. Adv Mater Res 2014;922:560–2. https://10.4028/www.scientific.net/AMR.922.560.
[151] Sauvage X, Lee S, Matsuda K, Horita Z. Origin of the influence of Cu or Ag micro-additions on the age hardening behavior of ultrafine-grained Al-Mg-Si alloys. J Alloys Compd 2017;710:199–204. https://doi.org/10.1016/j.jallcom.2017.03.250.
[152] Xu X, Zhu W, Yuan M, Liang C, Deng Y. The effect of Zn content on the microstructure and mechanical properties of the Al-mg-Si alloy. Mater. Charact. 2023;198:112714. https://doi.org/10.1016/j.matchar.2023.112714.
[153] Zhu S, Li Z, Yan L, Li X, Huang S, Yan H, et al. Natural aging behavior in pre-aged Al–Mg–Si–Cu alloys with and without Zn addition. J Alloys Compd 2019;773:496–502. https://doi.org/10.1016/j.jallcom.2018.09.244.
[154] Yang W, Shen W, Zhang R, Cao K, Zhang J, Liu L. Enhanced age-hardening by synergistic strengthening from MgSi and MgZn precipitates in Al-Mg-Si alloy with

Zn addition. Mater. Charact. 2020;169:110579. https://doi.org/10.1016/j.matchar.2020.110579.
[155] Ding XP, Cui H, Zhang JX, Li HX, Guo MX, Lin Z, et al. The effect of Zn on the age hardening response in an Al–Mg–Si alloy. Mater Des 2015;65:1229–35. https://doi.org/10.1016/j.matdes.2014.09.086.
[156] Cai Y-H, Wang C, Zhang J-S. Microstructural characteristics and aging response of Zn-containing Al-Mg-Si-Cu alloy. Int J Min Met Mater 2013;20:659–64. https://10.1007/s12613-013-0780-x.
[157] Guo MX, Zhang Y, Zhang XK, Zhang JS, Zhuang LZ. Non-isothermal precipitation behaviors of Al-Mg-Si-Cu alloys with different Zn contents. Mater Sci. Eng A 2016;669:20–32. https://doi.org/10.1016/j.msea.2016.05.060.
[158] Saito T, Wenner S, Osmundsen E, Marioara CD, Andersen SJ, Røyset J, Lefebvre W, Holmestad R. The effect of Zn on precipitation in Al–Mg–Si alloys. Philos Mag 2014;94:2410–25. https://10.1080/14786435.2014.913819.
[159] Marioara CD, Lervik A, Grønvold J, Lunder O, Wenner S, Furu T, Holmestad R. The correlation between intergranular corrosion resistance and copper content in the precipitate microstructure in an AA6005A alloy. Metall Mater Trans A 2018;49:5146–56. https://10.1007/s11661-018-4789-7.
[160] Zhang X, Zhou X, Nilsson J-O. Corrosion behaviour of AA6082 Al-Mg-Si alloy extrusion: the influence of quench cooling rate. Corros. Sci 2019;150:100–9. https://doi.org/10.1016/j.corsci.2019.01.030.
[161] Bartawi EH, Marioara CD, Shaban G, Rahimi E, Mishin OV, Sunde JK, Gonzalez-Garcia Y, Holmestad R, Ambat R. Effects of grain boundary chemistry and precipitate structure on intergranular corrosion in Al-Mg-Si alloys doped with Cu and Zn. Corros. Sci 2024;236:112227. https://doi.org/10.1016/j.corsci.2024.112227.
[162] Kairy SK, Alam T, Rometsch PA, Davies CHJ, Banerjee R, Birbilis N. Understanding the Origins of intergranular corrosion in copper-containing Al-Mg-Si alloys. Metall Mater Trans A 2016;47:985–9. https://10.1007/s11661-015-3296-3.
[163] Ahmed MS, Anwar MS, Islam MS, Arifuzzaman M. Experimental study on the effects of three alloying elements on the mechanical, corrosion and microstructural properties of aluminum alloys. Results Mater 2023;20:100485. https://doi.org/10.1016/j.rinma.2023.100485.
[164] Tai C-L, Pua Y-M, Chung T-F, Yang Y-L, Chen H-R, Chen C-Y, Wang S-H, Yu C-Y, Yang J-R. The effect of minor addition of Mn in AA7075 Al–Zn–Mg–Cu aluminum alloys on microstructural evolution and mechanical properties in warm forming and paint baking processes. Int. J. Lightweight Mater. Manuf 2023;6:521–33. https://doi.org/10.1016/j.ijlmm.2023.04.001.
[165] Langille MR, Diak BJ, De Geuser F, Deschamps A, Guiglionda G. Asymmetry of strain rate sensitivity between up- and down-changes in 6000 series aluminium alloys of varying Si content. Mater Sci. Eng A 2020;788:139517. https://doi.org/10.1016/j.msea.2020.139517.
[166] Rakhmonov J, Liu K, Pan L, Breton F, Chen XG. Enhanced mechanical properties of high-temperature-resistant Al–Cu cast alloy by microalloying with Mg. J Alloys Compd 2020;827:154305. https://doi.org/10.1016/j.jallcom.2020.154305.
[167] Xu Y, Zhang Z, Gao Z, Bai Y, Zhao P, Mao W. Effect of main elements (Zn、Mg and Cu) on the microstructure, castability and mechanical properties of 7xxx series aluminum alloys with Zr and Sc. Mater. Charact 2021;182:111559. https://doi.org/10.1016/j.matchar.2021.111559.
[168] Sokoluk M, Yuan J, Pan S, Li X. Nanoparticles enabled mechanism for hot cracking elimination in aluminum alloys. Mater Trans 2021;52:3083–96. https://doi.org/10.1007/s11661-021-06302-9.
[169] Liu X, Liu Y, Zhou Z, Wang K, Zhan Q, Xiao X. Grain refinement and crack inhibition of selective laser melted AA2024 aluminum alloy via inoculation with TiC–TiH2. Mater Sci. Eng A 2021;813:141171. https://doi.org/10.1016/j.msea.2021.141171.
[170] Yang H, Tian S, Gao T, Nie J, You Z, Liu G, et al. High-temperature mechanical properties of 2024 Al matrix nanocomposite reinforced by TiC network architecture. Mater Sci. Eng A 2019;763:138121. https://doi.org/10.1016/j.msea.2019.138121.
[171] Zhang M, Kelly P, Easton M, Taylor J. Crystallographic study of grain refinement in aluminum alloys using the edge-to-edge matching model. Acta Mater 2005;53:1427–38. https://doi.org/10.1016/j.actamat.2004.11.037.
[172] Li S-S, Qiu F, Yang H-Y, Liu S, Liu T-S, Chen L-Y, et al. Strengthening of dislocation and precipitation for high strength and toughness casting Al–Zn–Mg–Cu alloy via trace TiB2+TiC particles. Mater Sci. Eng A 2022;857:144107. https://doi.org/10.1016/j.msea.2022.144107.
[173] Yao X-Y, Qiu F, Yang H-Y, Shu S-L, Li T-T, Jiang Q-C. Role of in-situ nanocrystalline in solidification behaviors manipulation, microstructure refinement, and mechanical properties enhancement of Al-Cu4/Al-Mg1 alloys. Mater. Charact 2022;194:112408. https://doi.org/10.1016/j.matchar.2022.112408.
[174] Dong BX, Li Q, Yang HY, Liu TS, Qiu F, Shu SL, , et alZhang LC. Synergistic optimization in solidification microstructure and mechanical performance of novel (TiC N − TiB2)p/Al nanocomposites: design, tuning and mechanism. Composites, Part A 2022;155. https://doi.org/10.1016/j.compositesa.2022.106843.
[175] Ma XD, Yang HY, Dong BX, Shu SL, Wang Z, Shao Y, et al. Novel method to achieve synergetic strength–ductility improvement of Al–Cu alloy by in situ TiC–TiB2 particles via direct reaction synthesis. Mater Sci. Eng A 2023;869:144810. https://doi.org/10.1016/j.msea.2023.144810.
[176] Turnbull D, Vonnegut B. Nucleation Catalysis. Ind Eng Chem 2002;44:1292–8. https://doi.org/10.1021/ie50510a031.
[177] Liu T-S, Qiu F, Yang H-Y, Tan C-L, Dong B-X, Xie J-F, et al. Versatility of trace nano-TiC–TiB2 in collaborative control of solidification-rolling-welding microstructural evolution in Al–Mg–Si alloy for enhanced properties. Mater Sci. Eng A 2022;851:143661. https://doi.org/10.1016/j.msea.2022.143661.
[178] Geng R, Qiu F, Zhao Q-L, Gao Y-Y, Jiang Q-C. Effects of nanosized TiCp on the microstructure evolution and tensile properties of an Al-Mg-Si alloy during cold rolling. Mater Sci. Eng A 2019;743:98–105. https://doi.org/10.1016/j.msea.2018.11.078.
[179] Greer AL, Bunn AM, Tronche A, Evans PV, Bristow DJ. Modelling of inoculation of metallic melts: application to grain refinement of aluminium by Al–Ti–B. Acta Mater 2000;48:2823–35. https://doi.org/10.1016/S1359-6454(00)00094-X.
[180] Stjohn DH, Qian M, Easton MA, Cao P. The Interdependence Theory: the relationship between grain formation and nucleant selection. Acta Mater 2011;59:4907–21. https://doi.org/10.1016/j.actamat.2011.04.035.
[181] Zhang L, Jiang H, He J, Zhao J. A new model of growth restriction factor for hypoeutectic aluminium alloys. Scr. Mater 2020;179:99–101. https://doi.org/10.1016/j.scriptamat.2020.01.009.
[182] Wang K, Jiang HY, Jia YW, Zhou H, Wang QD, Ye B, et al. Nanoparticle-inhibited growth of primary aluminum in Al–10Si alloys. Acta Mater 2016;103:252–63. https://doi.org/10.1016/j.actamat.2015.10.005.
[183] Chen L-Y, Xu J-Q, Choi H, Konishi H, Jin S, Li X-C. Rapid control of phase growth by nanoparticles. Nat Commun 2014;5:3879. https://doi.org/10.1038/ncomms4879.
[184] Li H, Wang X, Chai L, Wang H, Chen Z, Xiang Z, et al. Microstructure and mechanical properties of an in-situ TiB2/Al-Zn-Mg-Cu-Zr composite fabricated by Melt-SHS process. Mater Sci. Eng A 2018;720:60–8. https://doi.org/10.1016/j.msea.2018.02.025.
[185] Zhao S, Zhang H, Cui Z, Chen D, Chen Z. Particle dispersion and grain refinement of in-situ TiB2 particle reinforced 7075 Al composite processed by elliptical cross-section torsion extrusion. J Alloys Compd 2020;834:155136. https://doi.org/10.1016/j.jallcom.2020.155136.
[186] Limmaneevichitr C, Eidhed W. Novel technique for grain refinement in aluminum casting by Al–Ti–B powder injection. Mater Sci. Eng A 2003;355:174–9. https://doi.org/10.1016/S0921-5093(03)00061-3.
[187] Chen G-C, Li X. Effect of TiC nano-treating on the fluidity and solidification behavior of aluminum alloy 6063. J Mater Process Technol 2024;324:118241. https://doi.org/10.1016/j.jmatprotec.2023.118241.
[188] Ma S, Wang Y, Wang X. Microstructures and mechanical properties of an Al-Cu-Mg-Sc alloy reinforced with in-situ TiB2 particulates. Mater Sci. Eng A 2020;788:139603. https://doi.org/10.1016/j.msea.2020.139603.
[189] Nadella R, Eskin DG, Du Q, Katgerman L. Macrosegregation in direct-chill casting of aluminium alloys. Prog Mater Sci 2008;53:421–80. https://doi.org/10.1016/j.pmatsci.2007.10.001.
[190] Liu X, Jia H-L, Wang C, Wu X, Zha M, Wang H-Y. Enhancing mechanical properties of twin-roll cast Al–Mg–Si–Fe alloys by regulating Fe-bearing phases and macro-segregation. Mater Sci. Eng A 2022;831:142256. https://doi.org/10.1016/j.msea.2021.142256.
[191] Liu X, Zhao Q, Ji Z, Wang B, Zhu Y, Jiang Q. Effectively mitigated macro-segregation and improved tensile properties of twin-roll casting Al-Cu strips via the addition of TiC nanoparticles. J Mater Process Technol 2021;296:117200. https://doi.org/10.1016/j.jmatprotec.2021.117200.
[192] Birol Y. Analysis of macro segregation in twin-roll cast aluminium strips via solidification curves. J Alloys Compd 2009;486:168–72. https://doi.org/10.1016/j.jallcom.2009.06.167.
[193] Šlapáková M, Zimina M, Zaunschirm S, Kastner J, Bajer J, Cieslar M. 3D analysis of macrosegregation in twin-roll cast AA3003 alloy. Mater. Charact 2016;118:44–9. https://doi.org/10.1016/j.matchar.2016.04.023.
[194] Kumar R, Gupta A, Kumar A, Chouhan RN, Khatirkar RK. Microstructure and texture development during deformation and recrystallisation in strip cast AA8011 aluminum alloy. J Alloys Compd 2018;742:369–82. https://doi.org/10.1016/j.jallcom.2018.01.280.
[195] Shiju L, Jiang T, Wang J, Chen L, Wei B, Li Y, et al. Effects of different external fields on the microstructure and mechanical properties of novel Al Cu Li alloy during twin-roll casting. Mater Sci. Eng A 2019;757:14–22. https://doi.org/10.1016/j.msea.2019.04.079.
[196] Sun KM, Li L, Chen SD, Xu GM, Chen G, Misra RDK, et al. A new approach to control centerline macrosegregation in Al-Mg-Si alloys during twin roll continuous casting. Mater Lett 2017;190:205–8. https://doi.org/10.1016/j.matlet.2016.12.109.
[197] Birol Y. The performance of Al–Ti–C grain refiners in twin-roll casting of aluminium foilstock. J Alloys Compd 2007;430:179–87. https://doi.org/10.1016/j.jallcom.2006.05.027.
[198] Liu X, Zhao Q, Jiang Q. Effects of cooling rate and TiC nanoparticles on the microstructure and tensile properties of an Al–Cu cast alloy. Mater Sci. Eng A 2020;790:139737. https://doi.org/10.1016/j.msea.2020.139737.
[199] Wang B, Zhao Q, Qiu F, Jiang Q. Effect of Mg and Si contents and TiC nanoparticles on the center segregation susceptibility of twin-roll cast Al–Mg–Si alloys. J Mater Res Technol 2023;25:411–9. https://doi.org/10.1016/j.jmrt.2023.05.240.
[200] Wang B, Ji Z, Qiu F, Zhao Q, Jiang Q. The effect of the TiC-TiB2 nanoparticles on the microstructure and mechanical properties of Al-Mn-Si strips fabricated by twin-roll casting. J Alloys Compd 2023;947:169648. https://doi.org/10.1016/j.jallcom.2023.169648.
[201] Lv Z, Du F, An Z, Huang H, Xu Z, Sun J. Centerline segregation mechanism of twin-roll cast A3003 strip. J Alloys Compd 2015;643:270–4. https://doi.org/10.1016/j.jallcom.2015.04.132.

[202] Martin JH, Yahata BD, Hundley JM, Mayer JA, Schaedler TA, Pollock TM. 3D printing of high-strength aluminium alloys. Nature 2017;549:365–9. https://doi.org/10.1038/nature23894.
[203] Choi H, Cho W-H, Konishi H, Kou S, Li X. Nanoparticle-induced superior hot tearing resistance of A206 alloy. Metall Mater Trans A 2012;44:1897–907. https://doi.org/10.1007/s11661-012-1531-8.
[204] Liu XC, Ye T, Li YZ, Pei XJ, Sun Z. Quasi-in-situ characterization of microstructure evolution in friction stir welding of aluminum alloy. J Mater Res Technol 2023;25:6380–94. https://doi.org/10.1016/j.jmrt.2023.07.101.
[205] Wang R, Zhu Q, Zuo Y, Cheng L, Wang J. The control of as-cast structure of 2024 aluminum alloy with intensive melt shearing and its effect on microstructure and mechanical properties after T4 treatment. J Mater Res Technol 2023;24:3179–93. https://doi.org/10.1016/j.jmrt.2023.03.225.
[206] Liu T-S, Qiu F, Yang H-Y, Shu S-L, Xie J-F, Jiang Q-C, et al. Insights into the influences of nanoparticles on microstructure evolution mechanism and mechanical properties of friction-stir-welded Al 6061 alloys. Mater Sci. Eng A 2023;871:144929. https://doi.org/10.1016/j.msea.2023.144929.
[207] Que Z, Wang Y, Fan Z, Hashimoto T, Zhou X. Enhanced heterogeneous nucleation of Al6(Fe,Mn) compound in Al alloys by interfacial segregation of Mn on TiB_2 particles surface. Mater Lett 2022;323:132570. https://doi.org/10.1016/j.matlet.2022.132570.
[208] Dai S, Zhang H, Bian Z, Geng J, Chen Z, Wang L, Wang M, Wang H. Insight into the recrystallization behavior and precipitation reaction of in-situ nano TiB_2/Al Cu Mg composite during heat treatment. Mater. Charact 2021;181:111458. https://doi.org/10.1016/j.matchar.2021.111458.
[209] Wang X-Y, Jiang J-T, Li G-A, Wang X-M, Shao W-Z, Zhen L. Particle-stimulated nucleation and recrystallization texture initiated by coarsened Al2CuLi phase in Al–Cu–Li alloy. J Mater Res Technol 2021;10:643–50. https://doi.org/10.1016/j.jmrt.2020.12.046.
[210] Wang L, Qiu F, Zhao Q, Zha M, Jiang Q. Superior high creep resistance of in situ nano-sized TiCx/Al-Cu-Mg composite. Sci Rep 2017;7:4540. https://doi.org/10.1038/s41598-017-04816-0.
[211] Geng R, Jia S-Q, Qiu F, Zhao Q-L, Jiang Q-C. Effects of nanosized TiC and TiB2 particles on the corrosion behavior of Al-Mg-Si alloy. Corros. Sci 2020;167:108479. https://doi.org/10.1016/j.corsci.2020.108479.
[212] Liu T-S, Qiu F, Dong B-X, Geng R, Zha M, Yang H-Y, et al. Role of trace nanoparticles in establishing fully optimized microstructure configuration of cold-rolled Al alloy. Mater Des 2021;206:109743. https://doi.org/10.1016/j.matdes.2021.109743.
[213] Wang H, Li Y, Xu G, Li J, Zhang T, Lu B, Yu W, Wang Y, Du Y. Effect of nano-TiC/TiB_2 particles on the recrystallization and precipitation behavior of AA2055-TiC+TiB2 alloys. Mater Sci. Eng A 2023;871:144927. https://doi.org/10.1016/j.msea.2023.144927.
[214] Chen Z, Sun GA, Wu Y, Mathon MH, Borbely A, Chen D, et al. Multi-scale study of microstructure evolution in hot extruded nano-sized TiB_2 particle reinforced aluminum composites. Mater Des 2017;116:577–90. https://doi.org/10.1016/j.matdes.2016.12.070.
[215] Doherty RD, Hughes DA, Humphreys FJ, Jonas JJ, Jensen DJ, Kassner ME, et al. Current issues in recrystallization: a review. Mater Sci. Eng A 1997;238:219–74. https://doi.org/10.1016/S0921-5093(97)00424-3.
[216] Zhang SL, Shi XX, Zhao YT, Zhang BR, Liang ZP, Yin HS, et al. Preparation, microstructures and mechanical properties of in-situ (TiB_2+ZrB_2)/AlSi9Cu3 composites. J Alloys Compd 2016;673:349–57. https://doi.org/10.1016/j.jallcom.2016.02.243.
[217] Xie Z, Jiang R, Li X, Zhang L, Li A, He Z. Microstructural evolution and mechanical properties of TiB2/2195 composites fabricated by ultrasonic-assisted in-situ casting. Ultrason Sonochem 2022;90:106203. https://doi.org/10.1016/j.ultsonch.2022.106203.
[218] Xu X, Zhao H, Hu Y, Zong L, Qin J, Zhang J, et al. Effect of hot compression on the microstructure evolution of aluminium bronze alloy. J Mater Res Technol 2022;19:3760–76. https://doi.org/10.1016/j.jmrt.2022.06.122.
[219] Li XM, Starink MJ. Identification and analysis of intermetallic phases in overaged Zr-containing and Cr-containing Al–Zn–Mg–Cu alloys. J Alloys Compd 2011;509:471–6. https://doi.org/10.1016/j.jallcom.2010.09.064.
[220] Wang L, Qiu F, Zhao Q, Wang H, Jiang Q. Simultaneously increasing the elevated-temperature tensile strength and plasticity of in situ nano-sized TiCx/Al-Cu-Mg composites. Mater. Charact 2017;125:7–12. https://doi.org/10.1016/j.matchar.2017.01.013.
[221] Wu X, Zhang H, Ma Z, Tao T, Gui J, Song W, et al. Interactions between Fe-rich intermetallics and Mg-Si phase in Al-7Si-xMg alloys. J J. Alloys Compd 2019;786:205–14. https://doi.org/10.1016/j.jallcom.2019.01.352.
[222] Ma Y, Addad A, Ji G, Zhang MX, Ji V. Atomic-scale investigation of the interface precipitation in a TiB2 nanoparticles reinforced Al-Zn-Mg-Cu matrix composite. Acta Mater 2019;185:287–99. https://doi.org/10.1016/j.actamat.2019.11.068.
[223] Zhao Y, Ma X, Zhao X, Chen H, Liu X. Enhanced aging kinetic of Al3BC/6061 Al composites and its micro-mechanism. J Alloys Compd 2017;726:1053–61. https://doi.org/10.1016/j.jallcom.2017.08.053.
[224] Arsenault RJ, Shi N. Dislocation generation due to differences between the coefficients of thermal expansion. Mater. Sci. Eng 1986;81:175–87. https://doi.org/10.1016/0025-5416(86)90261-2.
[225] Kuijpers NCW, Vermolen FJ, Vuik C, Koenis PTG, Nilsen KE, Zwaag SVD. The dependence of the β-AlFeSi to α-Al(FeMn)Si transformation kinetics in Al–Mg–Si alloys on the alloying elements. Mater Sci. Eng A 2005;394:9–19. https://doi.org/10.1016/j.msea.2004.09.073.
[226] Pal S, Mitra R, Bhanuprasad VV. Aging behaviour of Al–Cu–Mg alloy–SiC composites. Mater Sci. Eng A 2008;480:496–505. https://doi.org/10.1016/j.msea.2007.07.072.
[227] Cui Y, Jin T, Cao L, Liu F. Aging behavior of high volume fraction SiCp/Al composites fabricated by pressureless infiltration. J J. Alloys Compd 2016;681:233–9. https://doi.org/10.1016/j.jallcom.2016.04.127.
[228] Wang Z, Li C, Wang H, Zhu X, Wu M, Li J, et al. Aging behavior of nano-SiC/2014Al composite fabricated by powder metallurgy and hot extrusion techniques. J Mater Sci Technol 2016;32:1008–12. https://doi.org/10.1016/j.jmst.2016.07.011.
[229] Casati R, Fiocchi J, Fabrizi A, Lecis N, Bonollo F, Vedani M. Effect of ball milling on the ageing response of Al2618 composites reinforced with SiC and oxide nanoparticles. J Alloys Compd 2017;693:909–20. https://doi.org/10.1016/j.jallcom.2016.09.265.
[230] Zheng TQ, Pan SH, Liu J, Moodispaw M, Luo AA, Taub AI, et al. Study on nano-treating of Al-Mg-Si-Cu alloys with TiC nanoparticles. J Alloys Compd 2023;947. https://doi.org/10.1016/j.jallcom.2023.169405.
[231] Ma GN, Wang D, Liu ZY, Xiao BL, Ma ZY. An investigation on particle weakening in T6-treated SiC/Al–Zn–Mg–Cu composites. Mater. Charact 2019;158:109966. https://doi.org/10.1016/j.matchar.2019.109966.
[232] Yang H, Gao T, Zhang H, Nie J, Liu X. Enhanced age-hardening behavior in Al–Cu alloys induced by in-situ synthesized TiC nanoparticles. J Mater Sci Technol 2019;35:374–82. https://doi.org/10.1016/j.jmst.2018.09.029.
[233] Wang Z, Tan J, Sun BA, Scudino S, Prashanth KG, Zhang WW, Li YY, Eckert J. Fabrication and mechanical properties of Al-based metal matrix composites reinforced with $Mg_{65}Cu_{20}Zn_5Y_{10}$ metallic glass particles. Mater Sci. Eng A 2014;600:53–8. https://doi.org/10.1016/j.msea.2014.02.003.
[234] Liu TS, Qiu F, Yang HY, Tan CL, Dong BX, Xie JF, et al. Versatility of trace nano-TiC–TiB_2 in collaborative control of solidification-rolling-welding microstructural evolution in Al–Mg–Si alloy for enhanced properties. Mater Sci. Eng A 2022;851:143661. https://doi.org/10.1016/j.msea.2022.143661.
[235] Liu TS, Qiu F, Dong BX, Geng R, Zha M, Yang HY, et al. Role of trace nanoparticles in establishing fully optimized microstructure configuration of cold-rolled Al alloy. Mater Des 2021;206:109743. https://doi.org/10.1016/j.matdes.2021.109743.
[236] Reddy AP, Vamsirao P, Strengthening RN. Mechanical properties of SiC and graphite reinforced Al6061 hybrid nanocomposites processed through Ultrasonically assisted casting technique. Trans Indian Inst Met 2019;72:2533–46. https://doi.org/10.1007/s12666-019-01723-y.
[237] Sanaty-Zadeh A, Rohatgi PK. Corrigendum to: comparison between current models for the strength of particulate-reinforced metal matrix nanocomposites with emphasis on consideration of Hall–Petch effect. Mater Sci. Eng A 2012;551:112–8. https://doi.org/10.1016/j.msea.2011.10.043.
[238] Li JL, Xiong YC, Wang XD, Yan SJ, Yang C, He WW, et al. Microstructure and tensile properties of bulk nanostructured aluminum/graphene composites prepared via cryomilling. Mater Sci. Eng A 2015;626:400–5. https://doi.org/10.1016/j.msea.2014.12.102.
[239] Li Y, Liu W, Ortalan V, Li WF, Zhang Z, Vogt R, et al. HRTEM and EELS study of aluminum nitride in nanostructured Al 5083/B_4C processed via cryomilling. Acta Mater 2010;58:1732–40. https://doi.org/10.1016/j.actamat.2009.11.015.
[240] Kang Y-C, Chan SL-I. Tensile properties of nanometric Al_2O_3 particulate-reinforced aluminum matrix composites. Mater Chem Phys 2004;85:438–43. https://doi.org/10.1016/j.matchemphys.2004.02.002.
[241] Karbalaei Akbari M, Baharvandi HR, Shirvanimoghaddam K. Tensile and fracture behavior of nano/micro TiB_2 particle reinforced casting A356 aluminum alloy composites. Mater Des 2015;66:150–61. https://doi.org/10.1016/j.matdes.2014.10.048 (1980-2015).
[242] Wang Z, Song M, Sun C, He Y. Effects of particle size and distribution on the mechanical properties of SiC reinforced Al-Cu alloy composites. Mater Sci. Eng A 2011;528:1131–7. https://doi.org/10.1016/j.msea.2010.11.028.
[243] Yar AA, Montazerian M, Abdizadeh H, Baharvandi HR. Microstructure and mechanical properties of aluminum alloy matrix composite reinforced with nano-particle MgO. J Alloys Compd 2009;484:400–4. https://doi.org/10.1016/j.jallcom.2009.04.117.
[244] Radha A, Vijayakumar KR. An investigation of mechanical and wear properties of AA6061 reinforced with silicon carbide and graphene nano particles-Particulate composites. Mater Today: Proc 2016;3:2247–53. https://doi.org/10.1016/j.matpr.2016.04.133.
[245] Fadavi Boostani A, Tahamtan S, Jiang ZY, Wei D, Yazdani S, Azari Khosroshahi R, et al. Enhanced tensile properties of aluminium matrix composites reinforced with graphene encapsulated SiC nanoparticles. Composites, Part A 2015;68:155–63. https://doi.org/10.1016/j.compositesa.2014.10.010.
[246] Ding M, Xing WQ, Yu XY, Ma L, Zuo W, Ji ZQ. Effect of micro alumina particles additions on the interfacial behavior and mechanical properties of Sn-9Zn-1Al2O3 nanoparticles on low temperature wetting and soldering of 6061 aluminum alloys. J Alloys Compd 2018;739:481–8. https://doi.org/10.1016/j.jallcom.2017.12.247.
[247] Geng R, Jia SQ, Qiu F, Zhao QL, Jiang QC. Effects of nanosized TiC and TiB2 particles on the corrosion behavior of Al-Mg-Si alloy. Corros. Sci 2020;167:108479. https://doi.org/10.1016/j.corsci.2020.108479.
[248] Liu TS, Qiu F, Yang HY, Shu SL, Xie JF, Jiang QC, et al. Insights into the influences of nanoparticles on microstructure evolution mechanism and mechanical properties of friction-stir-welded Al 6061 alloys. Mater Sci. Eng A 2023;871:144929. https://doi.org/10.1016/j.msea.2023.144929.
[249] Zhu JW, Jiang WM, Li GY, Guan F, Yu Y, Fan ZT. Microstructure and mechanical properties of SiC_{np}/Al6082 aluminum matrix composites prepared by squeeze

casting combined with stir casting. J Mater Process Technol 2020;283:116699. https://doi.org/10.1016/j.jmatprotec.2020.116699.
[250] Li ZG, Chen L, Que BH, Lu L, Zhao GW, Zhang CS, Quan D. Fabrication and strengthening mechanism of dual-phased and bimodal-sized (Si_3N_{4p}+TiB_{2p})/6061Al hybrid composite. Mater Des 2022;220:110872. https://doi.org/10.1016/j.matdes.2022.110872.
[251] Xie KW, Nie JF, Hu KQ, Ma X, Liu XF. Improvement of high-temperature strength of 6061 Al matrix composite reinforced by dual-phased nano-AlN and submicron-Al_2O_3 particles. Trans. Nonferrous Met. Soc. China 2022;32:3197–211. https://doi.org/10.1016/S1003-6326(22)66013-8.
[252] Chen HS, Nie HH, Zhou J, Wang WX, Zhang P, Zhang YY, Wang JF, Liu RF. Microstructure and mechanical properties of B_4C/6061Al neutron absorber composite tube fabricated by spark plasma sintering and hot spinning. J Nucl Mater 2019;517:393–400. https://doi.org/10.1016/j.jnucmat.2018.12.048.
[253] Jia CP, Zhang P, Xu WR, Wang WX. Neutron shielding and mechanical properties of short carbon fiber reinforced aluminium 6061-boron carbide hybrid composite. Ceram Int 2021;47:10193–6. https://doi.org/10.1016/j.ceramint.2020.12.131.
[254] Chen HS, Wang WX, Nie HH, Zhou J, Li YL, Liu RF, et al. Microstructure evolution and mechanical properties of B_4C/6061Al neutron absorber composite sheets fabricated by powder metallurgy. J Alloys Compd 2018;730:342–51. https://doi.org/10.1016/j.jallcom.2017.09.312.
[255] Boppana SB, Dayanand S, Anil Kumar MR, Kumar V, Aravinda T. Synthesis and characterization of nano graphene and ZrO2 reinforced Al 6061 metal matrix composites. J Mater Res Technol 2020;9:7354–62. https://doi.org/10.1016/j.jmrt.2020.05.013.
[256] Zhang ZY, Zhao YT, Wang CL, Tao R, Fang Z, Sun Y, Kai XZ. High cycle fatigue behavior of in-situ ZrB2/AA6111 composites. Mater Sci. Eng A 2020;788:139590. https://doi.org/10.1016/j.msea.2020.139590.
[257] Jaber MH, Aziz GA, Mohammed AJ, Al-Aikawi HJ. Electrical conductivity, magnetic and fatigue properties of aluminum matrix composites reinforced with nano-titanium dioxide (TiO2). Nanocompos 2020;6:47–55. https://doi.org/10.1080/20550324.2020.1769976.
[258] Nieh TG, Lesuer DR, Syn CK. Tensile and fatigue properties of a 25 vol% SiC particulate reinforced 6090 Al composite at 300 °C. Metall. Mater 1995;32:707–12. https://doi.org/10.1016/0956-716X(95)91590-L.
[259] Polmear IJ, Couper MJ. Design and development of an experimental wrought aluminum alloy for use at elevated temperatures. Mater Trans 1988;19:1027–35. https://doi.org/10.1007/BF02628387.
[260] Tian W-S, Zhao Q-L, Zhang Q-Q, Qiu F, Jiang Q-C. Simultaneously increasing the high-temperature tensile strength and ductility of nano-sized TiCp reinforced Al-Cu matrix composites. Mater Sci. Eng A 2018;717:105–12. https://doi.org/10.1016/j.msea.2018.01.069.
[261] Hu KQ, Xu QF, Ma X, Sun QQ, Gao T, Liu XF. A novel heat-resistant Al–Si–Cu–Ni–Mg base material synergistically strengthened by Ni-rich intermetallics and nano-AlNp microskeletons. J Mater Sci Technol 2019;35:306–12. https://doi.org/10.1016/j.jmst.2018.09.051.
[262] Zan YN, Zhou YT, Zhao H, Liu ZY, Wang QZ, Wang D, Wang WG, Xiao BL, Ma ZY. Enhancing high-temperature strength of (B_4C+Al_2O_3)/Al designed for neutron absorbing materials by constructing lamellar structure. Composites Part B 2020;183:107674. https://doi.org/10.1016/j.compositesb.2019.107674.
[263] Zhang XY, Li WG, Ma JZ, Li Y, Deng Y, Yang MQ, et al. Temperature dependent strengthening mechanisms and yield strength for CNT/metal composites. Compos Struct 2020;244:112246. https://doi.org/10.1016/j.compstruct.2020.112246.
[264] Yoo SC, Kim J, Lee W, Hwang JY, Ryu HJ, Hong SH. Enhanced mechanical properties of boron nitride nanosheet/copper nanocomposites via a molecular-level mixing process. Composites Part B 2020;195:108088. https://doi.org/10.1016/j.compositesb.2020.108088.
[265] He PD, Kong H, Liu Q, Ferry M, Kruzic JJ, Li X. Elevated temperature mechanical properties of TiCN reinforced AlSi10Mg fabricated by laser powder bed fusion additive manufacturing. Mater Sci. Eng A 2021;811:141025. https://doi.org/10.1016/j.msea.2021.141025.
[266] Li J, Shi C, Liu E, He C, Zhao N. Microstructure evolution and tensile behavior of $MgAlB_{4w}$/Al composites at high temperatures. J Alloys Compd 2021;884:161088. https://doi.org/10.1016/j.jallcom.2021.161088.
[267] Morimune F, Hayase H, Shingu H, Kobayashi K, Ozaki R. The difference in the grain refining capacity of Al-Ti grain refiners with and without TiC. J. Jpn. Inst. Light Met 1976;26:320–6. https://doi.org/10.2464/jilm.26.320.
[268] Guemmaz M, Mosser A, Parlebas JC. Electronic changes induced by vacancies on spectral and elastic properties of titanium carbides and nitrides. J Electron Spectrosc Relat Phenom 2000;107:91–101. https://doi.org/10.1016/S0368-2048(00)00091-8.
[269] Frage N, Polak M, Dariel MP, Frumin N, Levin L. High-temperature phase equilibria in the Al-rich corner of the Al-Ti-C system. Metall Mater Trans A 1998:1341–5. https://doi.org/10.1007/s11661-998-0260-5.
[270] Hugosson HW, Korzhavyi P, Jansson U, Johansson B, Eriksson O. Phase stabilities and structural relaxations in substoichiometric TiC_{1-x}. Phys Rev B 2001;63:165116. https://doi.org/10.1103/PhysRevB.63.165116.
[271] Ren L, Gao T, Nie JF, Liu GL, Liu XF. A novel core-shell TiCx particle by modifying TiCx with B element and the preparation of the (TiC_x + AlN)/Al composite. J Alloys Compd 2022;894:162448. https://doi.org/10.1016/j.jallcom.2021.162448.
[272] Bian Y, Gao T, Liu G, Ma X, Ren Y, Liu X. Design of an in–situ multi–scale particles reinforced (Al2O3+ZrB2+AlN)/Al composite with high strength, elasticity modulus and thermal stability. Mater Sci. Eng A 2020;775:138983. https://doi.org/10.1016/j.msea.2020.138983.
[273] Zhu L, Liu TS, Duan TT, Li T-T, Qiu F, Yang HY, et al. Design of a new Al-Cu alloy manipulated by in-situ nanocrystals with superior high temperature tensile properties and its constitutive equation. Mater Des 2019;181:107945. https://doi.org/10.1016/j.matdes.2019.107945.
[274] Han G, Zhang WZ, Zhang GH, Feng ZJ, Wang YJ. High-temperature mechanical properties and fracture mechanisms of Al–Si piston alloy reinforced with in situ TiB_2 particles. Mater Sci. Eng A 2015;633:161–8. https://doi.org/10.1016/j.msea.2015.03.021.
[275] Wang HY, Jiang QC. Simultaneously increasing the elevated-temperature tensile strength and plasticity of in situ nano-sized TiC_x/Al-Cu-Mg composites. Mater. Charact 2017;125:7–12. https://doi.org/10.1016/j.matchar.2017.01.013.
[276] Takahashi Y, Shikama T, Yoshihara S, Aiura T, Noguchi H. Study on dominant mechanism of high-cycle fatigue life in 6061-T6 aluminum alloy through microanalyses of microstructurally small cracks. Acta Mater 2012;60:2554–67. https://doi.org/10.1016/j.actamat.2012.01.023.
[277] Liu T-S, Zhu L, Yang H-Y, Cui H-Y, Meng J, Qiu F, Dong B-X, Shu S-L, Jiang Q-C, Zhang L-C. Significantly enhanced fatigue resistance and mechanisms of hypoeutectic Al-Si composite calibrated using trace in-situ nanocrystals. Composites Part B 2023:111138. https://doi.org/10.1016/j.compositesb.2023.111138.
[278] Takahashi Y, Yoshitake H, Nakamichi R, Wada T, Takuma M, Shikama T, Noguchi H. Fatigue limit investigation of 6061-T6 aluminum alloy in giga-cycle regime. Mater Sci. Eng A 2014;614:243–9. https://doi.org/10.1016/j.msea.2014.07.039.
[279] Pineau A, Mcdowell DL, Busso EP, Antolovich SD. Failure of metals II: fatigue. Acta Mater 2016;107:484–507. https://doi.org/10.1016/j.actamat.2015.05.050.
[280] Geng JW, Li YG, Wang FF, Zhang CC, Chen D, Wang ML, et al. Revealing the complex effects of particle bands on fatigue crack growth in an extruded aluminium matrix composite. Int J Fatig 2022;157. https://doi.org/10.1016/j.ijfatigue.2022.106720.
[281] Abd-Elaziem W, Khedr M, Elsheikh AH, Liu J, Zeng Y, Sebae TA, et al. Influence of nanoparticles addition on the fatigue failure behavior of metal matrix composites: comprehensive review. Eng Fail Anal 2024;155:107751. https://doi.org/10.1016/j.engfailanal.2023.107751.
[282] Chawla N, Andres C, Davis LC, Jones JW, Allison JE. The interactive role of inclusions and SiC reinforcement on the high-cycle fatigue resistance of particle reinforced metal matrix composites. Metall Mater Trans A 2000;31:951–7. https://doi.org/10.1007/s11661-000-1013-2.
[283] Bonnen JJ, Allison JE, Jones JW. Fatigue behavior of a 2XXX series aluminum alloy reinforced with 15 vol Pct SiCp. Metall Trans A 1991;22:1007–19. https://doi.org/10.1016/0010-4361(91)90240-H.
[284] Chen Z. Effects of particle size on fatigue crack initiation and small crack growth in SiC particulate-reinforced aluminium alloy composites. Mater Lett 2004;58:2314–21. https://doi.org/10.1016/j.matlet.2004.02.034.
[285] Jody N, Hall J, Wayne Jones, Anil K. Particle size, volume fraction and matrix strength effects on fatigue behavior and particle fracture in 2124 aluminum-SiC_p composites. Mater. Sci. Eng. A 1994:69–80. https://doi.org/10.1016/0921-5093(94)90891-5.
[286] Hornbogen E, Gahr KHZ. Microstructure and fatigue crack growth in a γ-Fe-Ni-Al alloy. Acta Metall 1976;24:581–92. https://doi.org/10.1016/0001-6160(76)90104-8.
[287] Gray GT, Williams JC, Thompson AW. Roughness-induced crack closure: an explanation for microstructurally sensitive fatigue crack growth. Mater. Metall. Trans. A 1983;14:421–33. https://doi.org/10.1007/BF02644220.
[288] Chawla N, Habel U, Shen YL, Andres C, Jones JW, Allison JE. The effect of matrix microstructure on the tensile and fatigue behavior of SiC particle-reinforced 2080 Al matrix composites. Mater Trans 2000;31:531–40. https://doi.org/10.1007/s11661-000-0288-7.
[289] Alalkawi HJM, Hamdany AA, Alasadi AA. Influence of Nanoreinforced particles (Al2O3) on fatigue life and strength of aluminium based metal matrix composite. Al-Khwarizmi Engineering Journal 2017;13:91–9. https://doi.org/10.22153/kej.2017.03.005.
[290] Shin SE, Bae DH. Fatigue behavior of Al2024 alloy-matrix nanocomposites reinforced with multi-walled carbon nanotubes. Composites Part B 2018;134:61–8. https://doi.org/10.1016/j.compositesb.2017.09.034.
[291] Tóth L, Yarema SY. Formation of the science of fatigue of metals. Part 1. 1825–1870. Mater Sci 2006;42:673–80. https://doi.org/10.1007/s11003-006-0132-3.
[292] Mamoon A, Al-Jaafari A. Fatigue behavior of aluminum SiC nano composites material with different reinforcement ratio. IOP Conference Series: Mater. Sci. Eng 2020;870:012159. https://doi.org/10.1088/1757-899X/870/1/012159.
[293] Uematsu Y, Tokaji K, Kawamura M. Fatigue behaviour of SiC-particulate-reinforced aluminium alloy composites with different particle sizes at elevated temperatures. Compos Sci Technol 2008;68:2785–91. https://doi.org/10.1016/j.compscitech.2008.06.005.
[294] Senthilkumar R, Arunkumar N, Manzoor Hussian M. A comparative study on low cycle fatigue behaviour of nano and micro Al_2O_3 reinforced AA2014 particulate hybrid composites. Results Phys 2015;5:273–80. https://doi.org/10.1016/j.rinp.2015.09.004.
[295] Atrian A, Majzoobi GH, Enayati MH, Bakhtiari H. Mechanical and microstructural characterization of Al7075/SiC nanocomposites fabricated by dynamic compaction. Int. J. Miner 2014;21:295–303. https://doi.org/10.1007/s12613-014-0908-7.
[296] Ramesh CS, Hirianiah A, Noronha Noronha NP. A review on hot extrusion of Metal Matrix Composites (MMC's). Chin Geogr Sci 2014;4:30–5. https://doi.org/10.1007/s11769-002-0041-9.

[297] Xia J, Lewandowski JJ, Willard MA. Tension and fatigue behavior of Al-2124A/SiC-particulate metal matrix composites. Mater Sci. Eng A 2020;770:138518. https://doi.org/10.1016/j.msea.2019.138518.
[298] Srivatsan TS, Al-Hajri M. The fatigue and final fracture behavior of SiC particle reinforced 7034 aluminum matrix composites. Composites Part B 2002;33:391–404. https://doi.org/10.1016/S1359-8368(02)00025-2.
[299] Myriounis DP, Matikas TE, Hasan ST. Fatigue behaviour of SiC particulate-reinforced A359 aluminium matrix composites. Strain 2012;48:333–41. https://doi.org/10.1111/j.1475-1305.2011.00827.x.
[300] Chen C, Araby S, Demiral M, Cai R, Yang X, Wang W, Meng Q. Fatigue behavior and tribological properties of laser additive manufactured aluminum alloy/boron nitride nanosheet nanocomposites. J Mater Res Technol 2022;20:3930–48. https://doi.org/10.1016/j.jmrt.2022.08.124.

Yi-Cheng Gao: He is currently working toward the master's degree in Materials Processing Engineering at the School of Materials Science and Engineering, Jilin University, China. His main research interest is the microstructure construction and strengthening-toughening mechanism of aluminum alloy manipulated by nanoparticles.

Bai-Xin Dong: She is currently working toward a Ph. D in Materials Processing Engineering at the School of Materials Science and Engineering, Jilin University, China. Her main research interest is solidification microstructure manipulation and strengthening of Al alloy.

Hong-Yu Yang: She is currently working at the Department of Materials Science and Engineering, Jilin University, China. Her main research interests are the high efficiency control of microstructure and strengthening of alloy with nano-medium; Preparation of nano-functional ceramics, interface design and functional application of composite materials.

Xiao-Yan Yao: She is currently working toward the master's degree in Materials Processing Engineering at the School of Materials Science and Engineering, Jilin University, China. Her main research interests include micro-alloying and nano-mediated synergistic modulation of microstructure and toughening of Al–Mg–Si deformed alloys.

Jie Kang: He is now working in Jilin Liyuan Precision manufacturing Co., Ltd., as Chief Engineer. He mainly studies the research and development and trial production of extrusion of aluminum alloy.

Jia Meng: He is now working in FAW-Volkswagen Automotive Co., Ltd, as Supervisor of the automotive quality inspection department, He is mainly involved in quality testing and analysis of aluminum alloy components.

Chang-Jie Luo: He is now working in Shenzhen Cansinga Technology Co., Ltd, as Executive Director. He is a high-level talent in Shenzhen Bao'an District, Shenzhen Bao'an District 2020 May 4th Youth Medal winner. He has published more than 15 papers and applied for more than 50 patents.

Cheng-Gang Wang: He is now working in FAW Foundry Co., Ltd. as chief technical expert and senior engineer. He mainly studies the research and development and trial production of low-pressure and high-pressure casting products for non-ferrous and ferrous metal automotive structural parts.

Kuang Cao: He is now working in Jiangsu Dalishen Aluminum Industry Co., Ltd, serves as chairman of the board. He is mainly engaged in the production of wide and large-size aluminum and aluminum alloy plates, high-precision aluminum alloy sheets and strips and brazed aluminum alloy composite materials, as well as research and development.

Jian Qiao: He is a professor at School of Mechatronic Engineering and Automation at Foshan University. His research interests include the study of robot integration technology, precision control systems for super-resolution lasers, and inspection technology for high-brightness shaped curved products.

Shi-Li Shu: He received his Ph. D. from the School of Materials Science and Engineering of Jilin University in 2013, and is now an associate professor/doctoral supervisor at the School of Mechanical and Aerospace of Jilin University, engaged in laser additive manufacturing and bionic intelligent manufacturing research.

Ming Zhu: He is now working in Zhenjiang Xianfeng Automotive Parts Co., Ltd, as General Manager. He mainly studies the research and development and manufacture of aluminum alloy stamping and forming processes.

Feng Qiu: He is a professor at School of Materials Science and Engineering at Jilin University. Received his Ph. D of Materials Engineering at Jilin University in 2009. His research primarily focused on synthesis and processing, microstructure characterization, mechanical properties, physical properties of metal matrix composites; His research also extended to investigations on solidification microstructure and mechanical behaviors of aluminum alloys.

Qi-Chuan Jiang: He is a professor of the School of Materials Science and Engineering at Jilin University, China. Prof. Jiang is the leader of the research group of Metal Materials and Forming Processes of the Key Laboratory of Automobile Materials, Ministry of Education. He has been awarded the National Excellent Science and Technology Worker, the National Excellent Doctoral Dissertation Advisor, the China Foundry Outstanding Contribution Award (by Chinese Mechanical Engineering Society), and the Outstanding Figure of the Chinese Automobile Industry. He has been engaged in the research work on the metal solidification, and Al, Mg and steel matrix composites for over 30 years.